Navarra Center for International Development

Working Paper nº 01/2026

Score-driven long memory dynamics of worldwide regional temperature anomalies

Szabolcs Blazsek

Mercer University

Raven Amina Dupree

Mercer University

Luis Alberiko Gil-Alana

University of Navarra

Score-driven long memory dynamics of worldwide regional temperature anomalies

Szabolcs Blazsek[1,*], **Raven Amina Dupree**[1], **and Luis Alberiko Gil-Alana**[2]

[1]Stetson-Hatcher School of Business, Mercer University, Macon, United States

[2]School of Economics and Business, Universidad de Navarra, Pamplona, Spain

Abstract: We develop a score-driven fractionally integrated quasi-autoregressive model with Student's t innovations (t-FI-QAR), in which the degree of fractional integration d_t, the conditional mean, and the conditional scale evolve via likelihood-based updates. Using monthly U.S. National Oceanic and Atmospheric Administration (NOAA) land-and-ocean temperature anomalies for six regions (Arctic, Antarctic, Atlantic Ocean, Northeast Pacific Ocean, Northern and Southern Hemispheres) from January 1850 to October 2025, we show that d_t rises over time across all regions, implying increasingly persistent temperature dynamics. The increase is strongest in the Arctic and Northern Hemisphere, where we detect a structural shift over the past three decades consistent with a move toward non-stationary behavior. Significant but more moderate increases occur in the Atlantic, Northeast Pacific, and Southern Hemisphere, while the Antarctic exhibits a slight upward trend. Models that allow heavy tails and time-varying scale outperform homoscedastic specifications in likelihood-based criteria and diagnostics. The findings indicate that climate shocks now propagate more durably than in earlier periods, suggesting that stronger and more sustained mitigation and adaptation policies are needed to counter long-lived deviations in regional temperatures.

Keywords: Long memory processes; fractional degree of integration parameter; dynamic conditional score (DCS) models; generalized autoregressive score (GAS) models; climate change; global warming.

JEL classification codes: C22; C51; C52; Q54

[*]Correspondence to: Szabolcs Blazsek. Stetson-Hatcher Shcool of Business, Mercer University, 1501 Mercer University Drive, Macon, GA 31207, United States. E-mail: blazsek_s@mercer.edu

1 Introduction

Climate time series, such as long-run records of global and regional temperature anomalies, exhibit complex persistence patterns that standard short-memory or unit-root models often fail to capture adequately. Fractionally integrated FI(d) processes (Granger and Joyeux, 1980; Hosking, 1981), which allow the differencing parameter d to take non-integer values, provide a flexible continuum between short-memory I(0) and unit-root I(1) processes (e.g. Hamilton, 1994). Most applications in the climate and environmental literature assume a time-invariant memory parameter d (e.g. Yuan et al., 2014; Barassi et al., 2018; del Barrio Castro et al., 2025) and do not identify significant changes in persistence due to evolving climatic influences, alterations in observational networks, or structural breaks in climate dynamics.

Empirical evidence suggests that persistence in climate and environmental series d is dynamic. For example, wavelet-based methods (Lu and Guegan, 2011; Lu and Tao, 2012; Boubaker et al., 2017) and score-driven models (Bisaglia and Grigoletto, 2021) have been used to detect time-varying long-range dependence. We extend the latter work in our paper.

The class of score-driven models is a broadly applicable, likelihood-based framework for time-varying parameters such as location, scale, and shape of conditional distributions (Harvey and Chakravarty, 2008; Creal et al., 2008). Score-driven updates employ the scaled score of the conditional likelihood to generate data-adaptive parameter dynamics, which often yield robust filtering performance (Blasques et al., 2015; Gorgi et al., 2024).

We introduce the score-driven FI model for the t distribution, in which the degree of fractional integration d_t evolves endogenously alongside the conditional location and, in extended specifications, the conditional log scale. We propose the t-FI(d_t)-QAR family (FI quasi-autoregressive model), in which Student's t errors accommodate heavy tails commonly observed in climate anomaly records, and the dynamic memory parameter d_t is updated through a score-driven recursion. To address conditional heteroscedasticity and persistent scale effects, we consider two heteroscedastic variants: a t-FI-QAR-Beta-t-EGARCH model that imposes I(0) dynamics on the conditional log-scale and a t-FI-QAR-Beta-t-EIGARCH

counterpart that allows I(1) dynamics for the conditional log-scale. The model allows (i) dynamic long-memory behavior, (ii) resilience to outliers via heavy-tailed errors, and (iii) efficient, information-driven updates that adapt to changes in the data-generating process.

We use monthly data on the Arctic, Antarctic, Atlantic Ocean, Northeast Pacific Ocean, Northern Hemisphere, and Southern Hemisphere temperature anomalies from January 1850 to October 2025. The t-FI-QAR specification captures dynamics and annual stochastic seasonal effects in the conditional mean of temperature anomaly variables. The Beta-t-EGARCH and Beta-t-EIGARCH filters capture dynamics in the conditional variance of the errors.

We observe an increase in d_t throughout the sample period across all regions. The most pronounced increase is seen in the Arctic and the Northern Hemisphere. Significant increases in d_t are also noted for the Atlantic Ocean, the Northeast Pacific Ocean, and the Southern Hemisphere. A slight increment in d_t is estimated for the Antarctic. These findings suggest that climate shocks are expected to have longer-lasting impacts, and it is crucial to implement stronger policy measures to restore the original trends and mitigate anthropogenic effects.

In the remainder of this paper, Section 2 reviews the literature, Section 3 presents the methods, Section 4 describes the data, Section 5 summarizes the results, and Section 6 concludes.

2 Literature review

Fractional integration models appeared in the early 1980s (Granger, 1980, 1981; Granger and Joyeux, 1980; Hosking, 1981), and they became popular in the late 1990s (Baillie, 1996; Gil-Alana and Robinson, 1997). Gil-Alana and Robinson (1997) examined 14 US macroeconomic variables, which were earlier studied by Nelson and Plosser (1982) in the context of I(1) processes. They found that the 14 variables could be described better by FI(d) models. Subsequently, FI(d) models were applied in finance (Abbritti et al., 2016, 2023), climatology (Yuan et al., 2014; Proietti and Maddanu, 2022; Huang et al., 2024; del Barrio Castro et al., 2025), and environmental studies (Barassi et al., 2018; Blazsek et al., 2025b).

Dynamic FI(d) models relevant to the present paper have been investigated in several

papers, most of them using recursive or sequential estimation of the differencing parameter. For example, Caporale et al. (2020) recursively estimated the order of integration in the UK inflation rate. Cepni et al. (2025) proposed a time-varying estimation of the memory parameter in carbon price uncertainty. Wang and Ni (2025) proposed a recursive algorithm to estimate the Hurst exponent and the differencing parameter in ARFIMA (autoregressive fractionally integrated moving average) models by repeatedly applying an autoregressive filter until convergence is achieved. Another related paper is by Caporale et al. (2024), where they developed a dynamic factor model incorporating a fractional integration structure. Moreover, broader time-varying long memory models based on wavelets (Lu and Guegan, 2011; Lu and Tao, 2012; Boubaker et al., 2017) and score-driven models of fractional integration (Bisaglia and Grigoletto, 2021) were also suggested. We present an alternative to the latter work by extending it at several points.

Score-driven models, known as dynamic conditional score (DCS) or generalized autoregressive score (GAS) models, were introduced by Harvey and Chakravarty (2008) and Creal et al. (2008). See also Creal et al. (2011, 2013) and Harvey (2013). Some interesting properties of score-driven models are that (i) their updating terms generalize those of classical dynamic time series models (Creal et al., 2013; Harvey, 2013), (ii) they use information-theoretically effective filters (Blasques et al., 2015; Gorgi et al., 2024), and (iii) their outlier robustness is superior to that of classical time series models (Harvey, 2013; Caivano and Harvey, 2014). Applications of score-driven models used score-driven filters to model different properties of the probability distribution of the dependent variables, such as the conditional mean (Harvey, 2013), volatility (Harvey and Lange, 2017), association (Creal et al., 2013), shape parameters (Catania, 2021; Ayala et al., 2023), and regime-switching dynamics (Bernardi and Catania, 2019; Catania, 2021; Harvey and Palumbo, 2023), among several other applications.

To the best of our knowledge, relatively few works employ FI score-driven models. Janus et al. (2014) introduced FI score-driven filters of volatilities and copulas in a simultaneous equations model to capture the scale and dependence dynamics of several Dow Jones equi-

ties. Opschoor and Lucas (2019) introduced an FI score-driven multivariate model to model covariance matrix dynamics for intraday stock return data. Two recent papers employed FI univariate (Blazsek et al., 2025b) and multivariate (Blazsek et al., 2025a) score-driven location models. These four papers assume that the degree of fractional integration is time-invariant. For the present paper, a relevant work from the literature is by Bisaglia and Grigoletto (2021). They introduced a score-driven filter for the degree of fractional integration parameter and assumed a normal distribution with constant conditional variance for the error term.

3 Methods

The score-driven degree of the fractional integration model is

$$y_t = \mu_t + v_t = \mu_t + \exp(\lambda_t)\epsilon_t \tag{1}$$

for $t = 1, \ldots, T$, where $\mu_t = E(y_t|\mathcal{F}_{t-1}, \Theta)$ is the score-driven conditional mean of the demeaned dependent variable $y_t \in \mathbb{R}$ with $E(y_t) = 0$, where $\mathcal{F}_{t-1} = \sigma(y_1, \ldots, y_{t-1})$ and Θ is a vector of time-invariant parameters. The scaled error term $v_t|(\mathcal{F}_{t-1}, \Theta) \sim t[0, \exp(\lambda_t), \nu]$ has a conditional t distribution, where the degrees of freedom parameter $\nu \in \Theta$ with $2 < \nu < \infty$ and λ_t is the score-driven conditional log scale parameter. The standardized error term $\epsilon_t \sim t(0, 1, \nu)$ has the Student's t distribution. The conditional standard deviation (SD) of y_t is

$$\sigma_t = \mathrm{SD}(y_t|\mathcal{F}_{t-1}, \Theta) = \sqrt{\frac{\nu}{\nu - 2}} \exp(\lambda_t). \tag{2}$$

The log of the conditional density function of y_t is

$$\ln f(y_t|\mathcal{F}_{t-1}, \Theta) = \ln \Gamma\left(\frac{\nu+1}{2}\right) - \ln \Gamma\left(\frac{\nu}{2}\right) - \frac{1}{2}\ln(\pi\nu) - \lambda_t - \frac{\nu+1}{2}\ln\left[1 + \frac{(y_t - \mu_t)^2}{\nu \exp(2\lambda_t)}\right]. \tag{3}$$

First, the score-driven conditional mean μ_t is a t-FI(d_t)-QAR(p) filter:

$$(1 - L)^{d_t}(1 - \phi_1 L^1 - \ldots - \phi_p L^p)\mu_t = \psi_1 u_{\mu,t-1}, \tag{4}$$

where $d_t \in (0,1)$ is the score-driven degree of fractional integration parameter, L is the lag operator, and $(\phi_1, \ldots, \phi_p, \psi_1)' \in \Theta$. The scaled conditional score function $u_{\mu,t}$ is

$$\frac{\partial \ln f(y_t|\mathcal{F}_{t-1};\Theta)}{\partial \mu_t} = \frac{\nu+1}{\nu \exp(2\lambda_t)} u_{\mu,t} = \frac{\nu+1}{\nu \exp(2\lambda_t)} \times \frac{\nu \exp(\lambda_t)\epsilon_t}{\nu + \epsilon_t^2}, \tag{5}$$

where $u_{\mu,t}$ is defined by the second equality (Harvey, 2013). The scaled conditional score $u_{\mu,t}$ is a martingale difference sequence (MDS) (Harvey, 2013), and it is a bounded function of ϵ_t because $u_{\mu,t}$ is a continuously differentiable function of ϵ_t and if $|\epsilon_t| \to \infty$ then $u_{\mu,t} \to_p 0$. Due to the boundedness property, all unconditional moments of $u_{\mu,t}$ exist. The $u_{\mu,t} \to_p 0$ property shows that $u_{\mu,t}$ performs an asymptotic trimming of shocks captured by ϵ_t. Hence, the t-FI(d_t)-QAR(p) filter is robust to outliers. We note that if $\nu \to \infty$, i.e., $\epsilon_t \to_d N(0,1)$, then $u_{\mu,t} \to_p \exp(\lambda_t)\epsilon_t = v_t$. This shows that the normal distribution is a special case of the conditional mean filter, for which the updating term is a linear transformation of ϵ_t as in the moving average (MA) term of the Gaussian-ARMA(p,1) filter. We also note that the t-FI(d_t)-QAR(p) filter can be extended to the t-FI(d_t)-QARMA(p,q) filter straightforwardly.

Using the Maclaurin series (e.g., Hassler and Kokoszka, 2010), μ_t can also be written as

$$\mu_t = \phi_1 \mu_{t-1} + \ldots + \phi_p \mu_{t-p} + \sum_{j=0}^{\infty} \frac{\Gamma(j+d_t)}{\Gamma(j+1)\Gamma(d_t)} \psi_1 u_{\mu,t-1-j}, \tag{6}$$

where $\Gamma(x)$ is the gamma function. We set all variables for $t \leq 0$ to 0 to initialize this filter, similar to Bisaglia and Grigoletto (2021). Therefore, the infinite sum in Eq. (6) converges. The t-FI(d_t)-QAR(p) specification can capture stochastic seasonality in y_t by selecting the lag orders of μ_t according to the period of the seasonality. We note that to capture annual stochastic seasonality in the monthly time series data of our application, we use a lag order of 12.

Second, the score-driven degree of fractional integration d_t uses the link function

$$d_t = \frac{\exp(\tilde{d}_t)}{1+\exp(\tilde{d}_t)}, \tag{7}$$

which ensures that $d_t \in (0,1)$, where

$$\tilde{d}_t = \gamma \tilde{d}_{t-1} + (1-\gamma) u_{d,t-1}, \tag{8}$$

which is a score-driven exponentially weighted moving average (EWMA) filter, where $\gamma \in (0,1)$ is a smoothing parameter that can be estimated (i.e., $\gamma \in \Theta$) or chosen ex-ante. In our application, we choose $\gamma = 0.98$ a priori to simplify the estimation procedure. We considered alternatives for $\gamma \in (0.9,1)$, where different values of γ imply different levels of smoothing for $\tilde{d}_t$. The results were similar and are available from the authors upon request. We initialize $\tilde{d}_t$ from $E(\tilde{d}_t) = 0$. Hence, we initialize d_t from 0.5.

The conditional score function $u_{d,t}$ is

$$u_{d,t} = \frac{\partial \ln f(y_t|\mathcal{F}_{t-1};\Theta)}{\partial d_t} = \frac{(\nu+1)\epsilon_t}{\exp(\lambda_t)(\nu+\epsilon_t^2)} \times \left\{ \sum_{j=0}^{\infty} \frac{\Gamma(j+d_t)[\Psi^{(0)}(j+d_t) - \Psi^{(0)}(d_t)]}{\Gamma(j+1)\Gamma(d_t)} \psi_1 u_{\mu,t-1-j} \right\}, \tag{9}$$

where $\Psi^{(0)}(x)$ is the digamma function, also known as the polygamma function of order 0. The conditional score $u_{d,t}$ is an MDS (Harvey, 2013, Chapter 2), and it is a bounded function of ϵ_t because $u_{d,t}$ is a continuously differentiable function of ϵ_t and if $|\epsilon_t| \to \infty$ then $u_{d,t} \to_p 0$. Due to the boundedness property, all unconditional moments of $u_{d,t}$ exist. The $u_{d,t} \to_p 0$ property shows that $u_{d,t}$ performs an asymptotic trimming of shocks captured by ϵ_t. Hence, the conditional degree of the fractional integration filter is robust to outliers. We note that if $\nu \to \infty$, i.e., $\epsilon_t \to_d N(0,1)$, then conditional score function $u_{d,t}$ is given by:

$$u_{d,t} \to_p \frac{\epsilon_t}{\exp(\lambda_t)} \times \left\{ \sum_{j=0}^{\infty} \frac{\Gamma(j+d_t)[\Psi^{(0)}(j+d_t) - \Psi^{(0)}(d_t)]}{\Gamma(j+1)\Gamma(d_t)} \psi_1 \exp(\lambda_{t-1-j}) \epsilon_{t-1-j} \right\}. \tag{10}$$

This shows that by assuming the normal distribution for ϵ_t, we get a special case of the conditional degree of fractional integration model, for which the updating term is a linear function of ϵ_t, similar to the Gaussian-ARFIMA(p,d,1) filters, where d denotes the degree of fractional integration (see Gil-Alana and Hualde, 2009).

Third, for the log scale λ_t, we use (i) the Beta-t-EGARCH model (Harvey, 2013):

$$\lambda_t = \omega + \beta\lambda_{t-1} + \alpha u_{\lambda,t-1}, \tag{11}$$

where $(\omega, \beta, \alpha)' \in \Theta$, $|\beta| < 1$, and $\lambda_1 = \omega/(1-\beta)$, and (ii) the Beta-$t$-EIGARCH model:

$$\lambda_t = \lambda_{t-1} + \alpha u_{\lambda,t-1} \tag{12}$$

(Harvey, 2013, p. 113), where $\alpha \in \Theta$ and we estimate the initial value by parameter $\lambda_1 \in \Theta$. For both log scale filters, the conditional score function $u_{\lambda,t}$ is

$$\frac{\partial \ln f(y_t|\mathcal{F}_{t-1};\Theta)}{\partial \lambda_t} = \frac{(\nu+1)\epsilon_t^2}{\nu+\epsilon_t^2} - 1. \tag{13}$$

The scaled score $u_{\lambda,t}$ is an MDS (Harvey, 2013), and it is a bounded function of ϵ_t because $u_{\lambda,t}$ is a continuously differentiable function of ϵ_t and if $|\epsilon_t| \to \infty$ then $u_{\lambda,t} \to_p \nu$. Due to the boundedness property, all unconditional moments of $u_{\lambda,t}$ exist. The $u_{\lambda,t} \to_p \nu$ property shows that $u_{\lambda,t}$ performs an asymptotic Winsorizing of shocks captured by ϵ_t. Hence, the log scale filter is robust to outliers. If $\nu \to \infty$, i.e., $\epsilon_t \to_d N(0,1)$, then $u_{\lambda,t} \to_p \epsilon_t^2 - 1$. This shows that the normal distribution is a special case of the conditional mean model, for which the updating term is a quadratic transformation of ϵ_t, as in the Gaussian-GARCH(p,1) filters. Moreover, we note that $u_{\lambda,t}$ is i.i.d. since $u_{\lambda,t}$ is a continuous function of ϵ_t (White, 1984).

As a special case of the score-driven degree of fractional integration models in this section, we consider $\lambda_t = \lambda \in \Theta$ (i.e., homoscedastic errors), denoted as t-FI(d_t)-QAR(p). For this specification, $\Theta = (\phi_1, \phi_{12}, \psi_1, \lambda, \nu)'$. The score-driven degree of fractional integration models for the two conditional scale specifications are denoted as t-FI-QAR-Beta-t-EGARCH and t-FI-QAR-Beta-t-EIGARCH, respectively. For t-FI-QAR-Beta-t-EGARCH, $\Theta = (\phi_1, \phi_{12}, \psi_1, \omega, \beta, \alpha, \nu)'$. For t-FI-QAR-Beta-t-EIGARCH, $\Theta = (\phi_1, \phi_{12}, \psi_1, \omega, \lambda_1, \nu)'$.

We estimate all models using the maximum likelihood (ML) estimator method. See the

relevant works of Sowell (1992), Harvey (2013), and Blasques et al. (2022). We compare statistical performances using the log-likelihood (LL), Akaike information criterion (AIC), Bayesian information criterion (BIC), and Hannan-Quinn criterion (HQC) (Harvey, 2013).

We perform model diagnostics for ϵ_t, $u_{\mu,t}$, $u_{d,t}$, and $u_{\lambda,t}$ using the tests by Ljung and Box (1978) and Escanciano and Lobato (2009). The null hypothesis of the Ljung-Box (LB) test is that the time series consists of independent random variables, and the null hypothesis of the Escanciano-Lobato (EL) test is that the time series is an MDS. We use lag orders of 1, 5, 10, 25, and 50 for the LB test. The EL test involves an automatic lag-order selection.

4 Data

The data used correspond to average temperature anomalies in the Arctic, Antarctic, Mid-Atlantic, Northeast Pacific, and northern and southern hemispheres, obtained from the U.S. National Oceanic and Atmospheric Administration (NOAA) series, https://www.ncei.noaa.gov/access/monitoring/climate-at-a-glance/global/time-series. These series integrate sea surface and land surface temperature records from various long-term observation sets. The information used has a monthly resolution and covers the period from January 1850 to October 2025, corresponding to combined global land and ocean temperature anomalies calculated relative to the climatological average for the period 1901-2000.

Table 1 displays descriptive statistics of the temperature anomaly data. Figures 1 and 2 present their evolution from 1850 to 2025. We demeaned all variables by subtracting the sample average from each, which provides y_t (i.e., $E(y_t) = 0$) in the econometric model.

We provide estimates for the degree of fractional integration d using the following semi-parametric estimators: (i) the local Whittle (LW) estimator (Robinson, 1995); (ii) the exact LW (ELW) estimator, where the initial value of y_t is its sample average (Shimotsu and Phillips, 2005). (iii) the ELW estimator, where the initial value of y_t is y_1 (Shimotsu and Phillips, 2005). (iv) the two-step ELW estimator with unknown mean and time trend (Shimotsu, 2010), which uses the tapered estimator by Velasco (1999) in the first step and a modified ELW estimator

in the second step that uses the weighted average of the sample average of y_t and y_1 to approximate the initial value. (v) the two-step ELW estimator with unknown mean and time trend (Shimotsu, 2010), which uses the tapered estimator by Hurvich and Chen (2000) in the first step and a modified ELW estimator in the second step that uses the weighted average of the sample average of y_t and y_1 to approximate the initial value.

For estimators (i)-(v), an input argument is the bandwidth parameter, denoted δ. A low bandwidth leads to higher variance but lower bias in $\hat{d}$. A high bandwidth leads to lower variance but higher bias in $\hat{d}$. Alternative bandwidth parameters are suggested by Geweke and Porter-Hudak (1983); Robinson (1995); Delgado and Robinson (1996); Shimotsu and Phillips (2005); Henry (2007); Shimotsu (2010); Qu (2011); Baillie et al. (2014). Motivated by these, we consider $\delta \in \{0.5, 0.55, 0.6, 0.65, 0.7, 0.75, 0.8\}$.

We report results for all semiparametric estimators and bandwidths in Table 2. All estimates indicate long memory for all dependent variables with $0 < \hat{d} < 1$. Moreover, $\hat{d}$ significantly differs across alternative estimation methods and bandwidths and is a single estimate for each time series representing the average degree of fractional integration. Our score-driven model employs a flexible and robust approach for estimating the evolution of the degree of fractional integration. It controls for seasonality, heteroscedasticity, employs information-theoretically efficient filters for the conditional mean, log scale, and degree of fractional integration, and is robust to outliers. This provides an alternative method to the above LW method-based semiparametric estimators.

[APPROXIMATE LOCATION OF TABLES 1-2 AND FIGURES 1-2]

5 Results

We present the parameter estimates and model diagnostics for the t-FI-QAR, t-FI-QAR-Beta-t-EGARCH, and t-FI-QAR-Beta-t-EIGARCH specifications in Tables 3 and 4. We estimate t-FI-QAR for all dependent variables. For all specifications, we use lags 1 and 12 for the FI-QAR equation to simplify the estimation, but this can be updated in future work. In

this way, we control for both first-order dynamics and annual seasonality. For the t-FI-QAR specifications, the error term is homoscedastic. We improve that by using Beta-t-EGARCH or Beta-t-EIGARCH conditional standard deviation dynamics. In the first step, we estimated t-FI-QAR-Beta-t-EGARCH for all variables. In the results reported in Tables 3 and 4, we estimate the Beta-t-EIGARCH volatility model for those cases when β of the Beta-t-EGARCH filter converged to 1 (i.e., we found I(1) volatility dynamics). Results for t-FI-QAR-Beta-t-EIGARCH are reported for the Antarctic and Southern Hemisphere temperature anomaly variables, and results for t-FI-QAR-Beta-t-EGARCH are reported for Arctic, Atlantic Ocean, Northeast Pacific Ocean, and Northern Hemisphere temperature anomalies.

The parameter estimates indicate significant mean dynamics (ϕ_1, ϕ_{12}, and ψ_1). Parameter ϕ_1 is significant for all cases but for the Antarctic, ϕ_{12} is significant for all cases, and ψ_1 is also significant for all cases (Tables 3 and 4). We find significant log scale dynamics for all cases. The degrees of freedom ν estimates indicate heavy tails. The highest degrees of freedom parameter ν is estimated for the t-FI-QAR-Beta-t-EGARCH model for the Atlantic Ocean ($\hat{\nu} = 31.8161$). We also report LL, AIC, BIC, and HQC for each model in Tables 3 and 4. All those metrics indicate that the t-FI-QAR-Beta-t-EGARCH or t-FI-QAR-Beta-t-EIGARCH model outperforms the t-FI-QAR for the temperature anomaly data.

Tables 3 and 4 also present the p-values for the Ljung–Box and Escanciano–Lobato tests (Ljung and Box, 1978; Escanciano and Lobato, 2009) using lag orders 1, 5, 10, 25, and 50 for the Ljung–Box test and the optimal lag order for the Escanciano–Lobato test (Escanciano and Lobato, 2009). The p-values indicate correct specification for several filters, though the specification of μ_t may be updated by adding further lags to the score-driven equations. We use only lags μ_{t-1} and μ_{t-12} to simplify the statistical estimation procedures.

In Figures 3 and 4, we present the score-driven degree of factional integration parameter d_t for the best performing t-FI-QAR-Beta-t-EGARCH or t-FI-QAR-Beta-t-EIGARCH specification for each dependent variable. We note that as we initialize from $d_1 = 0.5$, for most variables, a burn-in period of 10-20 observations (i.e., the first 10-20 years of the sample

period) is needed to approximate the true value of d_t. The estimation results indicate a significant increase in d_t in the last three decades for the Arctic and the Northern Hemisphere, when the variable y_t became non-stationary. We find a significant increase in d_t for the Atlantic, Northeast Pacific Ocean, and the Southern Hemisphere. We also evidence a slightly increasing degree of fractional integration for the Antarctic. These results indicate that there are different levels and tendencies, but the degree of fractional integration for the temperature anomalies is increasing in every region. This suggests that temperature shocks are expected to last longer, their duration has increased over the last 30 years, and stronger policy measures are needed to recover to the original trend and stabilize temperature dynamics.

We present (i) the impact of ϵ_t to the scaled score function of location $u_{\mu,t}$ in Figures 5 and 6, (ii) the impact of ϵ_t to the score function of the degree of fractional integration $u_{d,t}$ in Figures 7 and 8, and (iii) the impact of ϵ_t to the score function of log scale $u_{\lambda,t}$ in Figures 9 and 10. As the maximum degrees of freedom is $\hat{\nu} = 31.8161$, all impact functions are bounded functions of ϵ_t. Hence, all score-driven filters in this paper are robust to outliers.

To highlight the importance of the heteroscedasticity-robust inference for the t-FI-QAR model, we exhibit the conditional standard deviation σ_t for temperature anomaly variables across all geographic regions from January 1850 to October 2025. This analysis utilizes the t-FI(d_t)-QAR(p)-Beta-t-EGARCH and t-FI(d_t)-QAR(p)-Beta-t-EIGARCH models, as illustrated in Figures 11 and 12. The estimates reveal significant and region-specific volatility dynamics.

In Supplementary Material A, we present the impact functions for $u_{\mu,t}$ and $u_{d,t}$, and the evolution of μ_t, d_t, ϵ_t, v_t, $u_{\mu,t}$, and $u_{d,t}$ from January 1850 to October 2025 for t-FI-QAR for all variables. In Supplementary Material B, we present the impact functions for $u_{\mu,t}$, $u_{d,t}$, and $u_{\lambda,t}$ and the evolution of μ_t, d_t, λ_t, σ_t, ϵ_t, v_t, $u_{\mu,t}$, $u_{d,t}$, $u_{\lambda,t}$ from January 1850 to October 2025 for t-FI-QAR-Beta-t-EGARCH or t-FI-QAR-Beta-t-EIGARCH for all variables.

[APPROXIMATE LOCATION OF TABLES 3-4 AND FIGURES 3-12]

6 Conclusions

This paper has introduced the t-FI(d_t)-QAR model, and two heteroscedastic extensions (t-FI-QAR-Beta-t-EGARCH and t-FI-QAR-Beta-t-EIGARCH) that allow the conditional log-scale to follow either I(0) or I(1) dynamics. Our methodology brings together three features that are especially relevant for long climate time series: (i) a time-varying fractional memory parameter d_t that is updated by the scaled score of the conditional likelihood, (ii) Student's t conditional errors to accommodate heavy tails and to increase robustness to extreme anomalies, and (iii) score-driven updates for the conditional mean, memory parameter, and, where applicable, the conditional log-scale, which deliver information-efficient and robust filtering.

Using combined land-and-ocean temperature anomaly series from NOAA for six regions (Arctic, Antarctic, Atlantic Ocean, Northeast Pacific Ocean, Northern Hemisphere, and Southern Hemisphere) from January 1850 to October 2025, we find the following primary results:

(i) Increasing persistence: For all regions, d_t has risen over the sample, indicating that temperature shocks have become more persistent. The increase is strongest and most pronounced in the Arctic and the Northern Hemisphere, where the series displays evidence of a structural shift affecting the last three decades toward non-stationary dynamics.

(ii) Regional heterogeneity: Significant increases in d_t are also estimated for the Atlantic Ocean, the Northeast Pacific Ocean, and the Southern Hemisphere, while the Antarctic shows smaller increases. Thus, the evolution of persistence is spatially heterogeneous.

(iii) Importance of heavy tails and heteroscedasticity: Models that jointly account for heavy-tailed errors (Student's t) and time-varying conditional scale (Beta-t-EGARCH or Beta-t-EIGARCH) outperform the homoscedastic t-FI-QAR in likelihood-based criteria and generally produce better diagnostic behavior for the score-driven updating series.

(iv) Robust updating and bounded impact functions: The score-driven updating terms for the conditional mean, memory parameter, and log-scale based on the t distribution are bounded functions of the standardized innovations; this produces automatic trimming of extreme shocks and lends robustness to outliers.

(v) Policy and scientific implications: The increase in the memory parameter implies that climate shocks, whether driven by natural variability or anthropogenic forcing, are likely to persist for longer durations than in earlier parts of the instrumental record. For policymakers, this means that transient mitigation or adaptation responses may be insufficient to return systems to prior states in the short run; stronger, sustained policy measures will be needed to counteract long-lived deviations. For climate scientists, the results underscore the value of allowing persistence to vary over time when characterizing and projecting climate dynamics.

While the proposed score-driven framework is flexible and robust, several important limitations should be considered. First, our models are observation-driven and apply a univariate approach to each regional series, meaning they do not explicitly account for cross-series dependence or common underlying drivers. Second, although the t distribution and the chosen score-driven specifications effectively capture heavy tails and heteroscedasticity, they cannot replace more comprehensive structural climate models that explain physical mechanisms in detail. Third, the choice of $\gamma = 0.98$ for the EWMA-type d_t recursion, along with the specific parametric forms used for the conditional location and log scale, is a practical decision; however, alternative filtering methods could also be investigated. Finally, formal proofs regarding the asymptotic properties of the maximum likelihood estimator, such as stationarity and invertibility, are areas that warrant further study.

The present paper could be extended in several ways, including: (i) Developing multivariate models that examine the joint evolution of d_t across different regions, which would help clarify both shared and local persistence dynamics. (ii) Incorporating exogenous factors, such as greenhouse gas concentrations, aerosol forcings, or volcanic events, into the score updates could aid in identifying the drivers behind changes in persistence. (iii) Extending the FI analysis to models that use Gegenbauer polynomials (see Gil-Alana and Hualde, 2009) could be beneficial, especially since singularities in these models occur at frequencies other than zero. (iv) Conducting comparative studies of the t-FI-QAR model against alternative time-varying long-memory estimators, like wavelet-based approaches, would provide valu-

able insights. (v) Finally, applying this framework to other environmental datasets would help assess the practical utility of the *t*-FI-QAR model for decision-making.

Funding

Luis Gil-Alana gratefully acknowledges financial support from the project from 'Ministerio de Ciencia, Innovación y Universidades' throughout the Grant PID2023-149516NB-I00/ AEI/10.13039/501100011033/FEDER, UE.

Conflict of interests

The authors declare no conflict of interest.

References

Abbritti, M., Carcel, H., Gil-Alana, L. A., and Moreno, A. (2023). Term premium in a fractionally cointegrated yield curve. *Journal of Banking and Finance*, 149:106777.

Abbritti, M., Gil-Alana, L. A., Lovcha, Y., and Moreno, A. (2016). Term structure persistence. *Journal of Financial Econometrics*, 14(2):331–352.

Ayala, A., Blazsek, S., and Escribano, A. (2023). Anticipating extreme losses using score-driven shape filters. *Studies in Nonlinear Dynamics & Econometrics*, 27(4):449–484.

Baillie, R. T. (1996). Long memory processes and fractional integration in econometrics. *Journal of Econometrics*, 73(1):5–59.

Baillie, R. T., Kapetanios, G., and Papailias, F. (2014). Bandwidth selection by cross-validation for forecasting long memory financial time series. *Journal of Empirical Finance*, 29:129–143.

Barassi, M. R., Spagnolo, N., and Zhao, Y. (2018). Fractional integration versus structural change: Testing the convergence of emissions. *Environmental and Resource Economics*, 71:923–968.

Bernardi, M. and Catania, L. (2019). Switching generalized autoregressive score copula models with application to systemic risk. *Journal of Applied Econometrics*, 34(1):43–65.

Bisaglia, L. and Grigoletto, M. (2021). A new time-varying model for forecasting long-memory series. *Statistical Methods & Applications*, 30(1):139–155.

Blasques, F., Koopman, S. J., and Lucas, A. (2015). Information-theoretic optimality of observation-driven time series models for continuous responses. *Biometrika*, 102(2):325–343.

Blasques, F., van Brummelen, J., Koopman, S. J., and Lucas, A. (2022). Maximum likelihood estimation for score-driven models. *Journal of Econometrics*, 227(2):325–346.

Blazsek, S., Escribano, A., and Licht, A. (2025a). Fractionally integrated multivariate score-driven location models with an application to climate data. *Studies in Nonlinear Dynamics & Econometrics*.

Blazsek, S., Lima, G. D. C., and Gil-Alana, L. A. (2025b). Score-driven fractionally integrated models of black carbon emissions: A cross-country study from 1820 to 2019. *Applied Economics Letters*.

Boubaker, H., Canarella, G., Gupta, R., and Miller, S. M. (2017). Time varying persistence of inflation. Evidence from wavelet based approach. *Studies in Nonlinear Dynamics & Econometrics*, 21(4):20160130.

Caivano, M. and Harvey, A. (2014). Time-series models with an EGB2 conditional distribution. *Journal of Time Series Analysis*, 35(6):558–571.

Caporale, G. M., Gil-Alana, L. A., and Piqueras-Martinez, P. J. (2024). Dynamic factor models and fractional integration with an application to US real economic activity. *Econometrics*, 12(4):39.

Caporale, G. M., Gil-Alana, L. A., and Trani, T. (2020). On the persistence of UK inflation: A long-range dependence approach. *International Journal of Finance & Economics*, 27(1):439–454.

Catania, L. (2021). Dynamic adaptive mixture models with an application to volatility and risk. *Journal of Financial Econometrics*, 19(4):531–564.

Cepni, O., Gupta, R., Gil-Alana, L. A., and Polat, O. (2025). Time variation in the persistence of carbon price uncertainty. The role of carbon policy uncertainty. *Quarterly Review of Economics and Finance*, 102:102004.

Creal, D., Koopman, S. J., and Lucas, A. (2008). A general framework for observation driven time-varying parameter models. Discussion Paper 08-108/4, Tinbergen Institute, https://papers.tinbergen.nl/08108.pdf.

Creal, D., Koopman, S. J., and Lucas, A. (2011). A dynamic multivariate heavy-tailed model for time-varying volatilities and correlations. *Journal of Business and Economic Statistics*, 29(4):552–563.

Creal, D., Koopman, S. J., and Lucas, A. (2013). Generalized autoregressive score models with applications. *Journal of Applied Econometrics*, 28(5):777–795.

del Barrio Castro, T., Escribano, A., and Sibbertsen, P. (2025). Modeling and forecasting the long memory of cyclical trends in paleoclimate data. *Energy Economics*, 147.

Delgado, M. and Robinson, P. M. (1996). Optimal spectral bandwidth for long memory. *Statistica Sinica*, 6(1):97–112.

Escanciano, J. C. and Lobato, I. N. (2009). An automatic portmanteau test for serial correlation. *Journal of Econometrics*, 151(2):140–149.

Geweke, J. and Porter-Hudak, S. (1983). The estimation and application of long memory time series models. *Journal of Time Series Analysis*, 4(4):221–238.

Gil-Alana, L. and Hualde, J. (2009). Fractional integration and cointegration: An overview and an empirical application. In Mills, T. and Patternson, K., editors, *Palgrave Handbook of Econometrics*, volume 2, pages 434–472. New York: Palgrave Macmillan.

Gil-Alana, L. A. and Robinson, P. M. (1997). Testing of unit roots and other nonstationary hypotheses. *Journal of Econometrics*, 80(2):241–268.

Gorgi, P., Lauria, C. S. A., and Luati, A. (2024). On the optimality of score-driven models. *Biometrika*, 111(3):865–880.

Granger, C. W. J. (1980). Long memory relationships and the aggregation of dynamic models. *Journal of Econometrics*, 14:227–238.

Granger, C. W. J. (1981). Some properties of time series data and their use in econometric model specification. *Journal of Econometrics*, 16:121–130.

Granger, C. W. J. and Joyeux, R. (1980). An introduction to long memory time series and fractionally differencing. *Journal of Time Series Analysis*, 1(1):15–29.

Hamilton, J. D. (1994). *Time Series Analysis*. Princeton: Princeton University Press.

Harvey, A. and Lange, R. J. (2017). Modeling the interactions between volatility and returns using EGARCH-M. *Journal of Time Series Analysis*, 39(6):909–919.

Harvey, A. C. (2013). *Dynamic Models for Volatility and Heavy Tails*. Cambridge: Cambridge University Press.

Harvey, A. C. and Chakravarty, T. (2008). Beta-t-(E)GARCH. Cambridge Working Papers in Economics 0840, University of Cambridge, Cambridge, http://www.econ.cam.ac.uk/research/repec/cam/pdf/cwpe0840.pdf.

Harvey, A. C. and Palumbo, D. (2023). Regime switching models for circular and linear time series. *Journal of Time Series Analysis*, 44(4):374–392.

Hassler, U. and Kokoszka, P. (2010). Impulse responses of fractionally integrated processes with long memory. *Econometric Theory*, 26(6):1855–1861.

Henry, M. (2007). Bandwidth choice, optimal rates and adaptivity in semiparametric estimation of long memory. In Teyssière, G. and Kirman, A. P., editors, *Long Memory in Economics*, pages 157–172. Berlin, Heidelberg: Springer.

Hosking, J. R. M. (1981). Fractional differencing. *Biometrika*, 68(1):165–176.

Huang, C., He, W., Liu, J., Nguyen, N. T., Yang, H., Lv, Y., Chen, H., and Zhao, M. (2024). Exploring the potential of long short-term memory networks for predicting net CO2 exchange across various ecosystems with multi-source data. *Journal of Geophysical Research: Atmospheres*, 129(7):e2023JD040418.

Hurvich, C. M. and Chen, W. W. (2000). An efficient taper for potentially overdifferenced long-memory time series. *Journal of Time Series Analysis*, 21(2):155–180.

Janus, P., Koopman, S. J., and Lucas, A. (2014). Long memory dynamics for multivariate dependence under heavy tails. *Journal of Empirical Finance*, 29(C):187–206.

Ljung, G. M. and Box, G. E. P. (1978). On a measure of a lack of fit in time series models. *Biometrika*, 65(2):297–303.

Lu, Z. and Guegan, D. (2011). Estimation of time-varying long memory parameter using wavelet method. *Communications in Statistics - Simulation and Computation*, 40(4):596–613.

Lu, Z. and Tao, Q. (2012). Time-varying long memory parameter estimation based on wavelets. *Chinese Journal of Applied Probability and Statistics*, 28(5):499–510.

Nelson, C. R. and Plosser, C. I. (1982). Trends and random walks in macroeconmic time series. *Journal of Monetary Economics*, 34(1):167–180.

Opschoor, A. and Lucas, A. (2019). Fractional integration and fat tails for realized covariance kernels. *Journal of Financial Econometrics*, 17(1):66–90.

Proietti, T. and Maddanu, F. (2022). Modelling cycles in climate series: The fractional sinusoidal waveform process. *Journal of Econometrics*, 239(1):105299.

Qu, Z. (2011). A test against spurious long memory. *Journal of Business & Economics Statistics*, 29(3):423–438.

Robinson, P. M. (1995). Gaussian semiparametric estimation of long range dependence. *Annals of Statistics*, 23(5):1630–1661.

Shimotsu, K. (2010). Exact local Whittle estimation of fractional integration with unknown mean and time trend. *Econometric Theory*, 26(2):501–540.

Shimotsu, K. and Phillips, P. C. B. (2005). Exact local Whittle estimation. *Annals of Statistics*, 30(4):1890–1933.

Sowell, F. (1992). Maximum likelihood estimation of stationary univariate fractionally integrated time series models. *Journal of Econometrics*, 53(1–3):165–188.

Velasco, C. (1999). Gaussian semiparametric estimation of non- stationary time series. *Journal of Time Series Analysis*, 20(1):87–127.

Wang, S. and Ni, N. (2025). A recursive method on estimating ARFIMA in agricultural time series. In Assa, H., Liu, P., and Wang, S., editors, *Quantitative Risk Management in Agricultural Business*, pages 217–248. Cham: Springer.

White, H. (1984). *Asymptotic Theory for Econometricians*. San Diego: Academic Press.

Yuan, N., Fu, Z., and Liu, S. (2014). Extracting climate memory using fractional integrated statistical model: A new perspective on climate prediction. *Scientific Reports*, 4:6577.

Table 1. Descriptive statistics.

Variable	Sample size	Minimum	Maximum	Median	Mean	SD
Arctic	2110	−3.7100	5.1300	0.1003	−0.0400	1.1870
Antarctic	2110	−1.6300	2.2200	0.0440	0.0300	0.4335
Atlantic Ocean	2110	−1.0900	1.8400	0.0991	0.0700	0.4592
Northeast Pacific Ocean	2110	−1.8800	1.7900	0.0532	0.0500	0.4809
Northern Hemisphere	2110	−1.0500	2.0200	0.0786	−0.0200	0.4887
Southern Hemisphere	2110	−0.5400	1.1000	0.0562	−0.0400	0.3047

Variable	Skewness	Kurtosis	Q 5%	Q 95%	IQ range	SW test
Arctic	0.5976	1.2057	−1.6545	2.3245	1.2700	0.0000
Antarctic	0.2634	1.7174	−0.6500	0.7900	0.4600	0.0000
Atlantic Ocean	0.4186	0.4098	−0.6100	0.8700	0.5925	0.0000
Northeast Pacific Ocean	−0.0402	0.5922	−0.7245	0.8600	0.6000	0.0000
Northern Hemisphere	1.1241	1.2380	−0.5300	1.1245	0.5100	0.0000
Southern Hemisphere	0.7873	−0.0735	−0.3300	0.6500	0.4300	0.0000

Notes: Standard deviation (SD); quantile 5% (Q 5%); quantile 95% (Q 95%); interquartile (IQ); Shapiro–Wilk (SW). We present the *p*-values for the SW test. *Data source:* U.S. National Oceanic and Atmospheric Administration (NOAA).

Table 2. Semiparametric estimates of the degree of fractional integration d.

LW estimator (Robinson, 1995):							
Variable/Bandwidth	0.5	0.55	0.6	0.65	0.7	0.75	0.8
Arctic	0.6002	0.5651	0.5316	0.5009	0.3811	0.3883	0.3698
Antarctic	0.3173	0.2656	0.2365	0.2233	0.1763	0.1835	0.1658
Atlantic Ocean	0.4420	0.4324	0.4971	0.5349	0.5821	0.6354	0.6823
Northeast Pacific Ocean	0.3132	0.3428	0.4058	0.4396	0.4789	0.5199	0.5799
Northern Hemisphere	0.6504	0.6703	0.7125	0.7411	0.6152	0.6291	0.6089
Southern Hemisphere	0.6511	0.6144	0.6647	0.6794	0.6390	0.6485	0.6352
ELW estimator (Shimotsu and Phillips, 2005), initial value of y_t is its sample average:							
Variable/Bandwidth	0.5	0.55	0.6	0.65	0.7	0.75	0.8
Arctic	0.6525	0.5875	0.5338	0.4831	0.3654	0.3743	0.3654
Antarctic	0.3401	0.2921	0.2483	0.2276	0.1876	0.1956	0.1839
Atlantic Ocean	0.5304	0.4704	0.5071	0.5284	0.5782	0.6462	0.7155
Northeast Pacific Ocean	0.3795	0.3770	0.4159	0.4450	0.4840	0.5319	0.6092
Northern Hemisphere	0.7194	0.6801	0.6766	0.6771	0.5619	0.5792	0.5713
Southern Hemisphere	0.6994	0.6152	0.6324	0.6297	0.5988	0.6157	0.6167
ELW estimator (Shimotsu and Phillips, 2005), initial value of y_t is y_1:							
Variable/Bandwidth	0.5	0.55	0.6	0.65	0.7	0.75	0.8
Arctic	0.5998	0.5498	0.5038	0.4541	0.3387	0.3514	0.3460
Antarctic	0.3225	0.2818	0.2409	0.2206	0.1845	0.1931	0.1820
Atlantic Ocean	0.5243	0.4638	0.5006	0.5233	0.5759	0.6476	0.7162
Northeast Pacific Ocean	0.3460	0.3506	0.3910	0.4325	0.4801	0.5334	0.6120
Northern Hemisphere	0.7063	0.6598	0.6512	0.6531	0.5339	0.5593	0.5555
Southern Hemisphere	0.6772	0.5947	0.6119	0.6115	0.5863	0.6071	0.6095
Two-step ELW estimator (Shimotsu, 2010; Velasco, 1999):							
Variable/Bandwidth	0.5	0.55	0.6	0.65	0.7	0.75	0.8
Arctic	0.6111	0.5947	0.5669	0.4587	0.3427	0.3539	0.3482
Antarctic	0.3323	0.2822	0.2410	0.2210	0.1865	0.1946	0.1836
Atlantic Ocean	0.5368	0.4686	0.5081	0.5276	0.5736	0.6420	0.7154
Northeast Pacific Ocean	0.3552	0.3602	0.4099	0.4378	0.4838	0.5355	0.6137
Northern Hemisphere	0.6484	0.6419	0.6348	0.6314	0.5784	0.5929	0.5870
Southern Hemisphere	0.6790	0.6221	0.6271	0.6229	0.6036	0.6176	0.6205
Two-step ELW estimator (Shimotsu, 2010; Hurvich and Chen, 2000):							
Variable/Bandwidth	0.5	0.55	0.6	0.65	0.7	0.75	0.8
Arctic	0.9319	0.8751	0.7883	0.6071	0.5001	0.5001	0.5001
Antarctic	0.9339	0.9267	0.7205	0.6610	0.5465	0.5438	0.5004
Atlantic Ocean	0.5368	0.4686	0.5081	0.5276	0.5736	0.7306	0.9394
Northeast Pacific Ocean	0.3552	0.3602	0.4099	0.4379	0.4838	0.7387	0.7605
Northern Hemisphere	0.6484	0.6419	0.6348	0.6314	0.5784	0.5929	0.5870
Southern Hemisphere	0.6790	0.6221	0.6270	0.6229	0.6036	0.6176	0.6205

Notes: Local Whittle (LW); exact LW (ELW).

Table 3. Parameter estimates and model diagnostics.

Statistics	Arctic t-FI-QAR	Arctic t-FI-QAR -Beta-t-EGARCH	Antarctic t-FI-QAR	Antarctic t-FI-QAR -Beta-t-EIGARCH	Atlantic Ocean t-FI-QAR	Atlantic Ocean t-FI-QAR -Beta-t-EGARCH
ϕ_1	0.0919***(0.0350)	0.0498***(0.0425)	0.0077(0.0889)	0.0002(0.0462)	0.5194***(0.0135)	0.5806***(0.0169)
ϕ_{12}	0.4044***(0.0374)	0.3957***(0.0418)	0.2832***(0.0816)	0.5498***(0.0473)	0.0876***(0.0147)	0.0919***(0.0166)
ψ_1	0.4762***(0.0353)	0.4269***(0.0339)	0.3112***(0.0353)	0.2194***(0.0230)	0.2194***(0.0287)	1.0012***(0.0312)
λ	−0.4622***(0.0231)		−1.1749***(0.0265)		−1.8641***(0.0156)	
ω		−0.3172***(0.0476)				−0.0373***(0.0101)
β		0.3581***(0.0887)				0.9801***(0.0054)
α		0.1643***(0.0206)		0.0134***(0.0031)		0.0242***(0.0038)
λ_1				−2.7346***(0.1031)		
ν	4.7799***(0.5144)	4.6576***(0.4890)	4.2555***(0.4852)	9.7832***(1.8999)	12.6019***(0.8475)	31.8161***(7.7460)
LL	−1.1723	**−1.1523**	−0.4894	**−0.3718**	0.3811	**0.4193**
AIC	2.3493	**2.3111**	0.9835	**0.7492**	−0.7575	**−0.8320**
BIC	2.3627	**2.3299**	0.9969	**0.7653**	−0.7441	**−0.8133**
HQC	2.3542	**2.3180**	0.9884	**0.7551**	−0.7526	**−0.8252**
LB(1) ϵ_t	0.0161	0.0019	0.0048	0.0115	**0.5053**	**0.7333**
LB(5) ϵ_t	**0.1029**	0.0071	0.0328	**0.0722**	0.0000	0.0000
LB(10) ϵ_t	**0.0551**	0.0026	**0.1082**	**0.1870**	0.0000	0.0000
LB(25) ϵ_t	0.0000	0.0000	0.0215	0.0000	0.0000	0.0001
LB(50) ϵ_t	0.0000	0.0000	0.0257	0.0000	0.0000	0.0056
LB(1) $u_{\mu,t}$	**0.2720**	0.0032	**0.9204**	**0.2347**	**0.7549**	**0.2350**
LB(5) $u_{\mu,t}$	**0.7964**	**0.0619**	**0.8092**	**0.1870**	0.0000	0.0000
LB(10) $u_{\mu,t}$	**0.7646**	0.0000	**0.7404**	**0.1783**	0.0001	0.0000
LB(25) $u_{\mu,t}$	0.0000	0.0000	0.0156	0.0023	0.0008	0.0000
LB(50) $u_{\mu,t}$	0.0000	0.0000	0.0024	0.0015	0.0050	0.0000
LB(1) $u_{d,t}$	0.0000	0.0000	**0.2174**	**0.7813**	0.0000	0.0000
LB(5) $u_{d,t}$	0.0000	0.0000	**0.3144**	**0.4431**	0.0000	0.0000
LB(10) $u_{d,t}$	0.0000	0.0000	0.0091	**0.3865**	0.0000	0.0000
LB(25) $u_{d,t}$	0.0000	0.0000	0.0001	0.0008	0.0000	0.0000
LB(50) $u_{d,t}$	0.0000	0.0000	0.0011	0.0249	0.0000	0.0000
LB(1) $u_{\lambda,t}$		**0.3813**		0.0003		**0.2747**
LB(5) $u_{\lambda,t}$		0.0000		0.0000		**0.2488**
LB(10) $u_{\lambda,t}$		0.0000		0.0000		**0.4992**
LB(25) $u_{\lambda,t}$		0.0000		0.0000		**0.5059**
LB(50) $u_{\lambda,t}$		0.0000		0.0000		**0.5663**
EL ϵ_t	0.0422	0.0001	0.0268	0.0052	0.0000	0.0000
EL $u_{\mu,t}$	**0.3086**	0.0023	**0.9266**	**0.3351**	0.0000	0.0000
EL $u_{d,t}$	0.0001	0.0000	**0.5199**	**0.8615**	0.0000	0.0000
EL $u_{\lambda,t}$		0.0000		0.0000		**0.0946**

Notes: Log-likelihood (LL); Akaike information criterion (AIC); Bayesian information criterion (BIC); Hannan–Quinn criterion (HQC); Ljung–Box (LB); Escanciano–Lobato (EL). Bold numbers indicate either superior likelihood-based metrics or p-values greater than 5%. *** indicates significance at the 1% level.

Table 4. Parameter estimates and model diagnostics.

Statistics	Northeast Pacific Ocean *t*-FI-QAR	Northeast Pacific Ocean *t*-FI-QAR -Beta-*t*-EGARCH	Northern Hemisphere *t*-FI-QAR	Northern Hemisphere *t*-FI-QAR -Beta-*t*-EGARCH	Southern Hemisphere *t*-FI-QAR	Southern Hemisphere *t*-FI-QAR -Beta-*t*-EIGARCH
ϕ_1	$0.4027^{***}(0.0196)$	$0.4297^{***}(0.0230)$	$0.4049^{***}(0.0171)$	$0.4275^{***}(0.0176)$	$0.5598^{***}(0.0178)$	$0.5658^{***}(0.0194)$
ϕ_{12}	$0.0701^{***}(0.0214)$	$0.0509^{***}(0.0223)$	$0.3403^{***}(0.0201)$	$0.2950^{***}(0.0220)$	$0.2148^{***}(0.0182)$	$0.1995^{***}(0.0182)$
ψ_1	$0.9506^{***}(0.0314)$	$0.8802^{***}(0.0319)$	$0.5813^{***}(0.0317)$	$0.5481^{***}(0.0304)$	$0.6174^{***}(0.0291)$	$0.5929^{***}(0.0293)$
λ	$-1.4842^{***}(0.0145)$		$-1.8872^{***}(0.0188)$		$-2.3939^{***}(0.0182)$	
ω		$-0.0558^{***}(0.0162)$		$-1.3434^{***}(0.2597)$		
β		$0.9630^{***}(0.0108)$		0.2891(0.1377)		
α		$0.0271^{***}(0.0039)$		$0.0824^{***}(0.0139)$		$0.0078^{***}(0.0021)$
λ_1						$-2.7750^{***}(0.0831)$
ν	$20.6117^{***}(2.2413)$	$23.9622^{***}(4.0680)$	$9.2739^{***}(1.1646)$	$9.4382^{***}(1.2859)$	$16.8177^{***}(3.3407)$	$24.2836^{***}(6.7637)$
LL	0.0281	**0.0567**	0.3778	**0.3862**	0.9387	**0.9474**
AIC	−0.0514	**−0.1068**	−0.7508	**−0.7657**	−1.8726	**−1.8891**
BIC	−0.0380	**−0.0881**	−0.7374	**−0.7469**	−1.8592	**−1.8731**
HQC	−0.0465	**−0.0999**	−0.7459	**−0.7588**	−1.8677	**−1.8833**
LB(1) ϵ_t	**0.8918**	**0.5351**	**0.6172**	**0.4589**	0.0061	0.0201
LB(5) ϵ_t	**0.1272**	0.0298	**0.4480**	**0.4043**	0.0000	0.0000
LB(10) ϵ_t	**0.2371**	**0.1132**	**0.1129**	0.0402	0.0000	0.0000
LB(25) ϵ_t	**0.3968**	**0.3177**	0.0000	0.0000	0.0000	0.0000
LB(50) ϵ_t	**0.4596**	**0.5941**	0.0000	0.0000	0.0000	0.0000
LB(1) $u_{\mu,t}$	**0.5298**	**0.3984**	**0.3552**	**0.1868**	0.0097	**0.0764**
LB(5) $u_{\mu,t}$	0.0440	0.0021	**0.3108**	**0.2079**	0.0000	0.0000
LB(10) $u_{\mu,t}$	**0.1058**	0.0095	**0.0668**	0.0144	0.0000	0.0000
LB(25) $u_{\mu,t}$	**0.3346**	**0.0578**	0.0000	0.0000	0.0000	0.0000
LB(50) $u_{\mu,t}$	**0.3537**	**0.1065**	0.0000	0.0000	0.0000	0.0000
LB(1) $u_{d,t}$	0.0000	0.0002	**0.5575**	**0.5356**	**0.6716**	**0.4808**
LB(5) $u_{d,t}$	0.0000	0.0003	0.0007	0.0152	0.0000	0.0000
LB(10) $u_{d,t}$	0.0000	0.0000	0.0037	0.0048	0.0000	0.0000
LB(25) $u_{d,t}$	0.0000	0.0000	0.0000	0.0000	0.0000	0.0000
LB(50) $u_{d,t}$	**0.3537**	0.0000	0.0000	0.0000	0.0000	0.0000
LB(1) $u_{\lambda,t}$		0.0022				**0.1281**
LB(5) $u_{\lambda,t}$		0.0336				**0.1059**
LB(10) $u_{\lambda,t}$		**0.1550**				**0.2473**
LB(25) $u_{\lambda,t}$		**0.4421**				**0.0928**
LB(50) $u_{\lambda,t}$		**0.4027**				0.0108
EL ϵ_t	**0.0590**	0.0054	**0.0754**	**0.0720**	0.0000	0.0000
EL $u_{\mu,t}$	0.0018	0.0018	**0.0674**	**0.0639**	0.0000	0.0000
EL $u_{d,t}$	0.0170	0.0142	0.0383	**0.7617**	0.0000	0.0000
EL $u_{\lambda,t}$		0.0145				0.0012

Notes: Log-likelihood (LL); Akaike information criterion (AIC); Bayesian information criterion (BIC); Hannan–Quinn criterion (HQC); Ljung–Box (LB); Escanciano–Lobato (EL). Bold numbers indicate either superior likelihood-based metrics or *p*-values greater than 5%. *** indicates significance at the 1% level.

(a) Arctic temperature anomalies

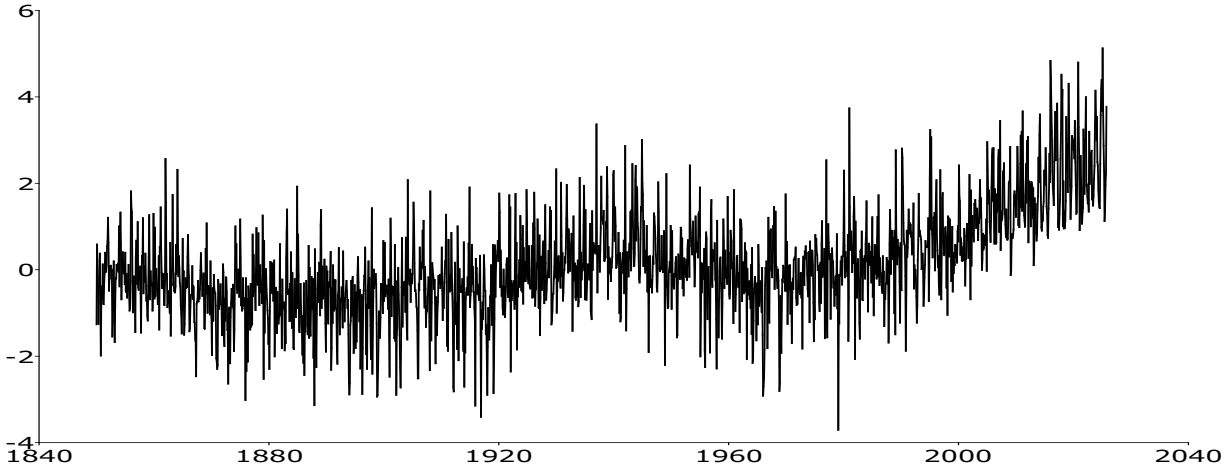

(b) Antarctic temperature anomalies

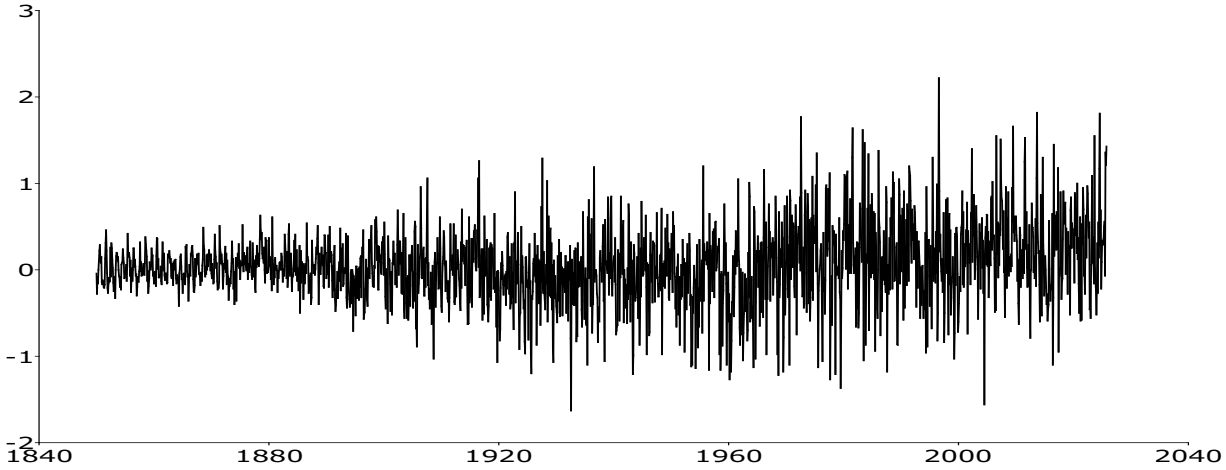

(c) Atlantic Ocean temperature anomalies

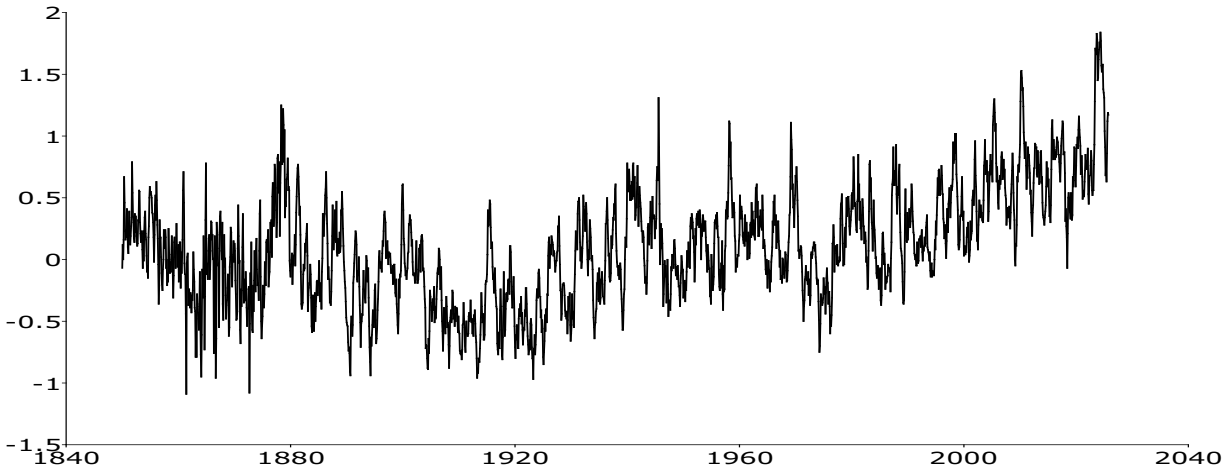

Figure 1. Temperature anomalies from January 1850 to October 2025. *Data source:* U.S. National Oceanic and Atmospheric Administration (NOAA).

(a) Northeast Pacific Ocean temperature anomalies

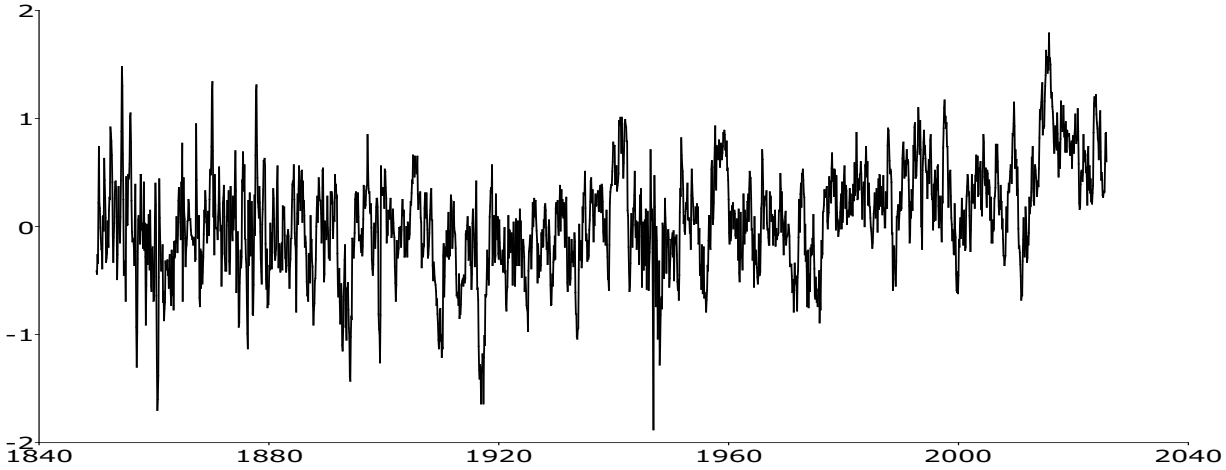

(b) Northern Hemisphere temperature anomalies

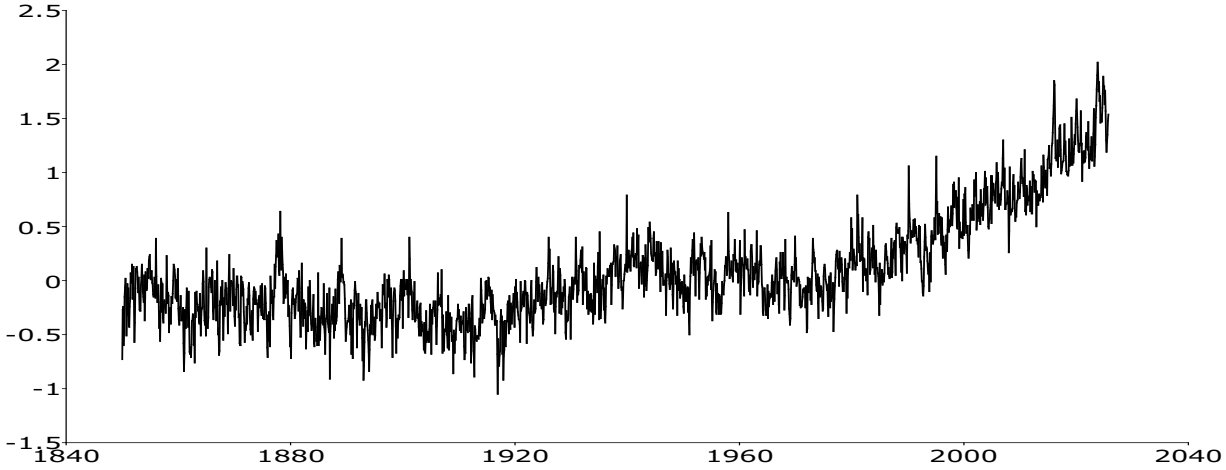

(c) Southern Hemisphere temperature anomalies

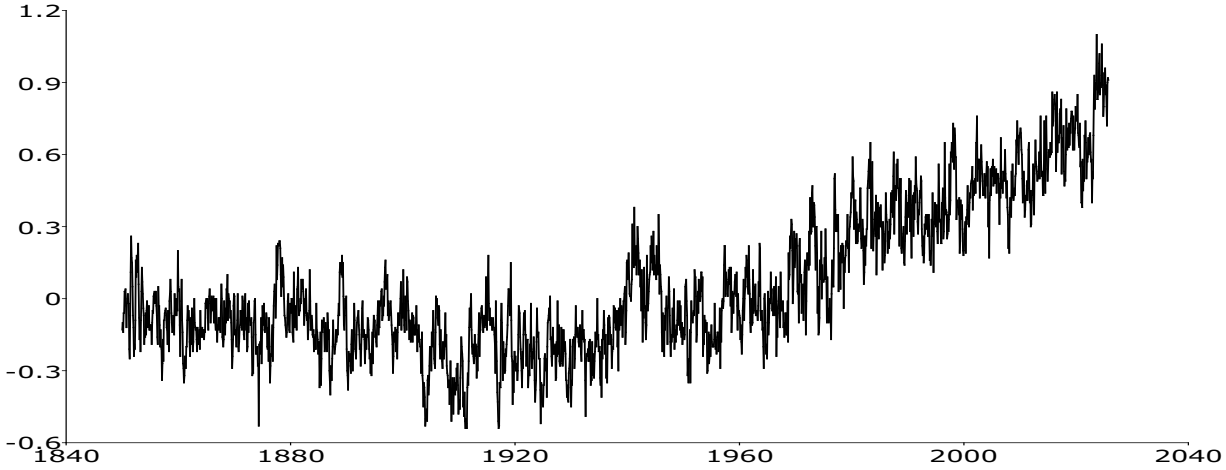

Figure 2. Temperature anomalies from January 1850 to October 2025. *Data source:* U.S. National Oceanic and Atmospheric Administration (NOAA).

(a) Arctic temperature anomalies, degree of fractional integration d_t for t-FI-QAR-Beta-t-EGARCH

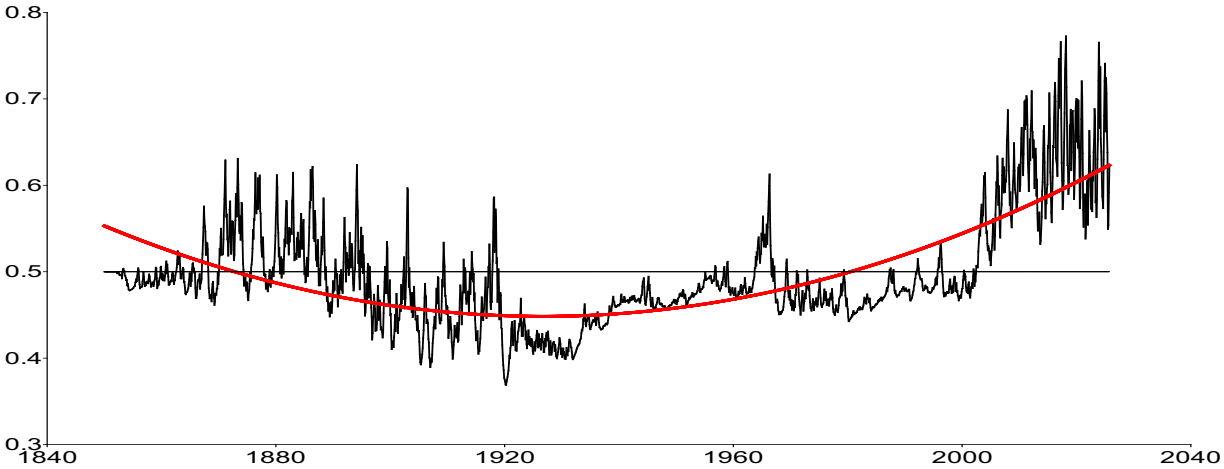

(b) Antarctic temperature anomalies, degree of fractional integration d_t for t-FI-QAR-Beta-t-EIGARCH

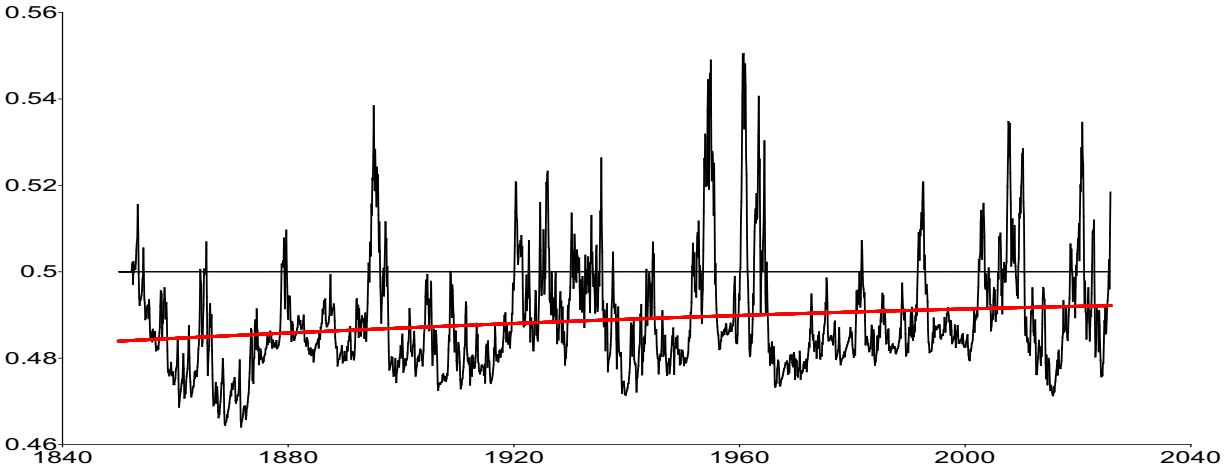

(c) Atlantic Ocean temperature anomalies, degree of fractional integration d_t for t-FI-QAR-Beta-t-EGARCH

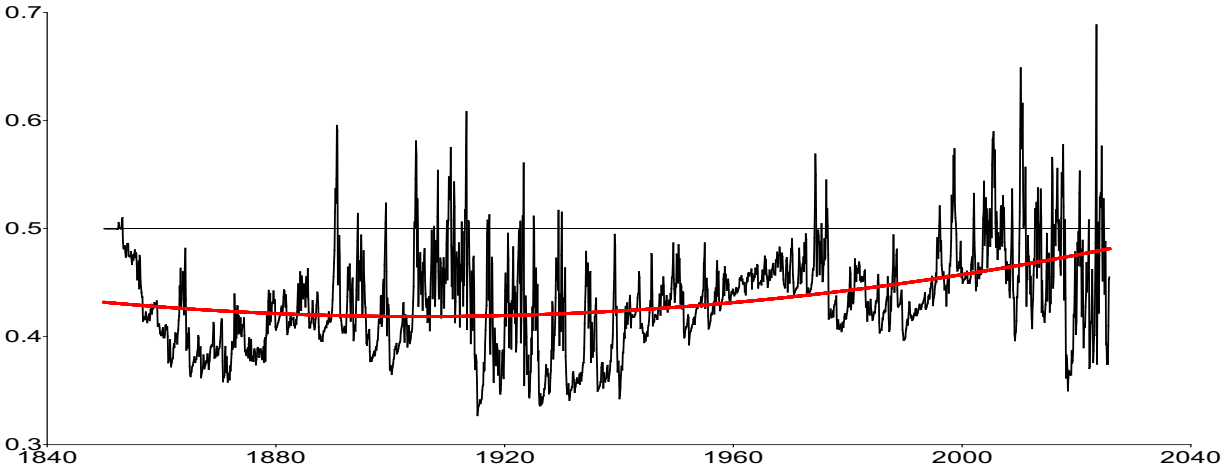

Figure 3. Degree of fractional integration of temperature anomalies d_t from January 1850 to October 2025 for the t-FI(d_t)-QAR(p)-Beta-t-EGARCH and t-FI(d_t)-QAR(p)-Beta-t-EIGARCH models. *Notes:* We present the degree of fractional integration of temperature anomalies d_t (black) and the fitted quadratic polynomial (red).

(a) Northeast Pacific Ocean temperature anomalies, degree of fractional integration d_t for t-FI-QAR-Beta-t-EGARCH

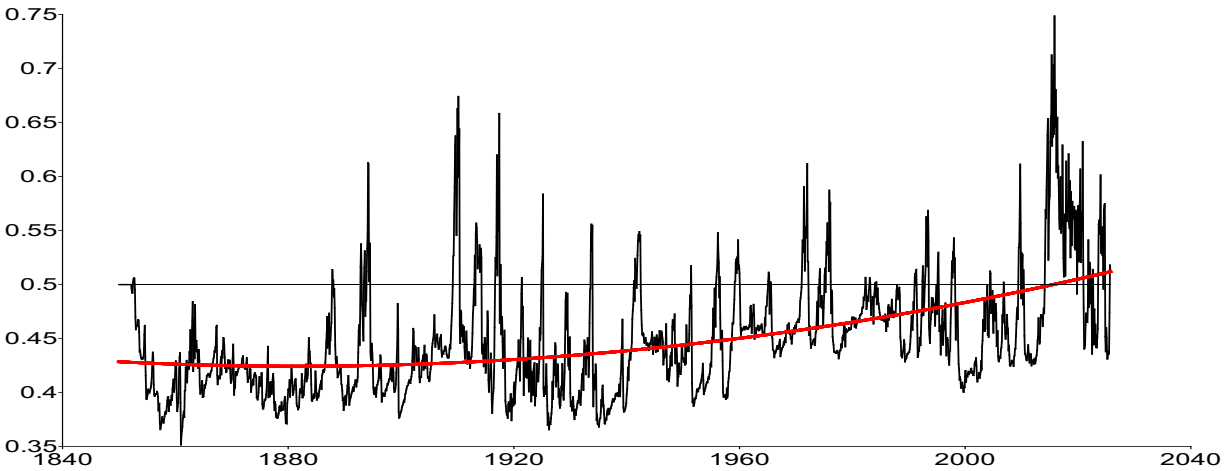

(b) Northern Hemisphere temperature anomalies, degree of fractional integration d_t for t-FI-QAR-Beta-t-EGARCH

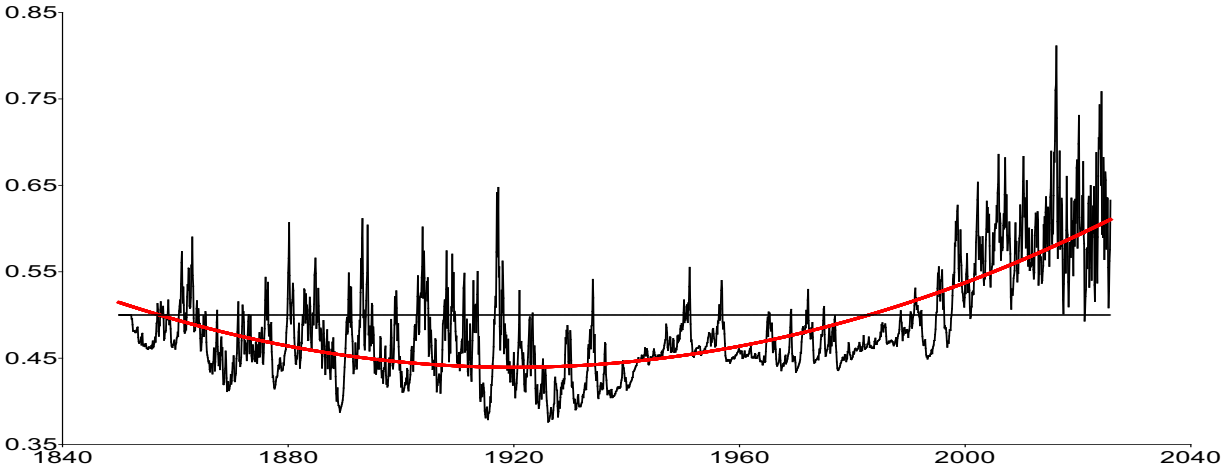

(c) Southern Hemisphere temperature anomalies, degree of fractional integration d_t for t-FI-QAR-Beta-t-EIGARCH

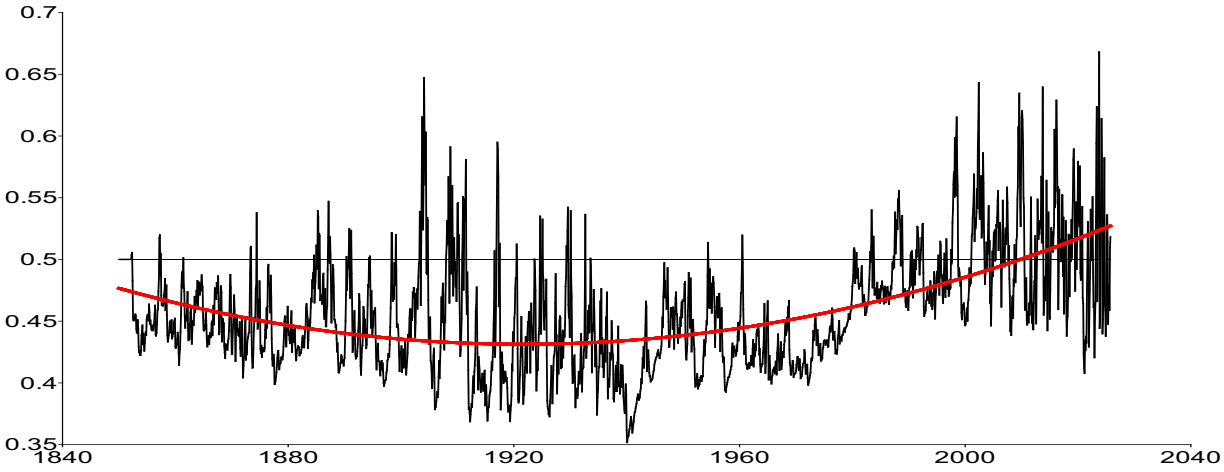

Figure 4. Degree of fractional integration of temperature anomalies d_t from January 1850 to October 2025 for the t-FI(d_t)-QAR(p)-Beta-t-EGARCH and t-FI(d_t)-QAR(p)-Beta-t-EIGARCH models.. *Notes:* We present the degree of fractional integration of temperature anomalies d_t (black) and the fitted quadratic polynomial (red).

(a) Arctic temperature anomalies, $u_{\mu,t}$ as a function of ϵ_t for t-FI-QAR-Beta-t-EGARCH

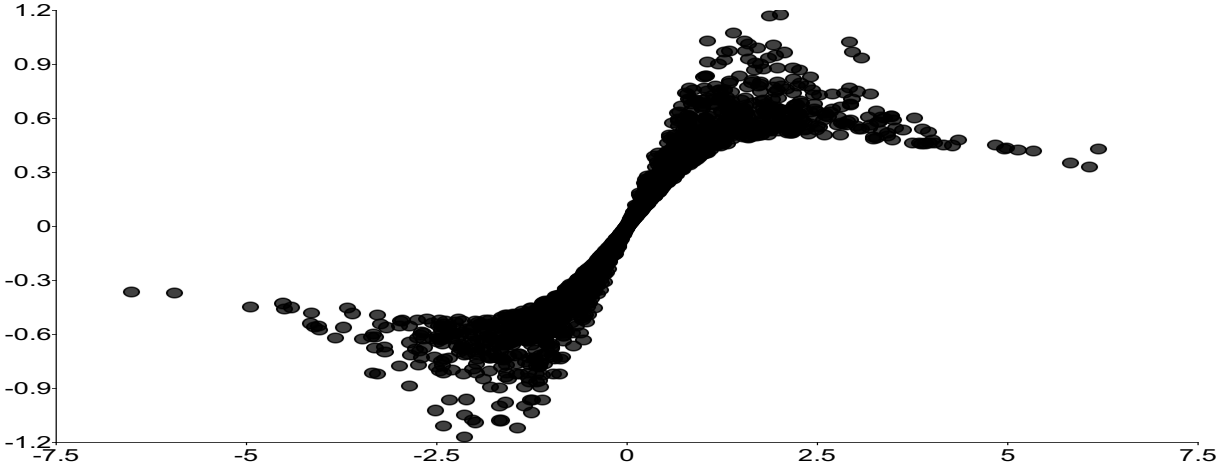

(b) Antarctic temperature anomalies, $u_{\mu,t}$ as a function of ϵ_t for t-FI-QAR-Beta-t-EIGARCH

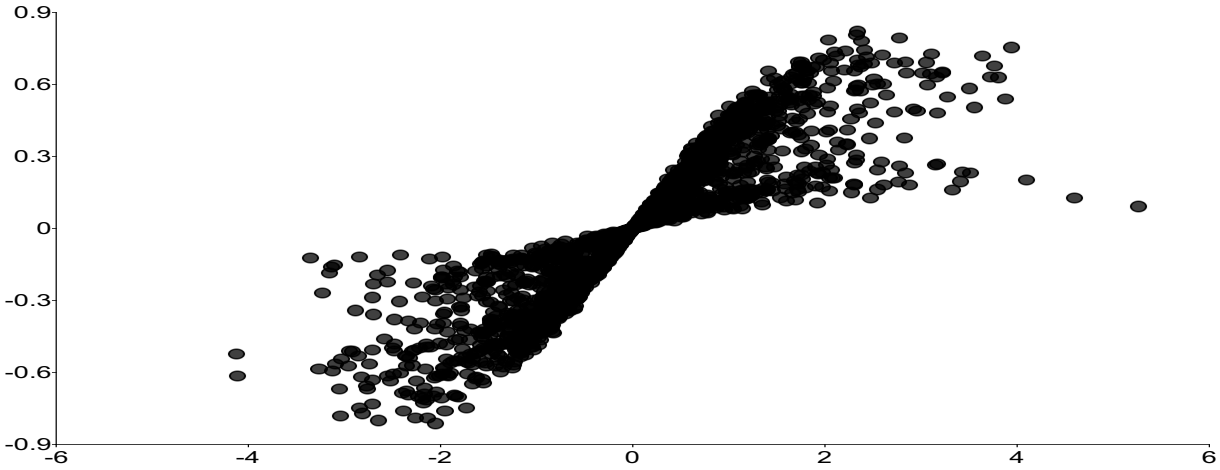

(c) Atlantic Ocean temperature anomalies, $u_{\mu,t}$ as a function of ϵ_t for t-FI-QAR-Beta-t-EGARCH

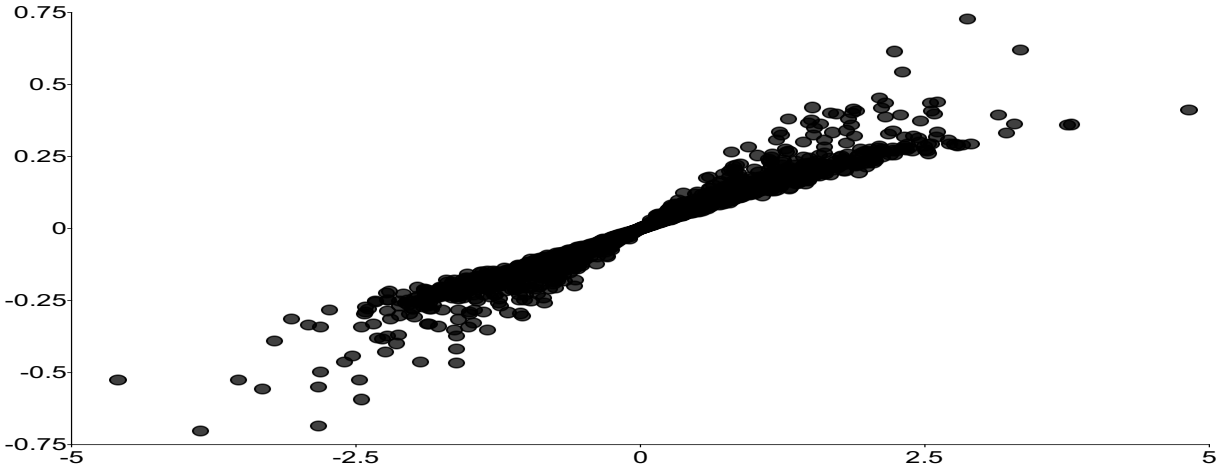

Figure 5. Impact of shocks on updating terms: $u_{\mu,t}$ as a function of ϵ_t from January 1850 to October 2025 for the t-FI(d_t)-QAR(p)-Beta-t-EGARCH and t-FI(d_t)-QAR(p)-Beta-t-EIGARCH models.

(a) Northeast Pacific Ocean temperature anomalies, $u_{\mu,t}$ as a function of ϵ_t for t-FI-QAR-Beta-t-EGARCH

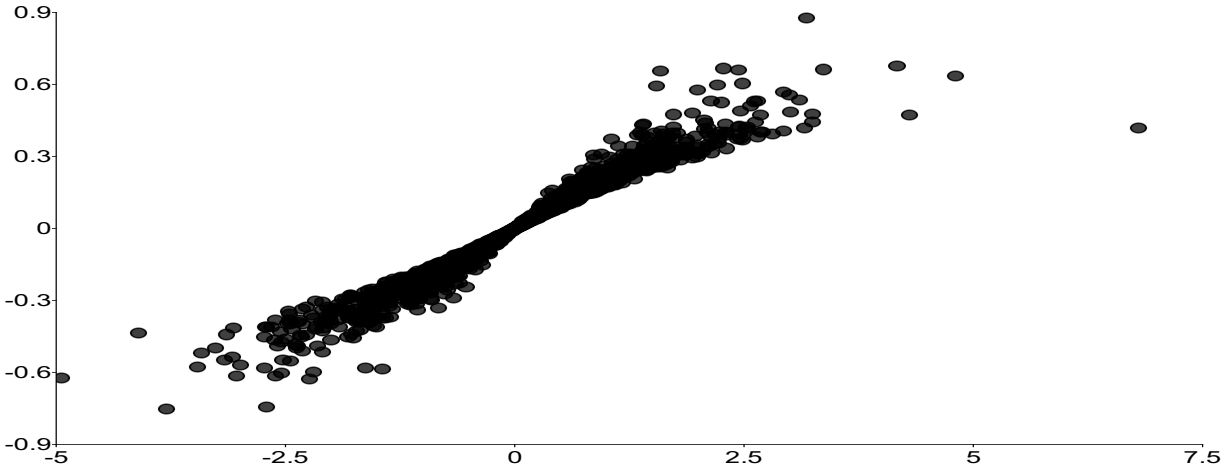

(b) Northern Hemisphere temperature anomalies, $u_{\mu,t}$ as a function of ϵ_t for t-FI-QAR-Beta-t-EGARCH

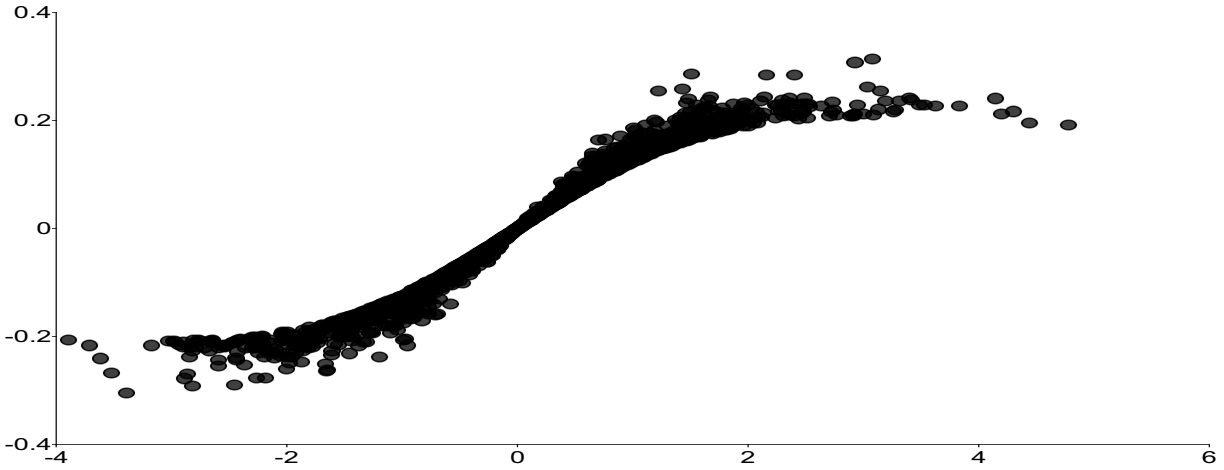

(c) Southern Hemisphere temperature anomalies, $u_{\mu,t}$ as a function of ϵ_t for t-FI-QAR-Beta-t-EIGARCH

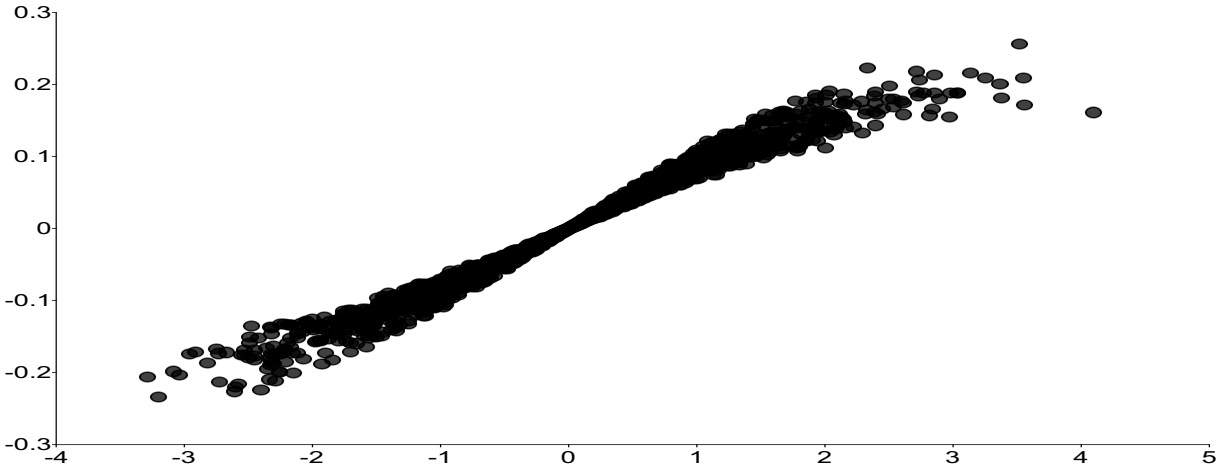

Figure 6. Impact of shocks on updating terms: $u_{\mu,t}$ as a function of ϵ_t from January 1850 to October 2025 for the t-FI(d_t)-QAR(p)-Beta-t-EGARCH and t-FI(d_t)-QAR(p)-Beta-t-EIGARCH models.

(a) Arctic temperature anomalies, $u_{d,t}$ as a function of ϵ_t for t-FI-QAR-Beta-t-EGARCH

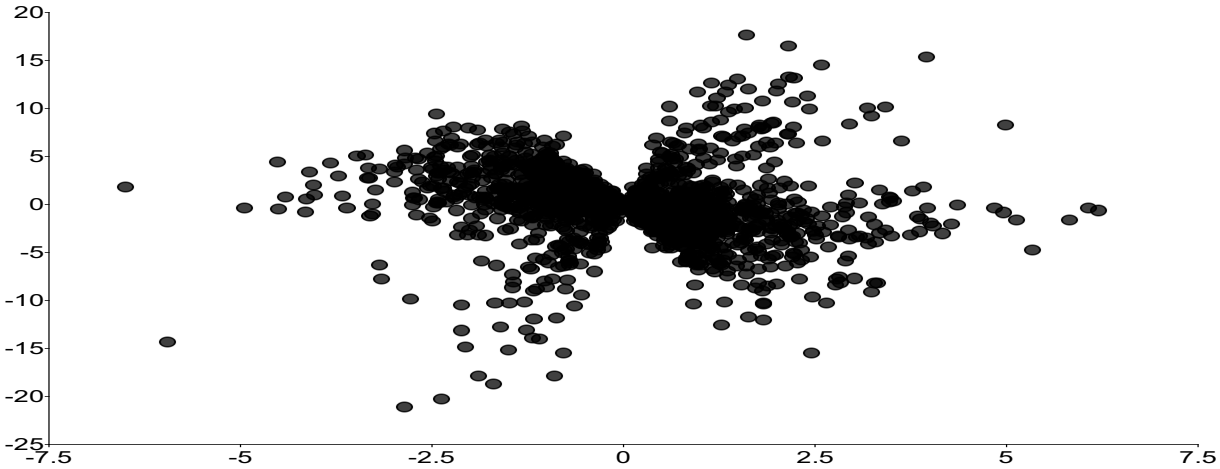

(b) Antarctic temperature anomalies, $u_{d,t}$ as a function of ϵ_t for t-FI-QAR-Beta-t-EIGARCH

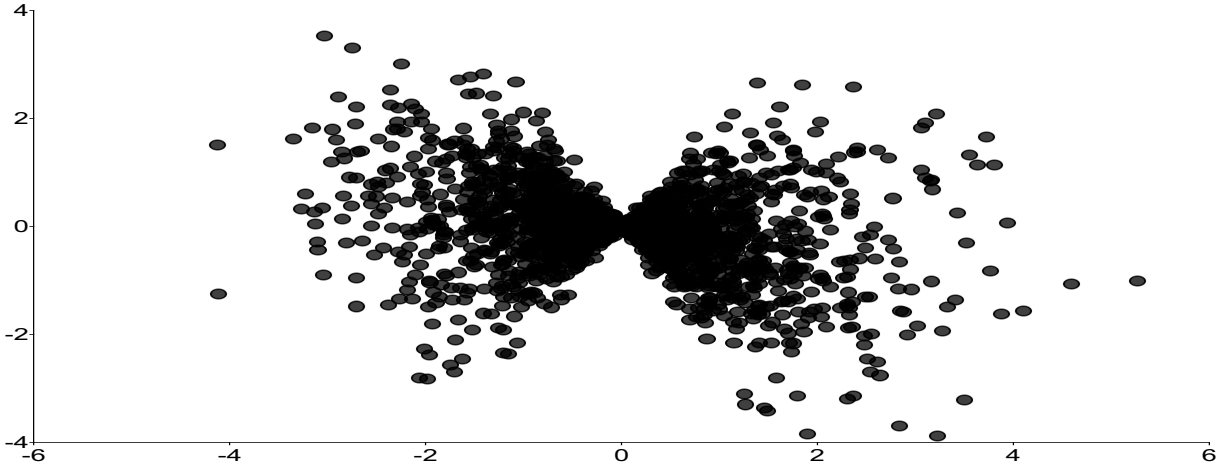

(c) Atlantic Ocean temperature anomalies, $u_{d,t}$ as a function of ϵ_t for t-FI-QAR-Beta-t-EGARCH

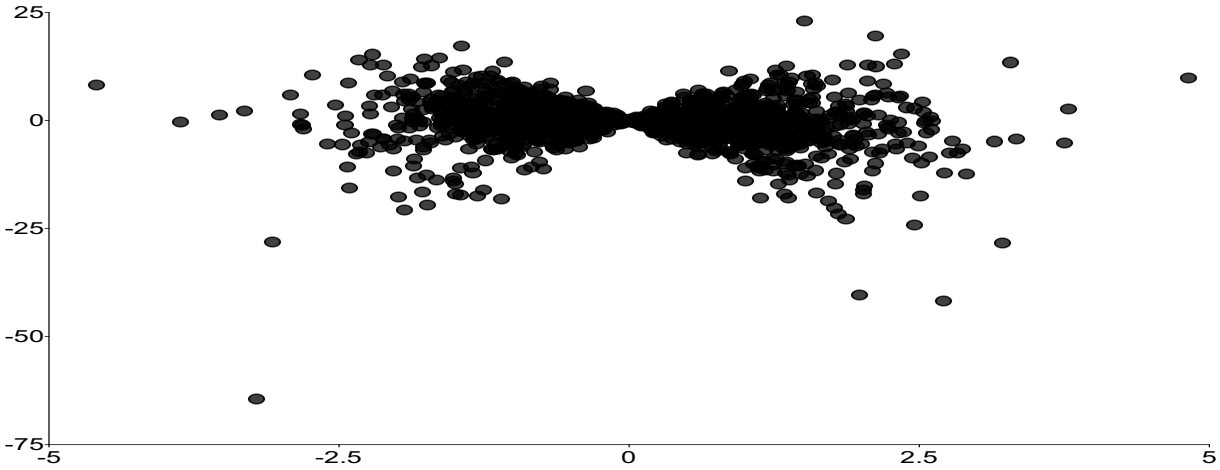

Figure 7. Impact of shocks on updating terms: $u_{d,t}$ as a function of ϵ_t from January 1850 to October 2025 for the t-FI(d_t)-QAR(p)-Beta-t-EGARCH and t-FI(d_t)-QAR(p)-Beta-t-EIGARCH models.

(a) Northeast Pacific Ocean temperature anomalies, $u_{d,t}$ as a function of ϵ_t for t-FI-QAR-Beta-t-EGARCH

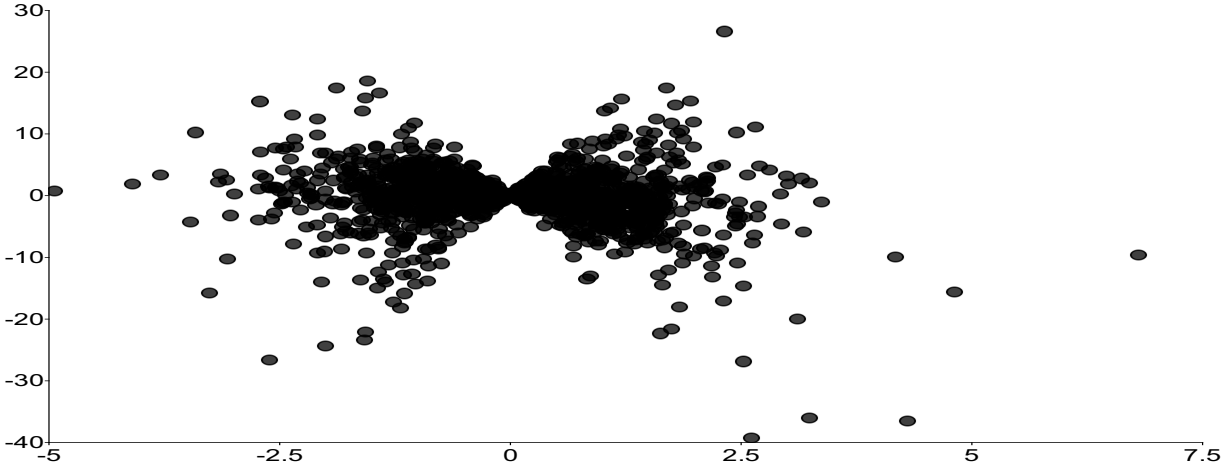

(b) Northern Hemisphere temperature anomalies, $u_{d,t}$ as a function of ϵ_t for t-FI-QAR-Beta-t-EGARCH

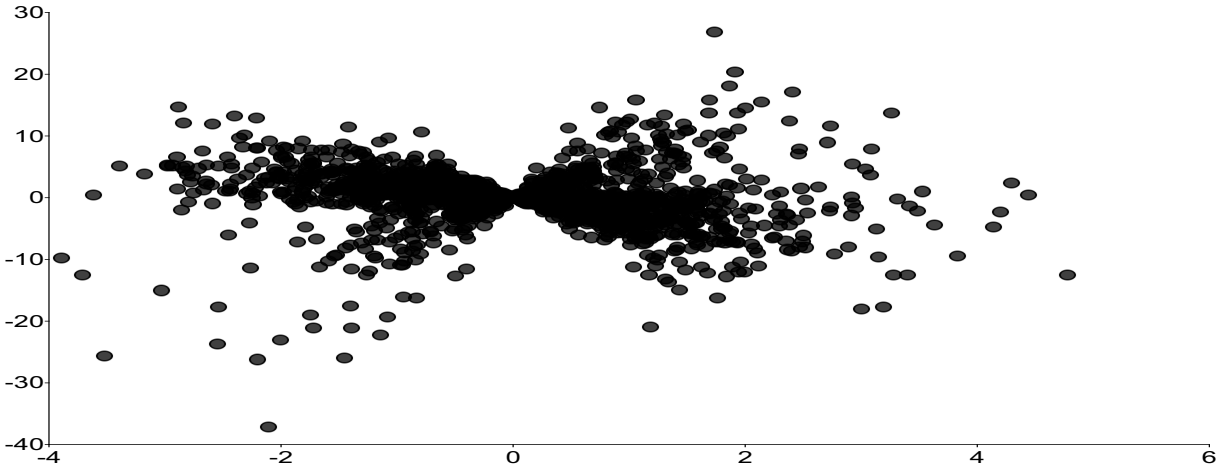

(c) Southern Hemisphere temperature anomalies, $u_{d,t}$ as a function of ϵ_t for t-FI-QAR-Beta-t-EIGARCH

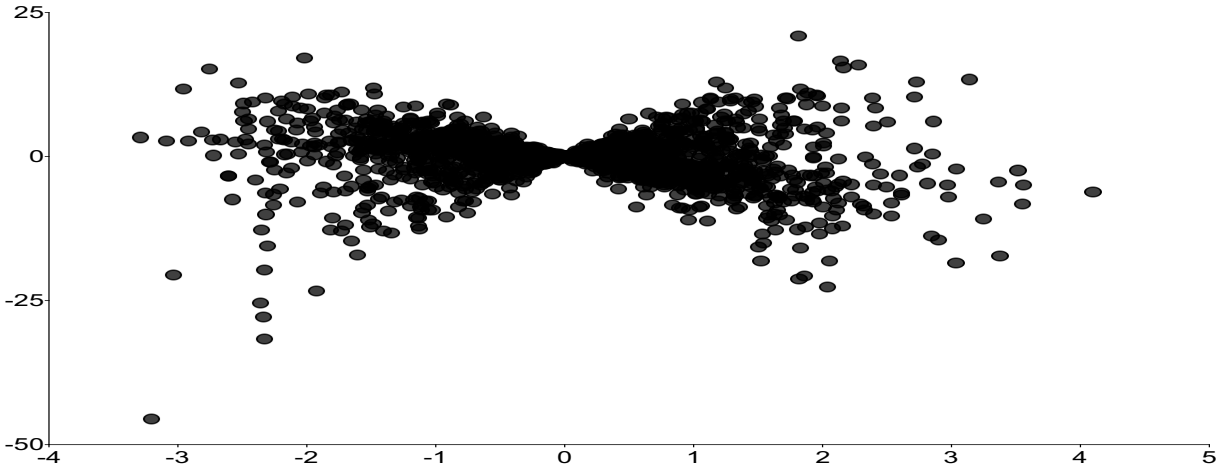

Figure 8. Impact of shocks on updating terms: $u_{d,t}$ as a function of ϵ_t from January 1850 to October 2025 for the t-FI(d_t)-QAR(p)-Beta-t-EGARCH and t-FI(d_t)-QAR(p)-Beta-t-EIGARCH models.

(a) Arctic temperature anomalies, $u_{\lambda,t}$ as a function of ϵ_t for t-FI-QAR-Beta-t-EGARCH

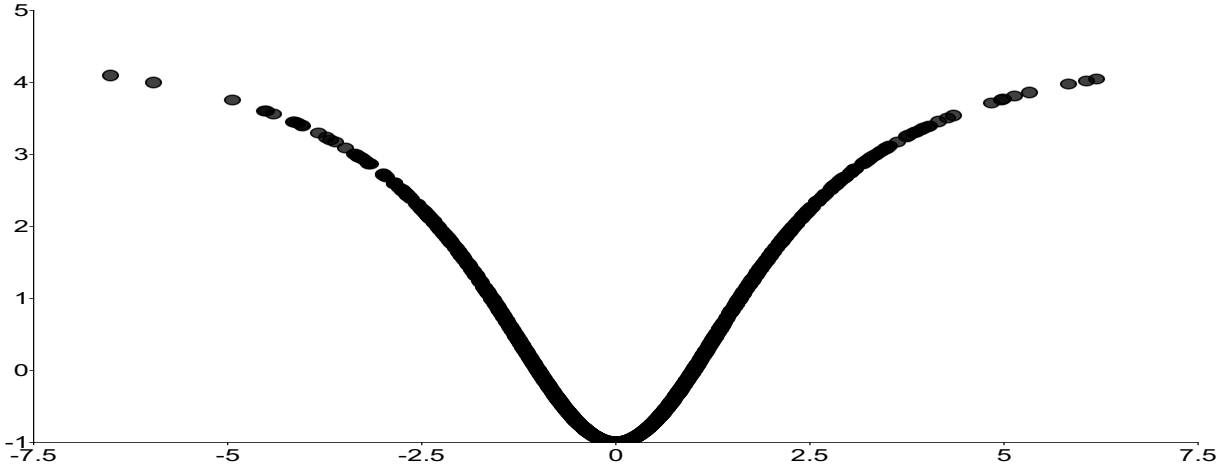

(b) Antarctic temperature anomalies, $u_{\lambda,t}$ as a function of ϵ_t for t-FI-QAR-Beta-t-EIGARCH

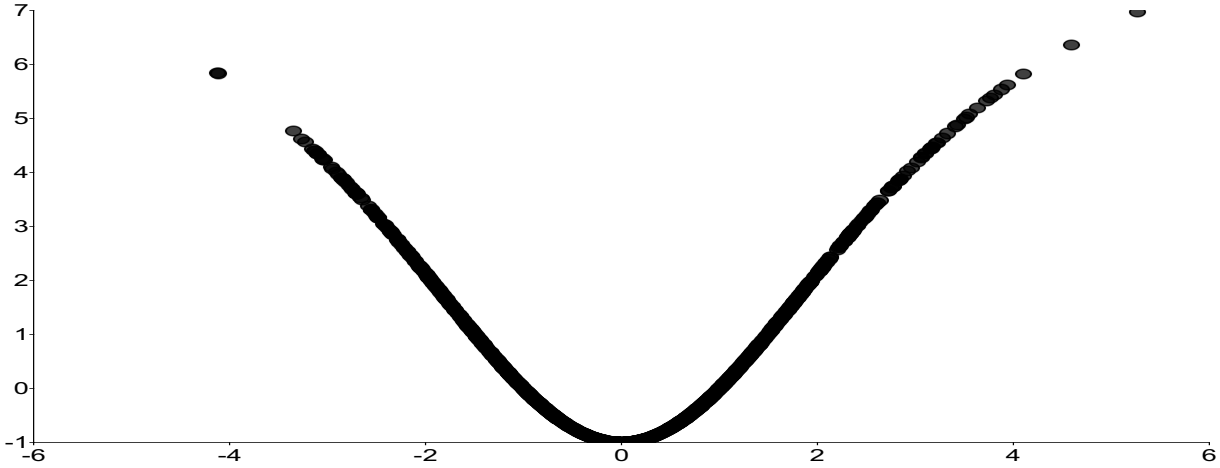

(c) Atlantic Ocean temperature anomalies, $u_{\lambda,t}$ as a function of ϵ_t for t-FI-QAR-Beta-t-EGARCH

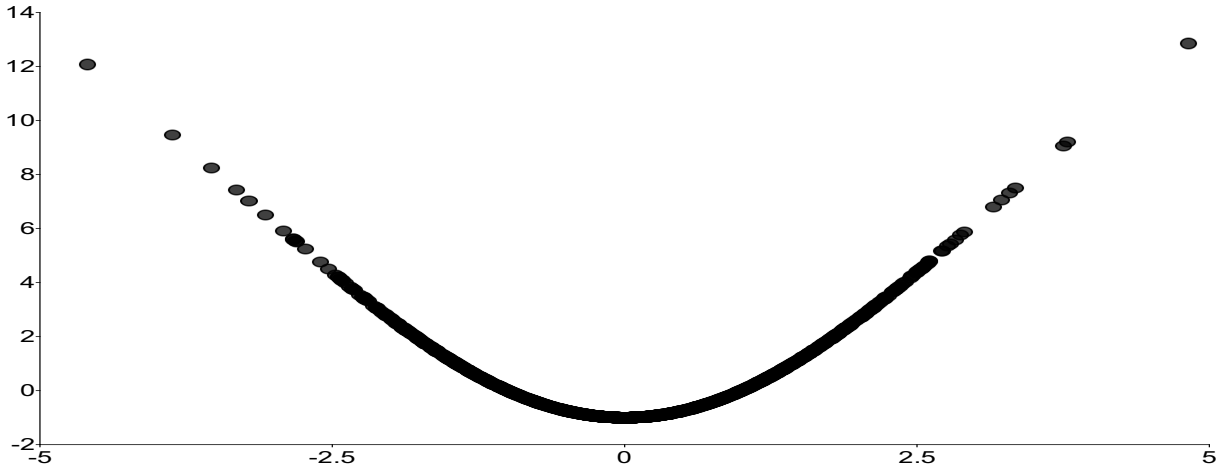

Figure 9. Impact of shocks on updating terms: $u_{\lambda,t}$ as a function of ϵ_t from January 1850 to October 2025 for the t-FI(d_t)-QAR(p)-Beta-t-EGARCH and t-FI(d_t)-QAR(p)-Beta-t-EIGARCH models.

(a) Northeast Pacific Ocean temperature anomalies, $u_{\lambda,t}$ as a function of ϵ_t for t-FI-QAR-Beta-t-EGARCH

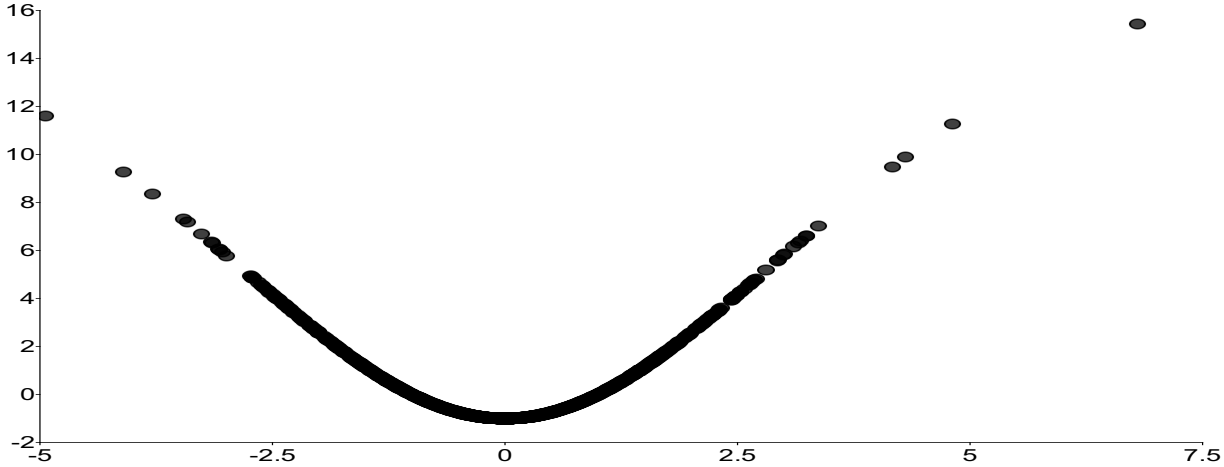

(b) Northern Hemisphere temperature anomalies, $u_{\lambda,t}$ as a function of ϵ_t for t-FI-QAR-Beta-t-EGARCH

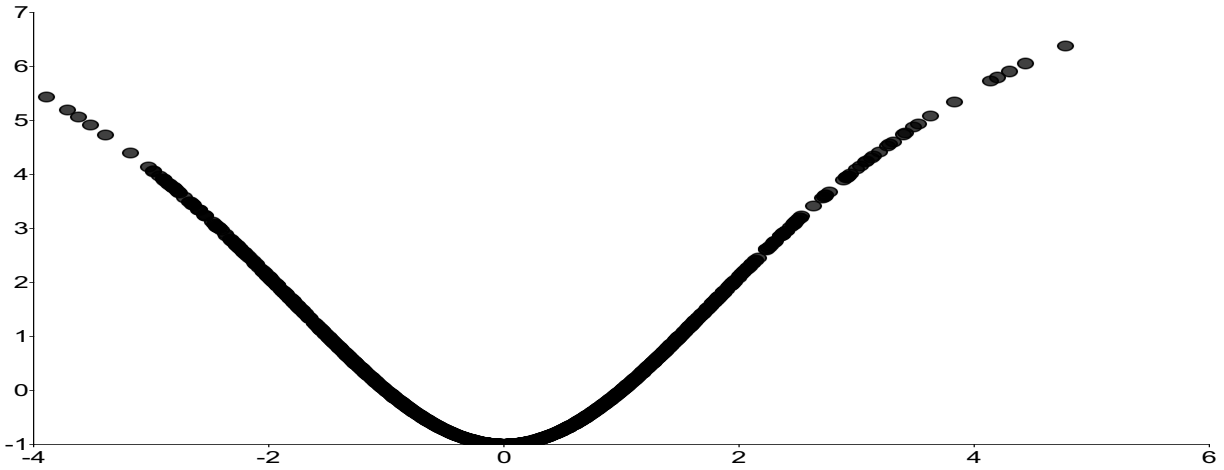

(c) Southern Hemisphere temperature anomalies, $u_{\lambda,t}$ as a function of ϵ_t for t-FI-QAR-Beta-t-EIGARCH

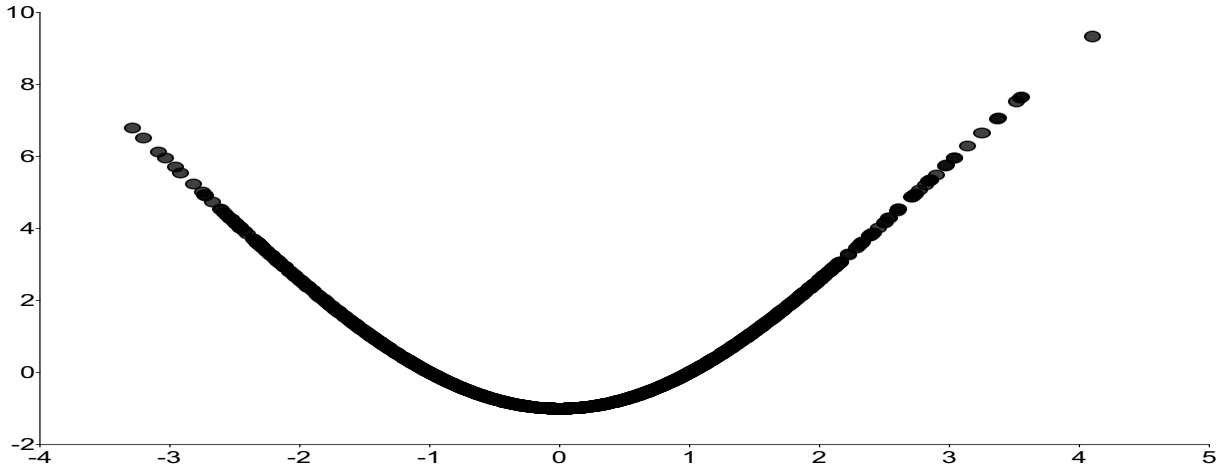

Figure 10. Impact of shocks on updating terms: $u_{\lambda,t}$ as a function of ϵ_t from January 1850 to October 2025 for the t-FI(d_t)-QAR(p)-Beta-t-EGARCH and t-FI(d_t)-QAR(p)-Beta-t-EIGARCH models.

(a) Arctic temperature anomalies, conditional standard deviation σ_t for t-FI-QAR-Beta-t-EGARCH

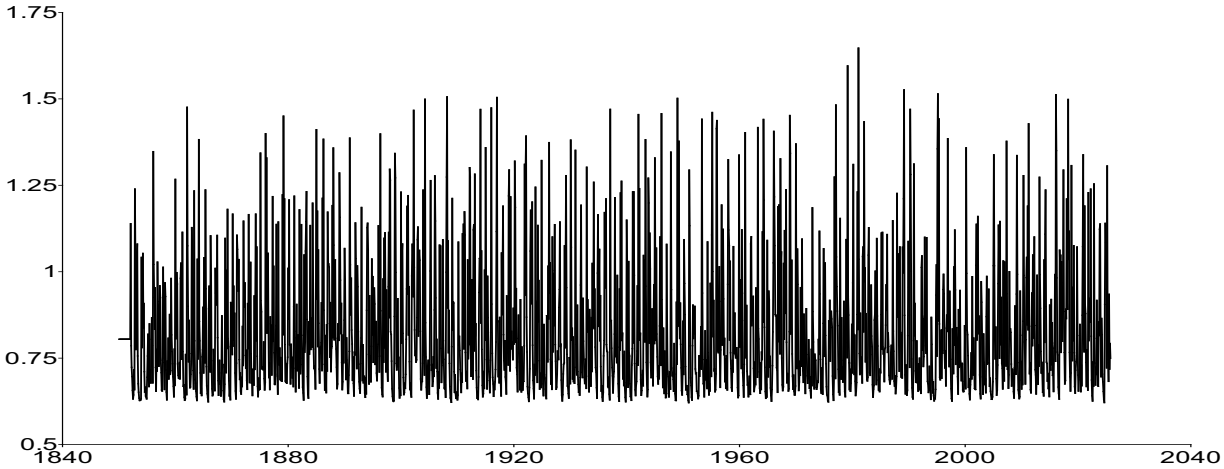

(b) Antarctic temperature anomalies, conditional standard deviation σ_t for t-FI-QAR-Beta-t-EIGARCH

(c) Atlantic Ocean temperature anomalies, conditional standard deviation σ_t for t-FI-QAR-Beta-t-EGARCH

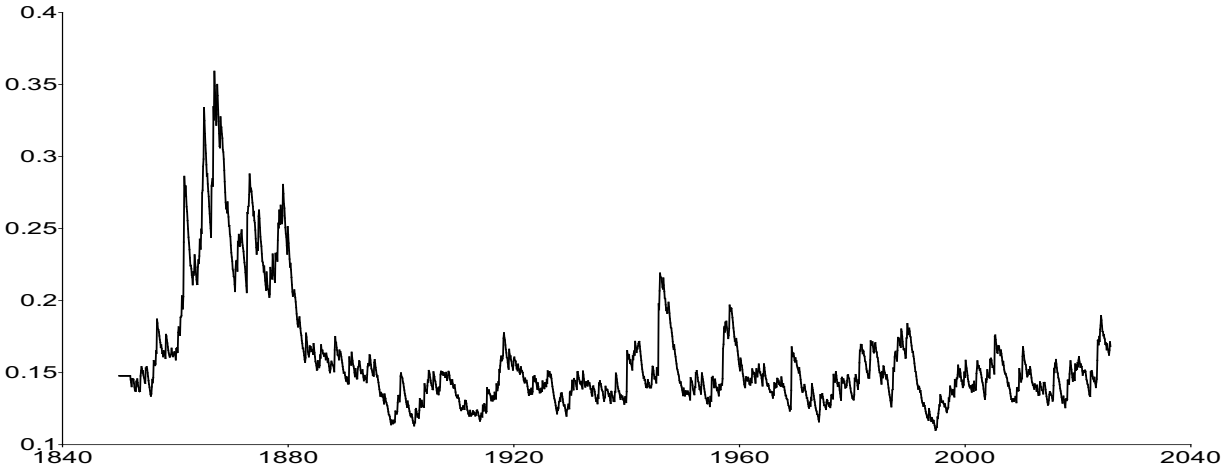

Figure 11. Conditional standard deviation σ_t from January 1850 to October 2025 for the t-FI(d_t)-QAR(p)-Beta-t-EGARCH and t-FI(d_t)-QAR(p)-Beta-t-EIGARCH models.

(a) Northeast Pacific Ocean temperature anomalies, conditional standard deviation σ_t for t-FI-QAR-Beta-t-EGARCH

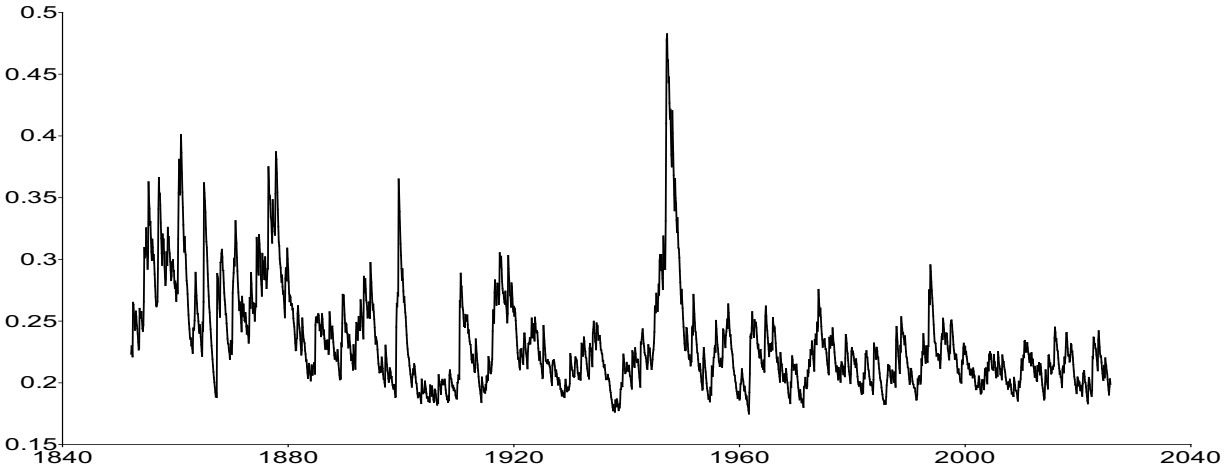

(b) Northern Hemisphere temperature anomalies, conditional standard deviation σ_t for t-FI-QAR-Beta-t-EGARCH

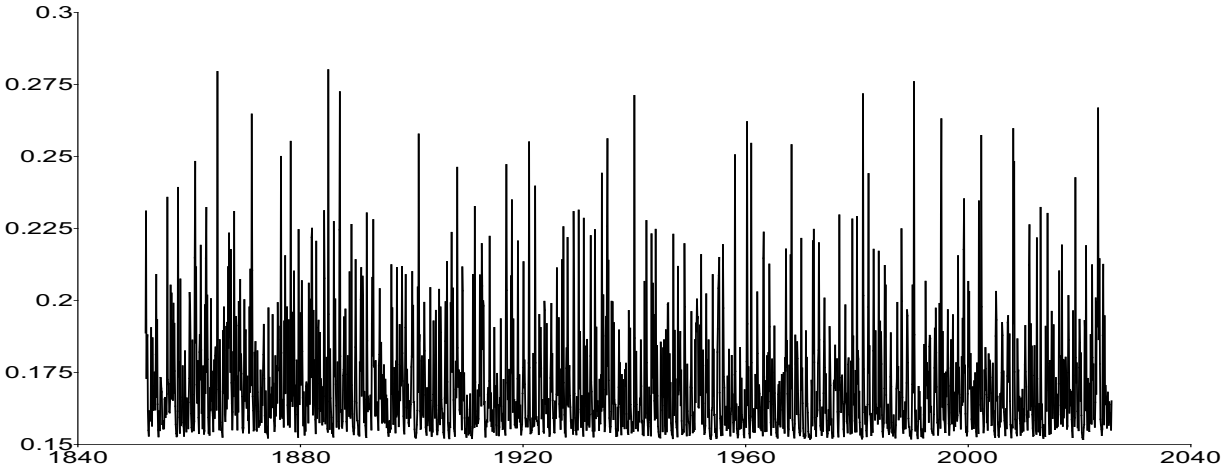

(c) Southern Hemisphere temperature anomalies, conditional standard deviation σ_t for t-FI-QAR-Beta-t-EIGARCH

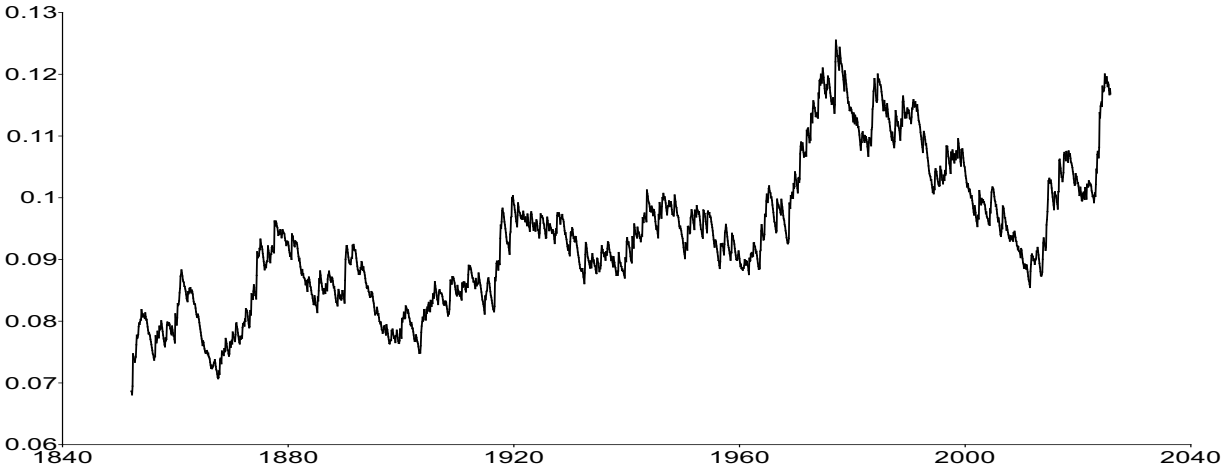

Figure 12. Conditional standard deviation σ_t from January 1850 to October 2025 for the t-FI(d_t)-QAR(p)-Beta-t-EGARCH and t-FI(d_t)-QAR(p)-Beta-t-EIGARCH models.

Supplementary Material

Score-driven long memory dynamics of worldwide regional temperature anomalies

Szabolcs Blazsek[1,*], **Raven Amina Dupree**[1], **and Luis Alberiko Gil-Alana**[2]

[1]Stetson-Hatcher School of Business, Mercer University, Macon, United States

[2]School of Economics and Business, Universidad de Navarra, Pamplona, Spain

Abstract: We develop a score-driven fractionally integrated quasi-autoregressive model with Student's t innovations (t-FI-QAR), in which the degree of fractional integration d_t, the conditional mean, and the conditional scale evolve via likelihood-based updates. Using monthly U.S. National Oceanic and Atmospheric Administration (NOAA) land-and-ocean temperature anomalies for six regions (Arctic, Antarctic, Atlantic Ocean, Northeast Pacific Ocean, Northern and Southern Hemispheres) from January 1850 to October 2025, we show that d_t rises over time across all regions, implying increasingly persistent temperature dynamics. The increase is strongest in the Arctic and Northern Hemisphere, where we detect a structural shift over the past three decades consistent with a move toward non-stationary behavior. Significant but more moderate increases occur in the Atlantic, Northeast Pacific, and Southern Hemisphere, while the Antarctic exhibits a slight upward trend. Models that allow heavy tails and time-varying scale outperform homoscedastic specifications in likelihood-based criteria and diagnostics. The findings indicate that climate shocks now propagate more durably than in earlier periods, suggesting that stronger and more sustained mitigation and adaptation policies are needed to counter long-lived deviations in regional temperatures.

Keywords: Long memory processes; fractional degree of integration parameter; dynamic conditional score (DCS) models; generalized autoregressive score (GAS) models; climate change; global warming.

JEL classification codes: C22; C51; C52; Q54

[*]Correspondence to: Szabolcs Blazsek. Stetson-Hatcher Shcool of Business, Mercer University, 1501 Mercer University Drive, Macon, GA 31207, United States. E-mail: blazsek_s@mercer.edu

Supplementary Material A

(a) Arctic temperature anomalies, $u_{\mu,t}$ as a function of ϵ_t for t-FI-QAR

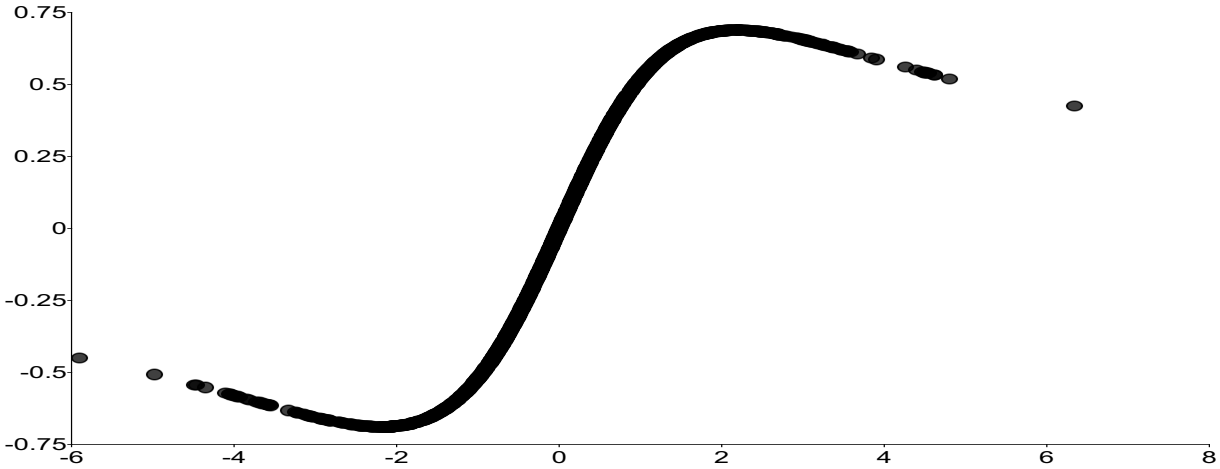

(b) Antarctic temperature anomalies, $u_{\mu,t}$ as a function of ϵ_t for t-FI-QAR

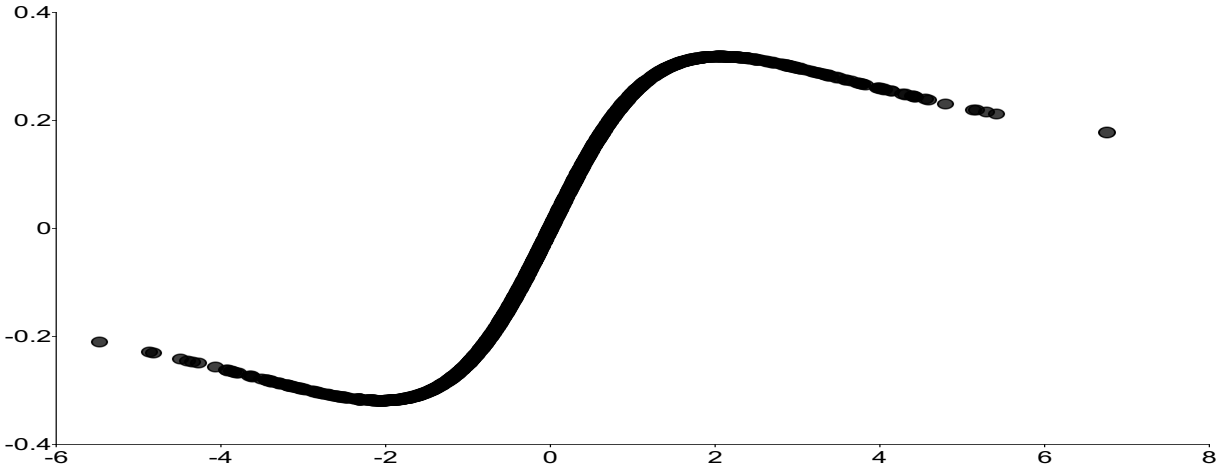

(c) Atlantic Ocean temperature anomalies, $u_{\mu,t}$ as a function of ϵ_t for t-FI-QAR

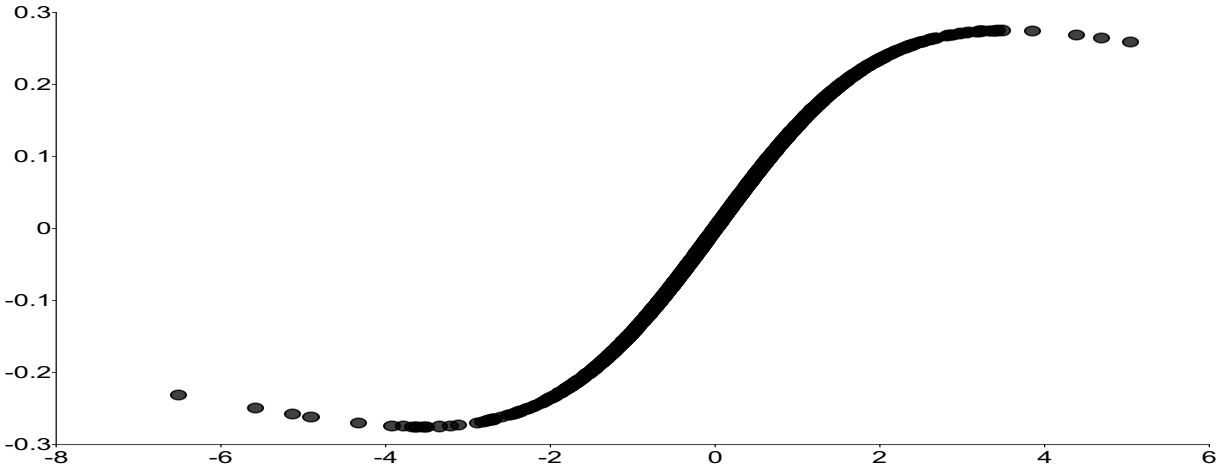

Figure A1. Impact of shocks on updating terms: $u_{\mu,t}$ as a function of ϵ_t from January 1850 to October 2025 for the t-FI(d_t)-QAR(p) model.

(a) Northeast Pacific Ocean temperature anomalies, $u_{\mu,t}$ as a function of ϵ_t for t-FI-QAR

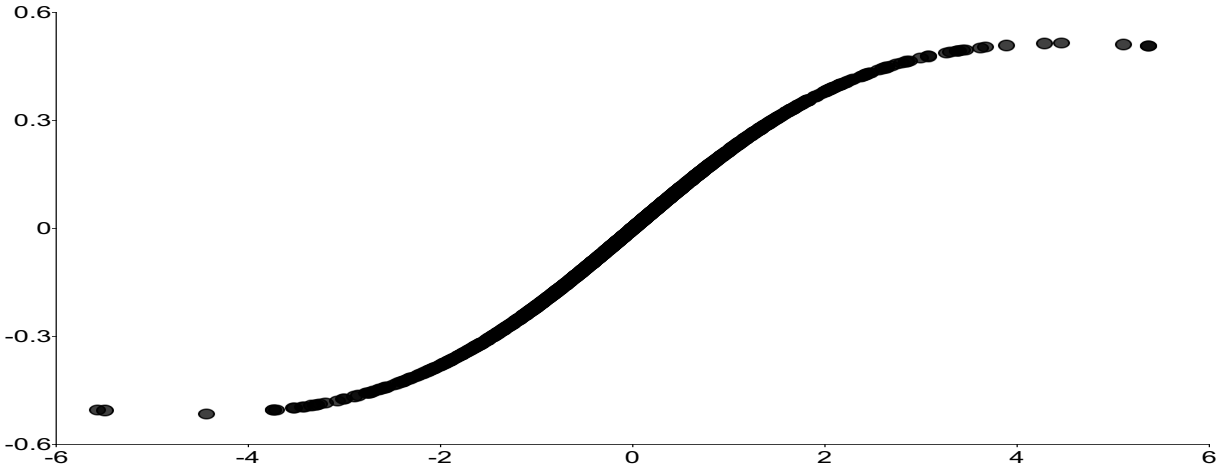

(b) Northern Hemisphere temperature anomalies, $u_{\mu,t}$ as a function of ϵ_t for t-FI-QAR

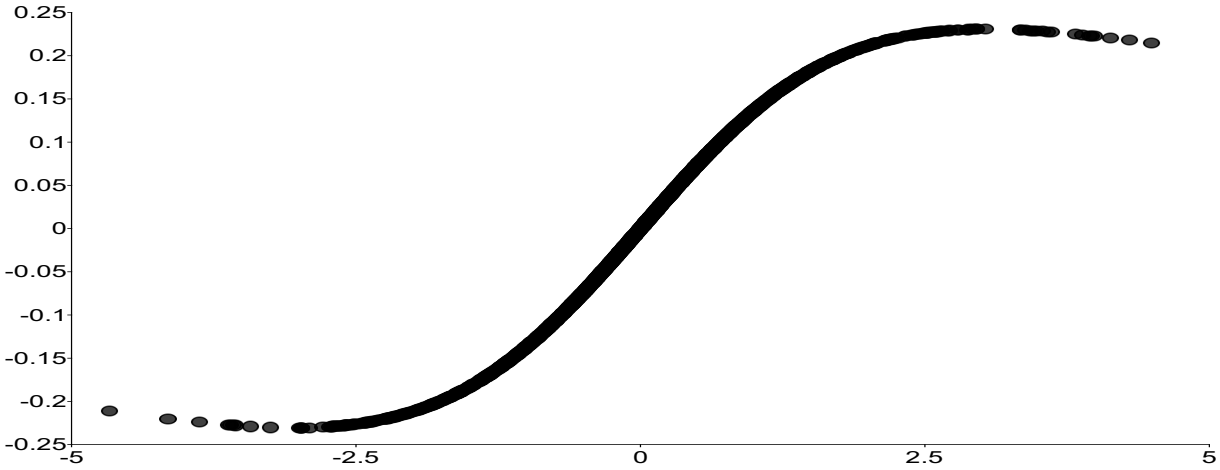

(c) Southern Hemisphere temperature anomalies, $u_{\mu,t}$ as a function of ϵ_t for t-FI-QAR

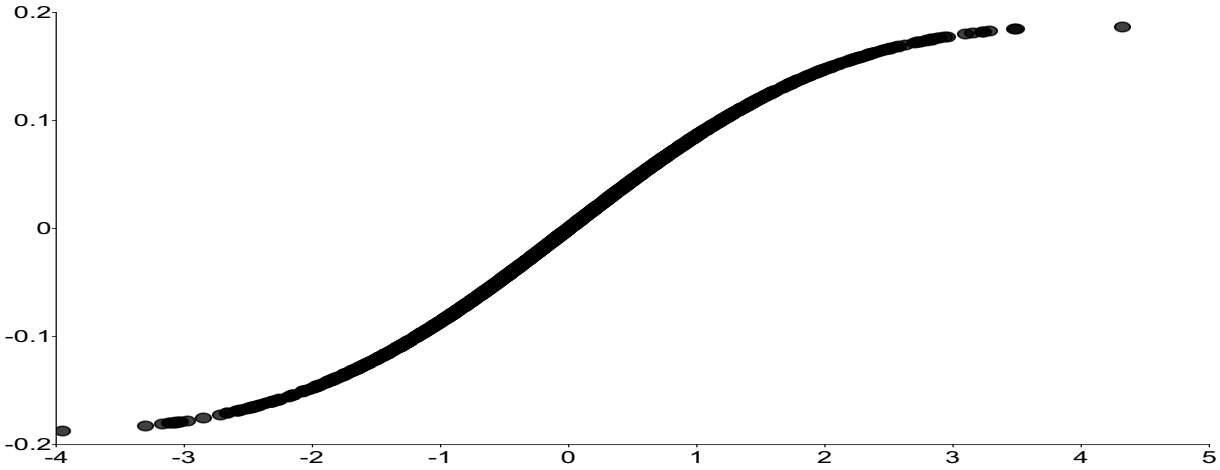

Figure A2. Impact of shocks on updating terms: $u_{\mu,t}$ as a function of ϵ_t from January 1850 to October 2025 for the t-FI(d_t)-QAR(p) model.

(a) Arctic temperature anomalies, $u_{d,t}$ as a function of ϵ_t for t-FI-QAR

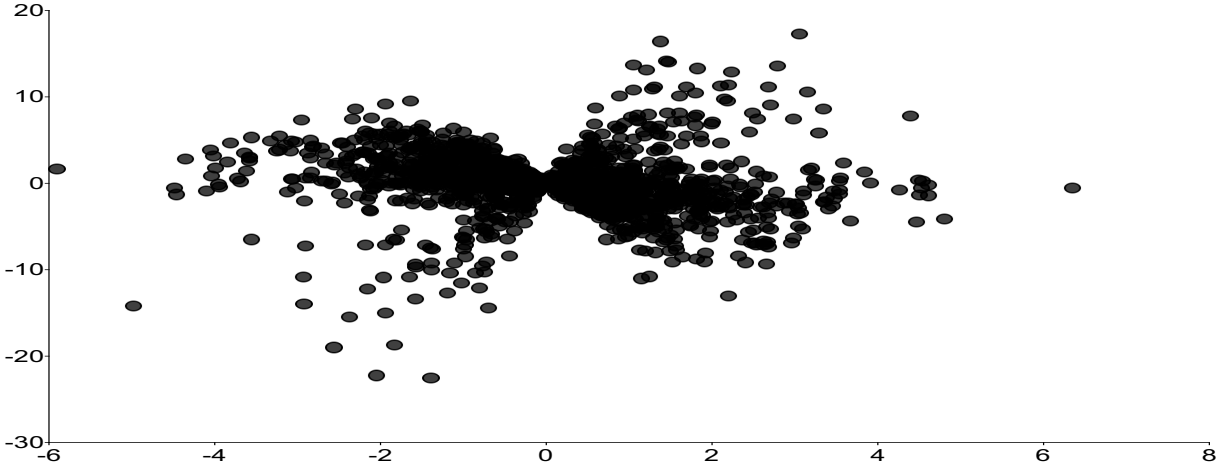

(b) Antarctic temperature anomalies, $u_{d,t}$ as a function of ϵ_t for t-FI-QAR

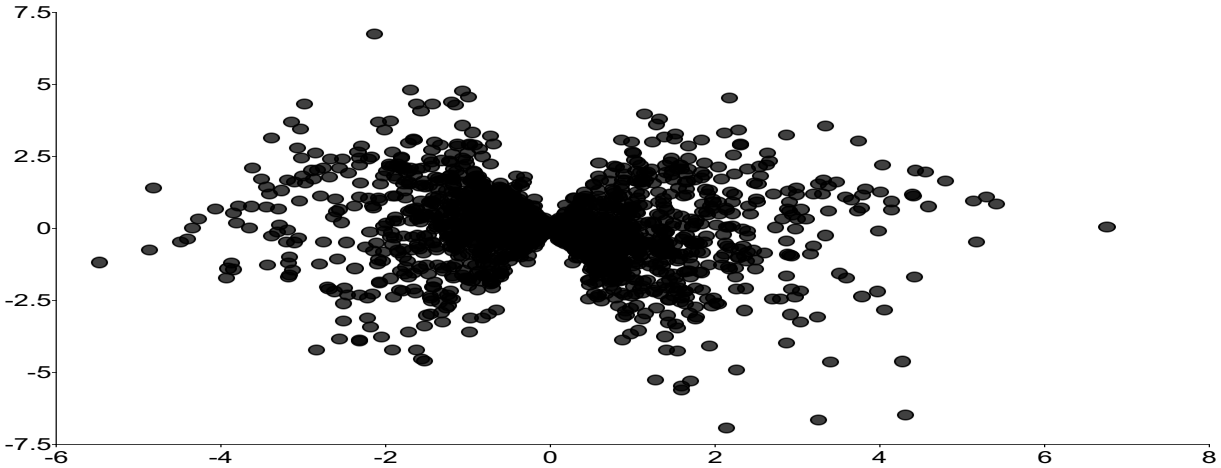

(c) Atlantic Ocean temperature anomalies, $u_{d,t}$ as a function of ϵ_t for t-FI-QAR

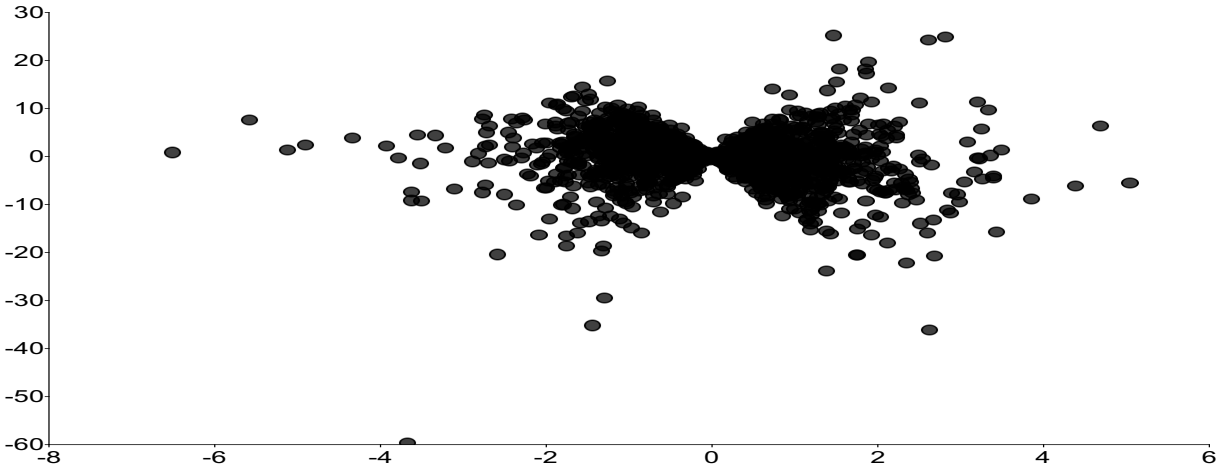

Figure A3. Impact of shocks on updating terms: $u_{d,t}$ as a function of ϵ_t from January 1850 to October 2025 for the t-FI(d_t)-QAR(p) model.

(a) Northeast Pacific Ocean temperature anomalies, $u_{d,t}$ as a function of ϵ_t for t-FI-QAR

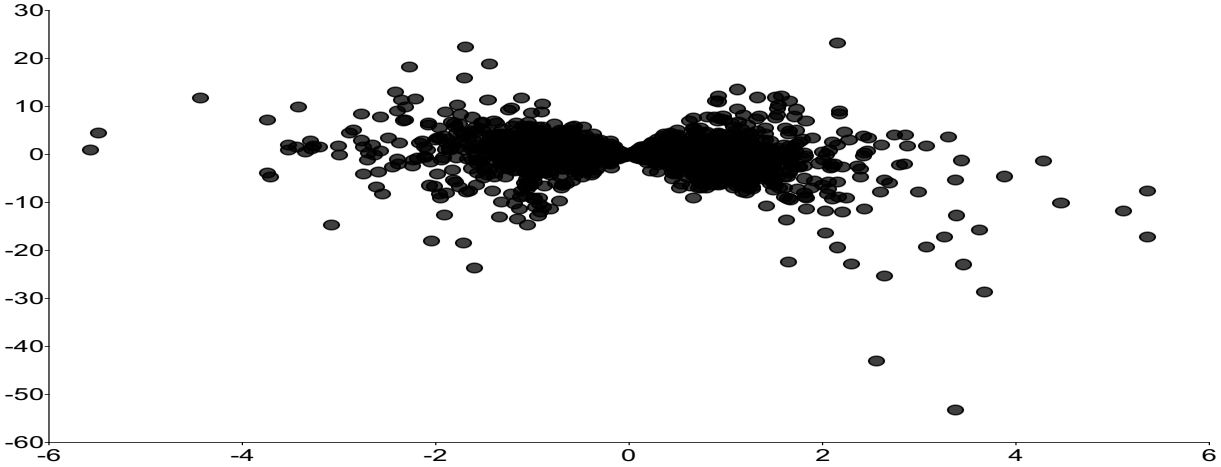

(b) Northern Hemisphere temperature anomalies, $u_{d,t}$ as a function of ϵ_t for t-FI-QAR

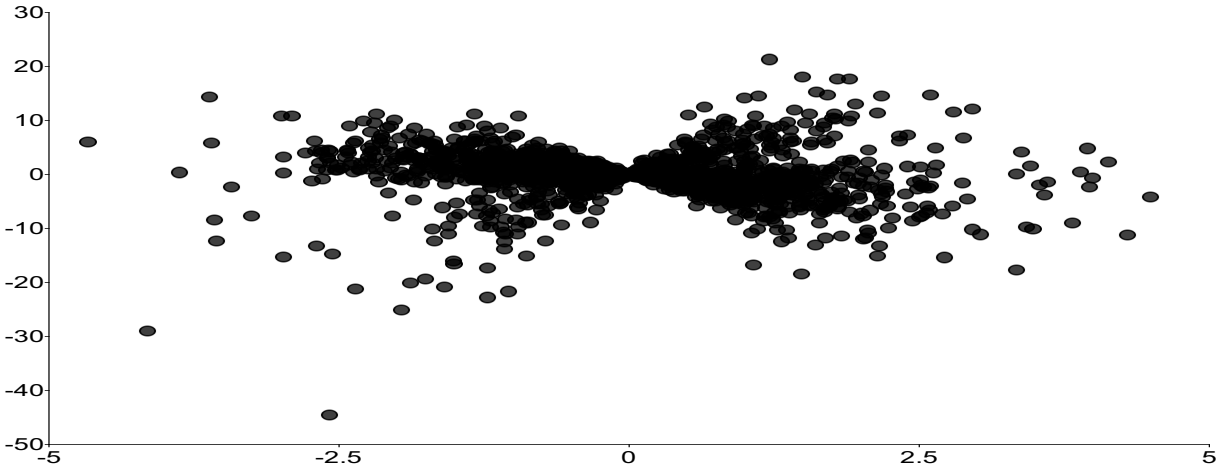

(c) Southern Hemisphere temperature anomalies, $u_{d,t}$ as a function of ϵ_t for t-FI-QAR

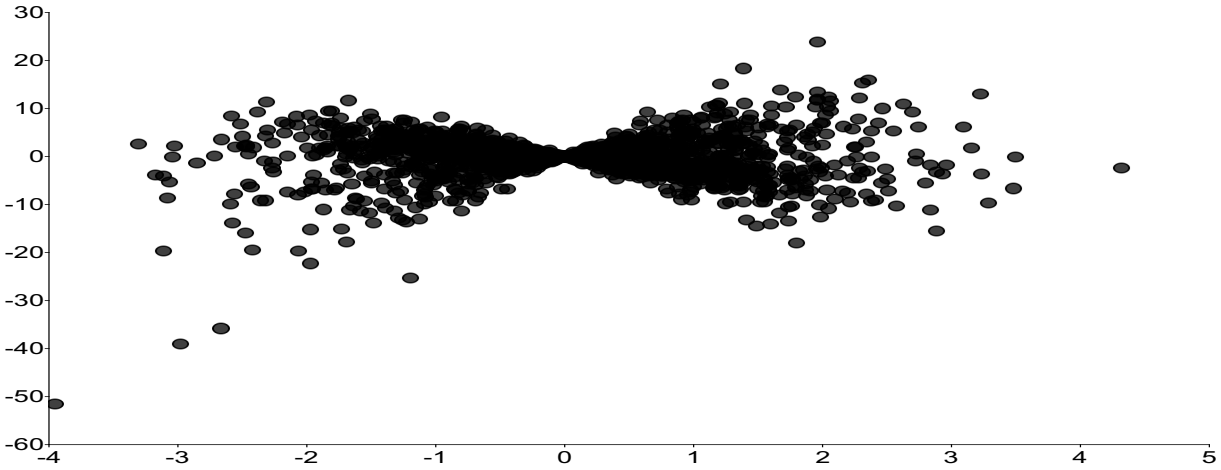

Figure A4. Impact of shocks on updating terms: $u_{d,t}$ as a function of ϵ_t from January 1850 to October 2025 for the t-FI(d_t)-QAR(p) model.

(a) Arctic temperature anomalies, y_t and μ_t for t-FI-QAR

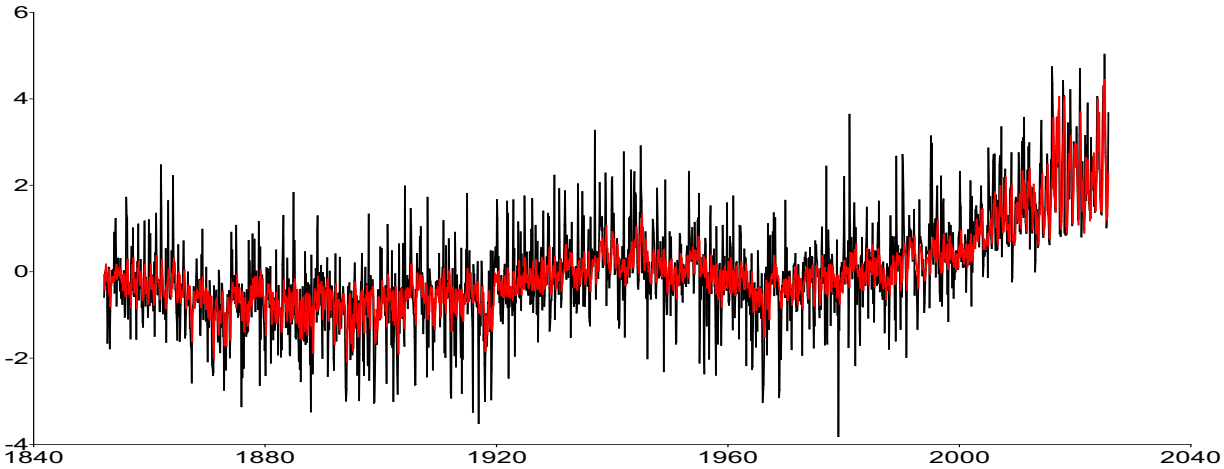

(b) Antarctic temperature anomalies, y_t and μ_t for t-FI-QAR

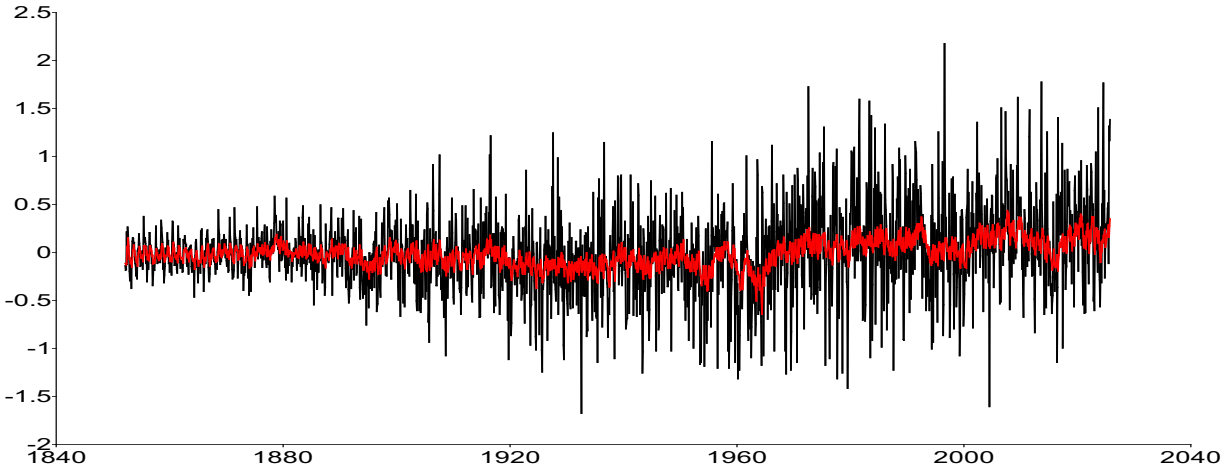

(c) Atlantic Ocean temperature anomalies, y_t and μ_t for t-FI-QAR

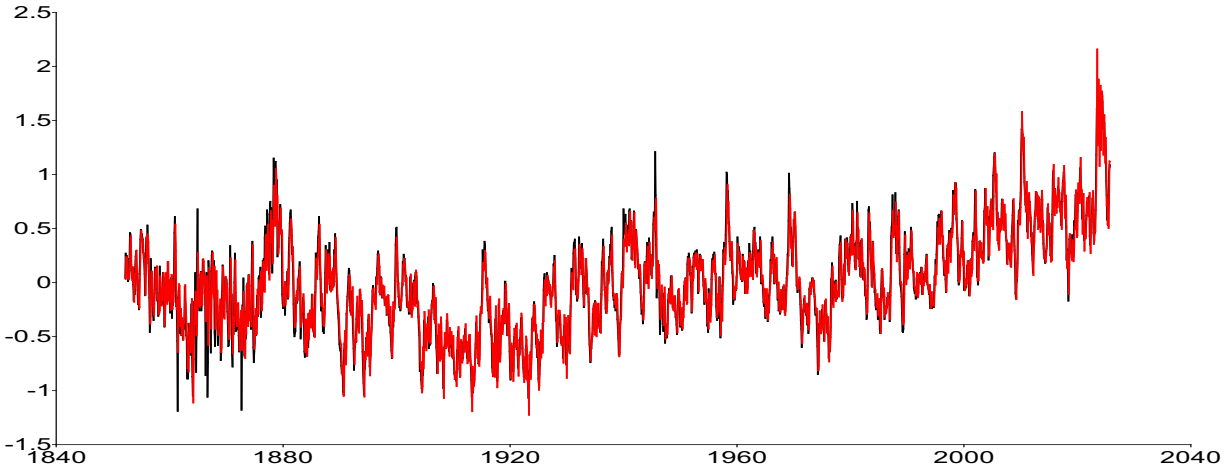

Figure A5. Evolution of y_t (black) and μ_t (red) from January 1850 to October 2025 for the t-FI(d_t)-QAR(p) model.

(a) Northeast Pacific Ocean temperature anomalies, y_t and μ_t for t-FI-QAR

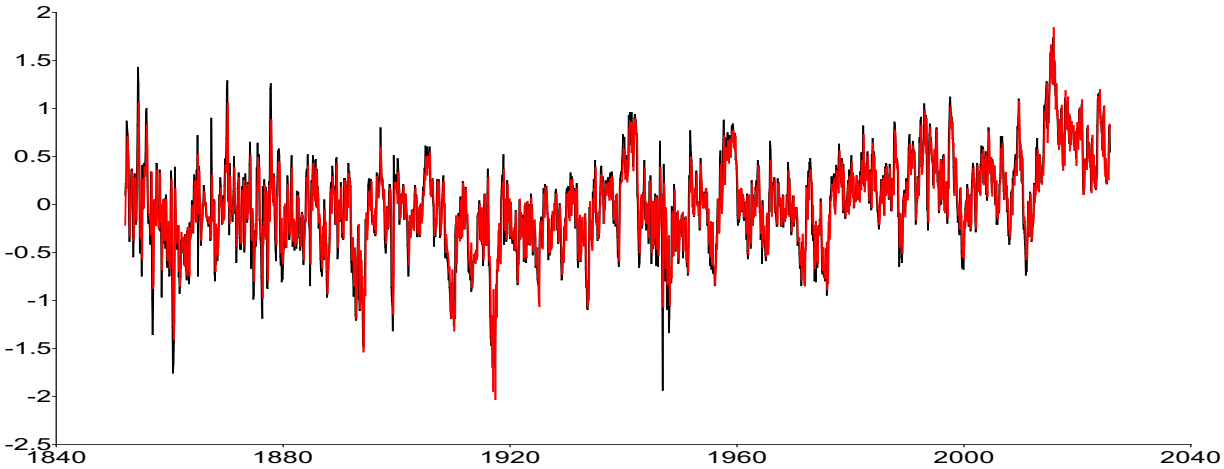

(b) Northern Hemisphere temperature anomalies, y_t and μ_t for t-FI-QAR

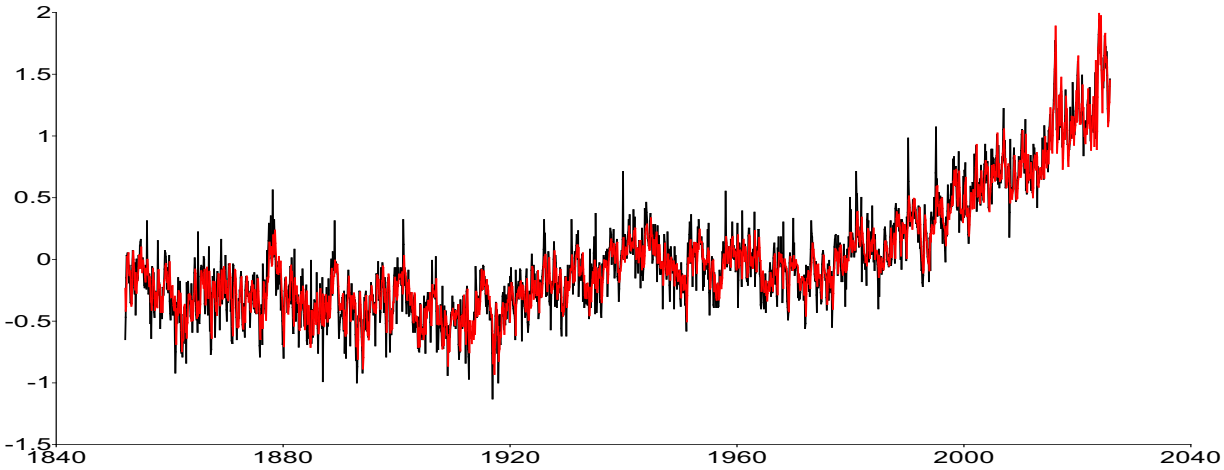

(c) Southern Hemisphere temperature anomalies, y_t and μ_t for t-FI-QAR

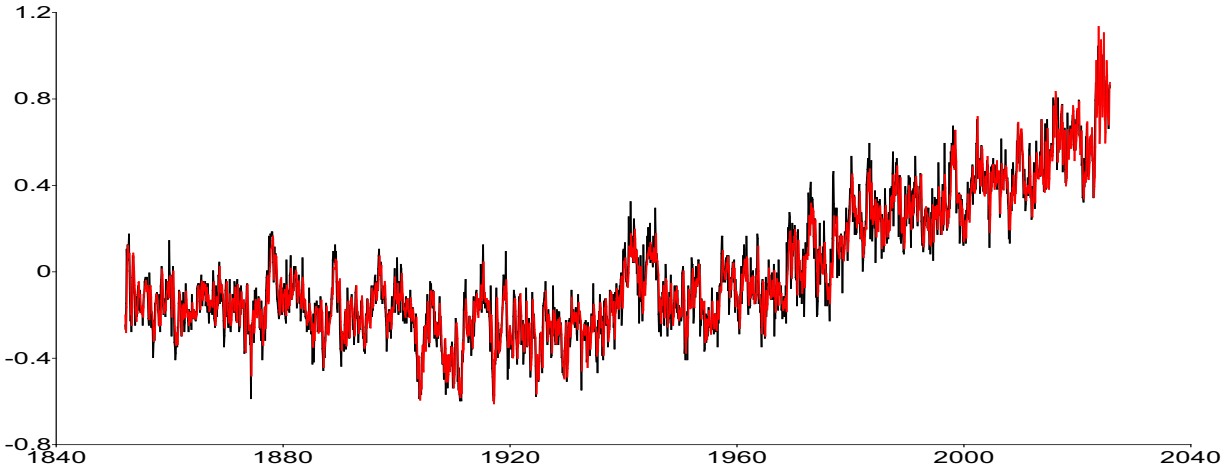

Figure A6. Evolution of y_t (black) and μ_t (red) from January 1850 to October 2025 for the t-FI(d_t)-QAR(p) model.

(a) Arctic temperature anomalies, degree of fractional integration d_t for t-FI-QAR

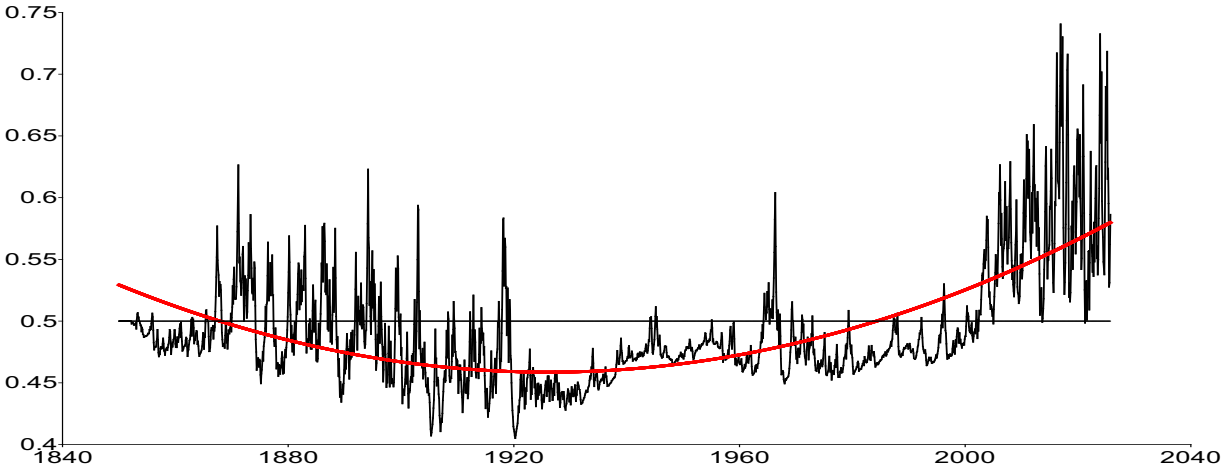

(b) Antarctic temperature anomalies, degree of fractional integration d_t for t-FI-QAR

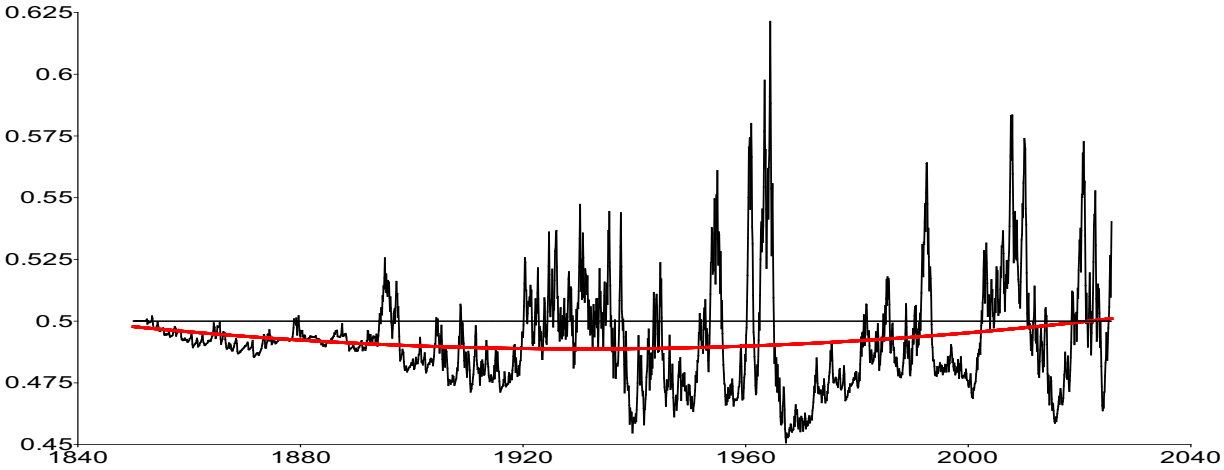

(c) Atlantic Ocean temperature anomalies, degree of fractional integration d_t for t-FI-QAR

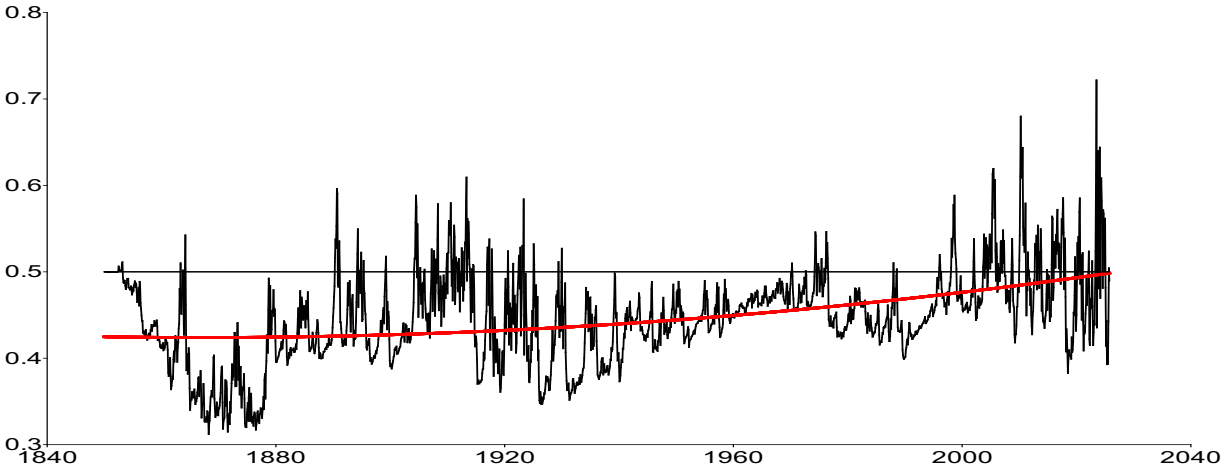

Figure A7. Degree of fractional integration of temperature anomalies d_t from January 1850 to October 2025 for the t-FI(d_t)-QAR(p) model.
Notes: We present the degree of fractional integration of temperature anomalies d_t (black) and the fitted quadratic polynomial (red).

(a) Northeast Pacific Ocean temperature anomalies, degree of fractional integration d_t for t-FI-QAR

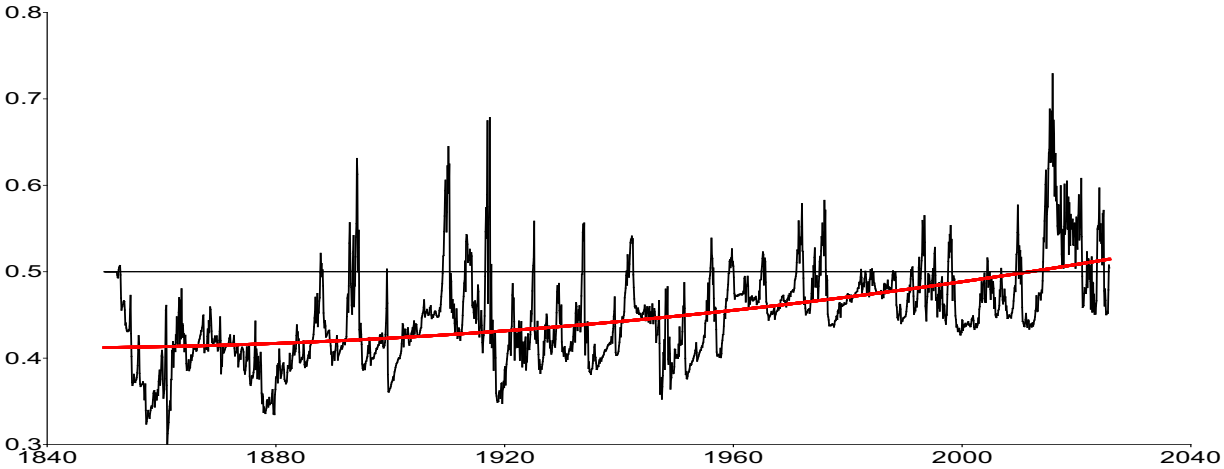

(b) Northern Hemisphere temperature anomalies, degree of fractional integration d_t for t-FI-QAR

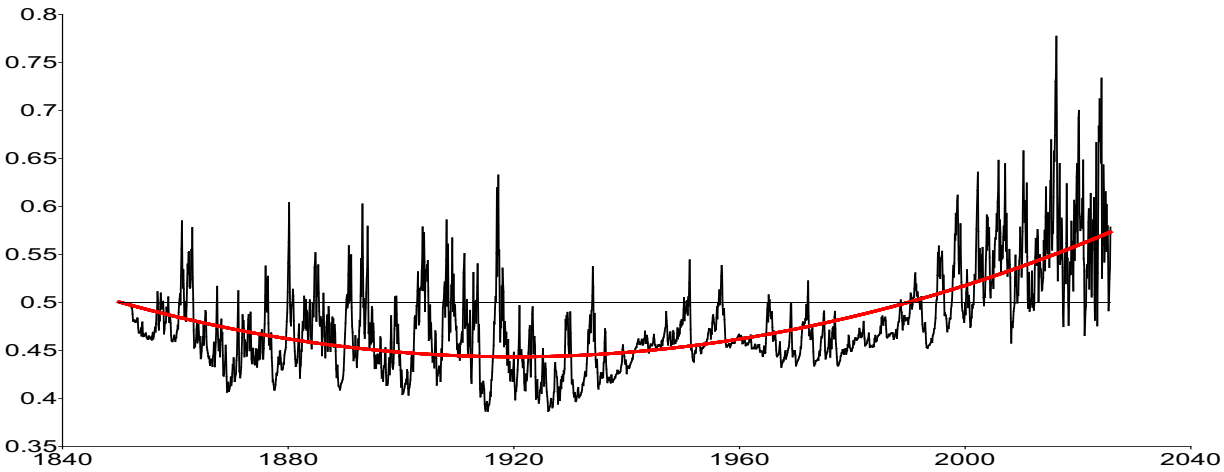

(c) Southern Hemisphere temperature anomalies, degree of fractional integration d_t for t-FI-QAR

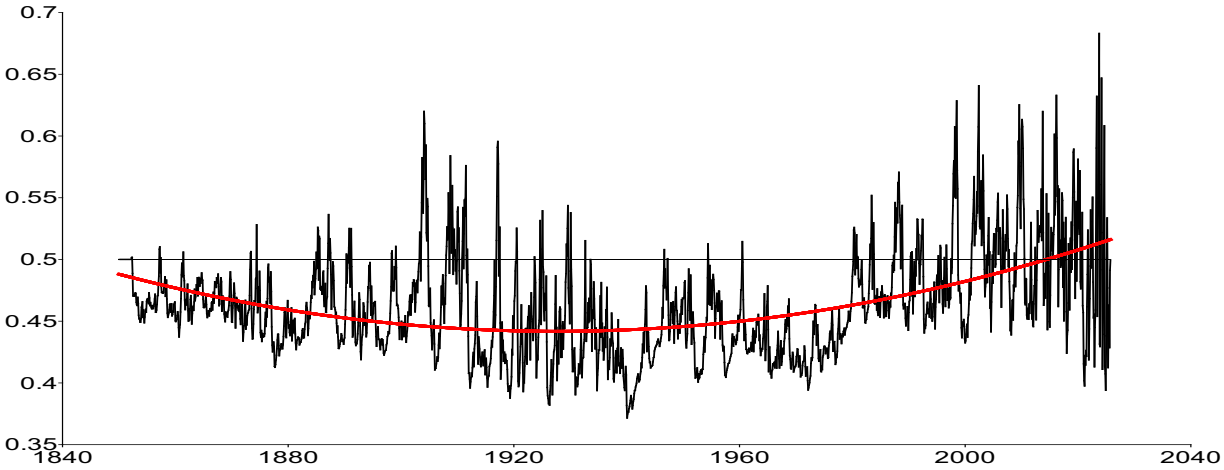

Figure A8. Degree of fractional integration of temperature anomalies d_t from January 1850 to October 2025 for the t-FI(d_t)-QAR(p) model. *Notes:* We present the degree of fractional integration of temperature anomalies d_t (black) and the fitted quadratic polynomial (red).

(a) Arctic temperature anomalies, standardized error term ϵ_t for t-FI-QAR

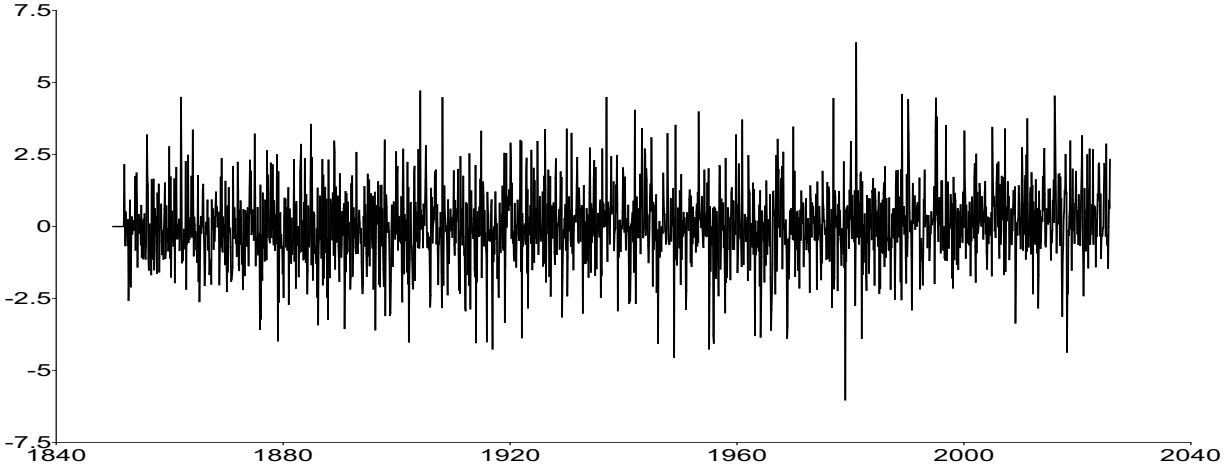

(b) Antarctic temperature anomalies, standardized error term ϵ_t for t-FI-QAR

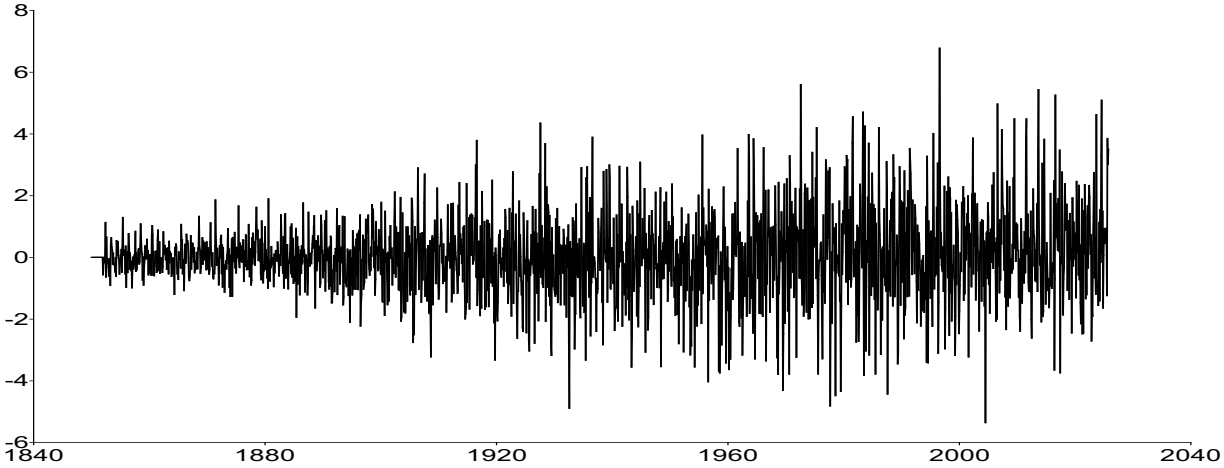

(c) Atlantic Ocean temperature anomalies, standardized error term ϵ_t for t-FI-QAR

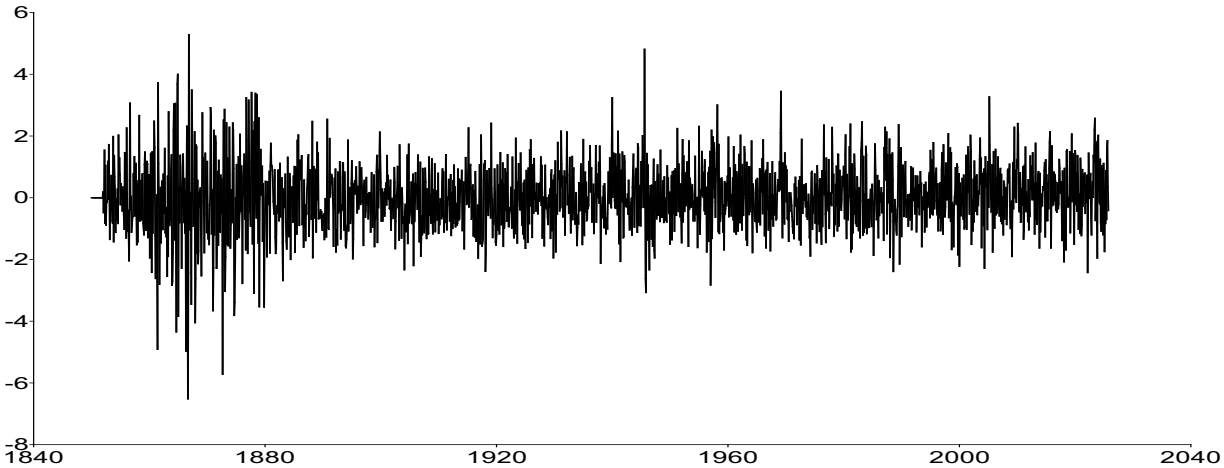

Figure A9. Standardized error term ϵ_t from January 1850 to October 2025 for the t-FI(d_t)-QAR(p) model.

(a) Northeast Pacific Ocean temperature anomalies, standardized error term ϵ_t for t-FI-QAR

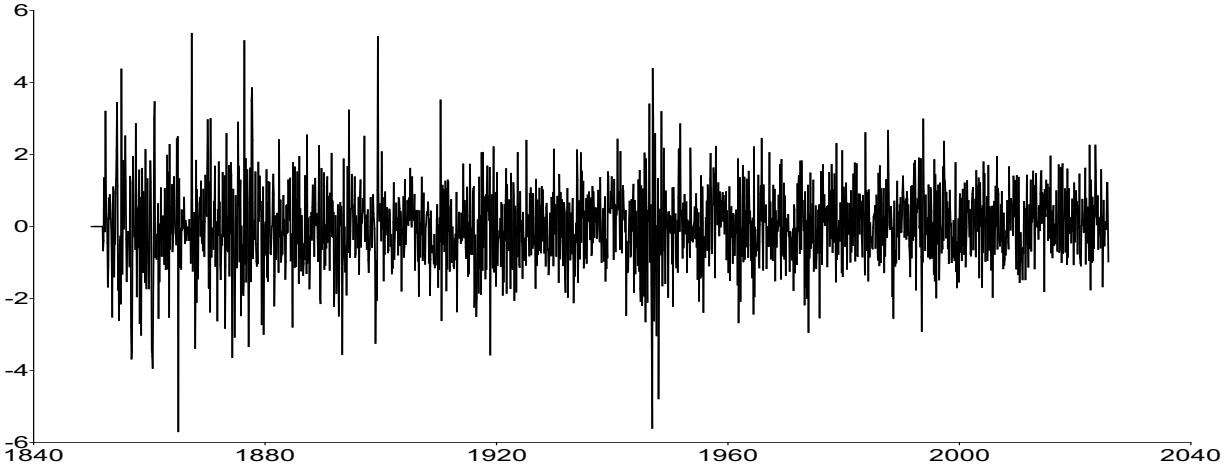

(b) Northern Hemisphere temperature anomalies, standardized error term ϵ_t for t-FI-QAR

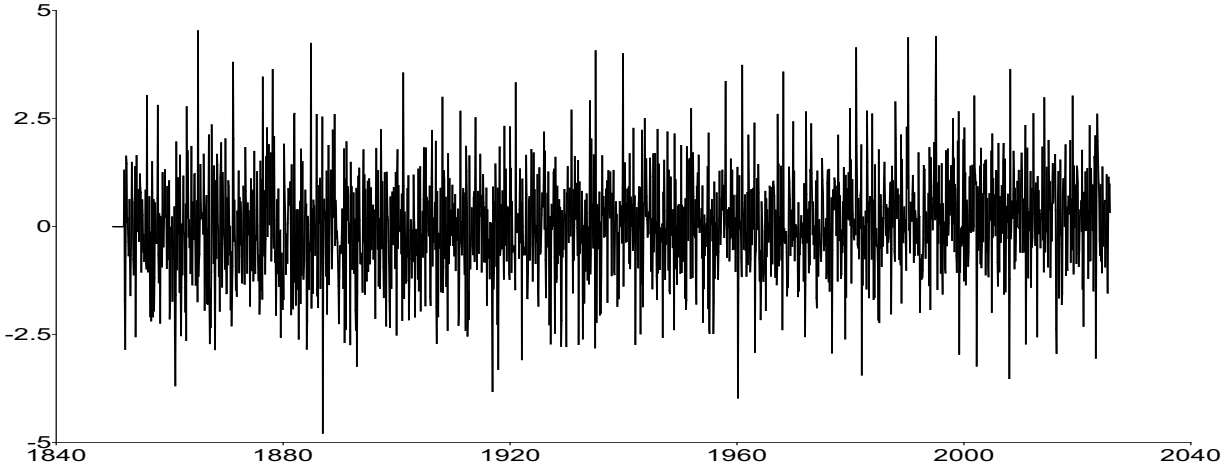

(c) Southern Hemisphere temperature anomalies, standardized error term ϵ_t for t-FI-QAR

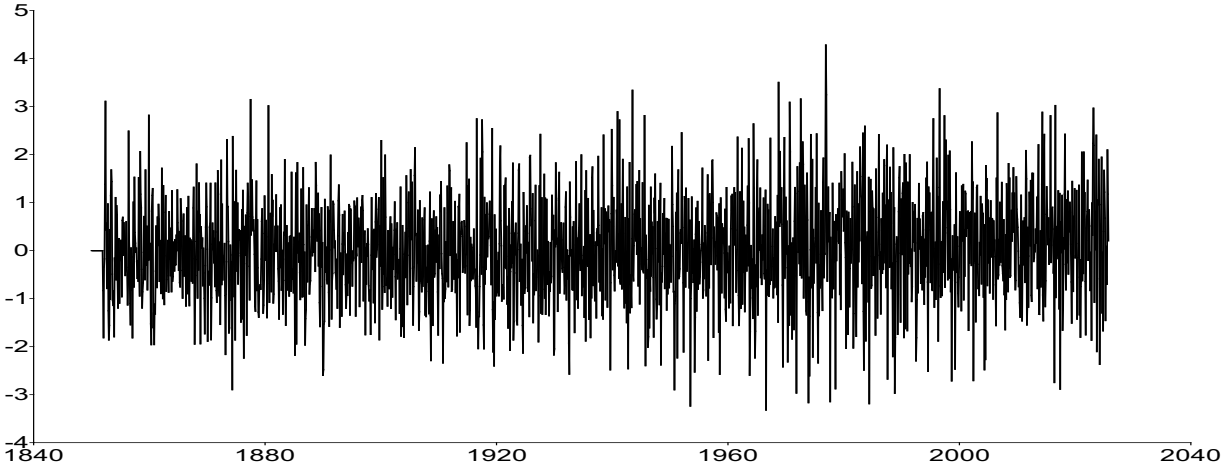

Figure A10. Standardized error term ϵ_t from January 1850 to October 2025 for the t-FI(d_t)-QAR(p) model.

(a) Arctic temperature anomalies, scaled error term v_t for t-FI-QAR

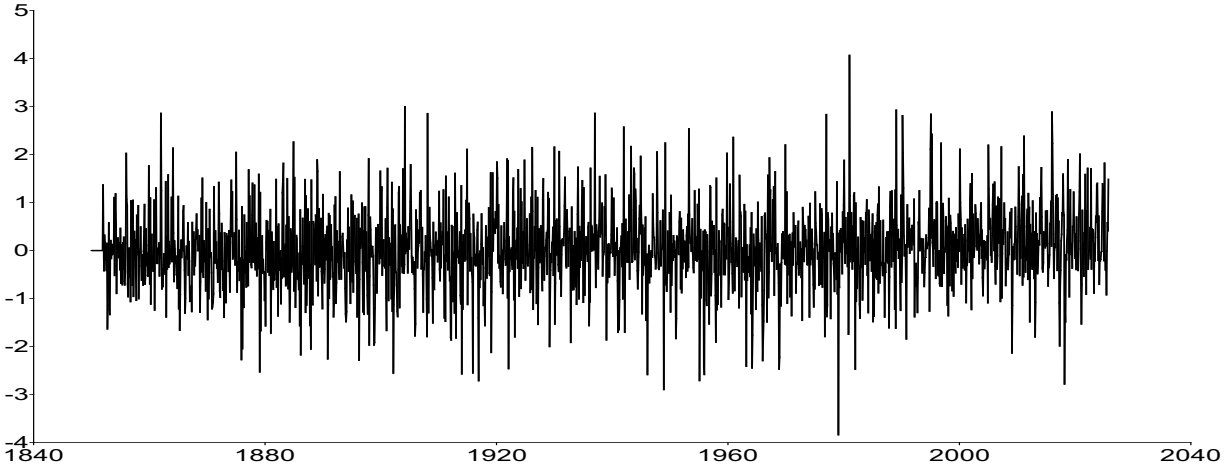

(b) Antarctic temperature anomalies, scaled error term v_t for t-FI-QAR

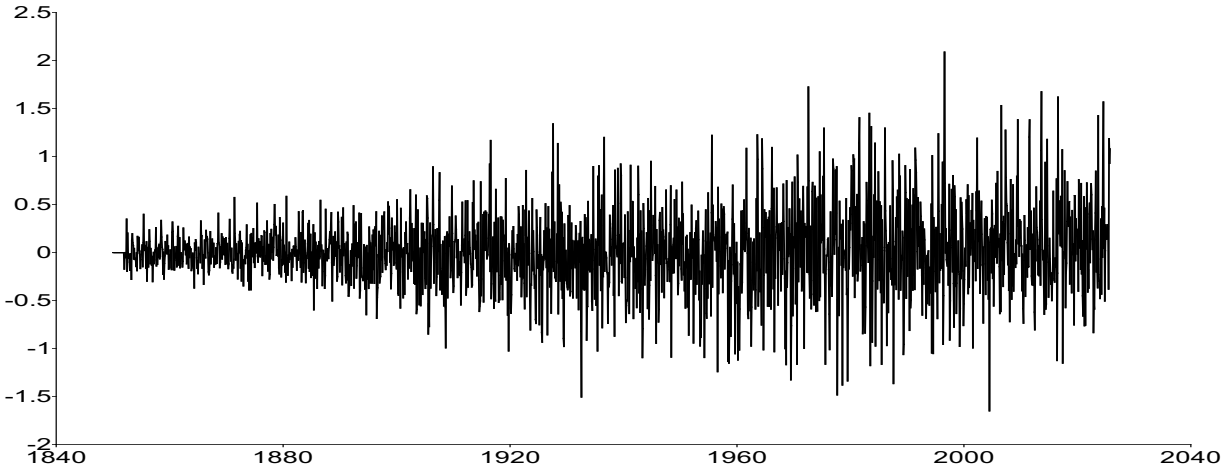

(c) Atlantic Ocean temperature anomalies, scaled error term v_t for t-FI-QAR

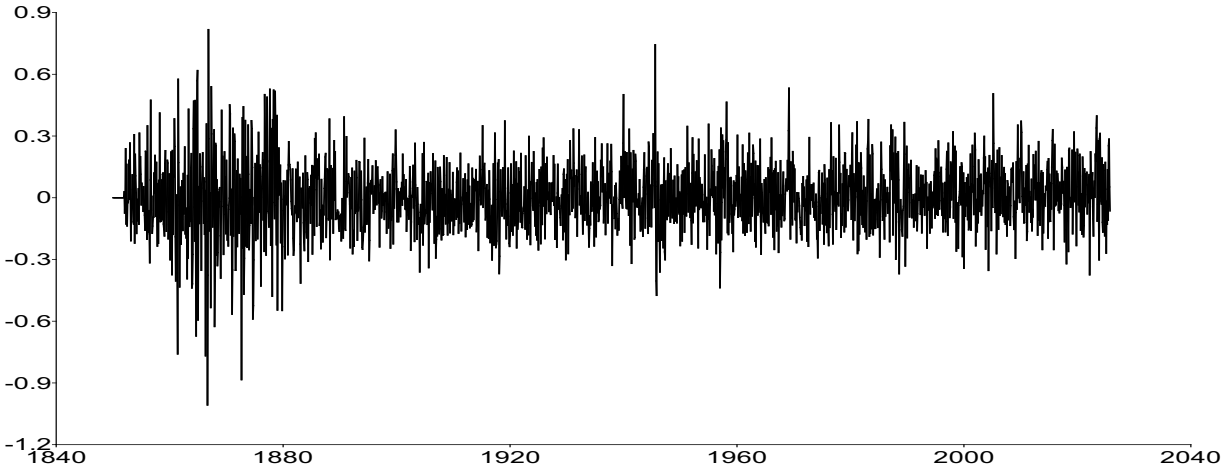

Figure A11. Scaled error term v_t from January 1850 to October 2025 for the t-FI(d_t)-QAR(p) model.

(a) Northeast Pacific Ocean temperature anomalies, scaled error term v_t for t-FI-QAR

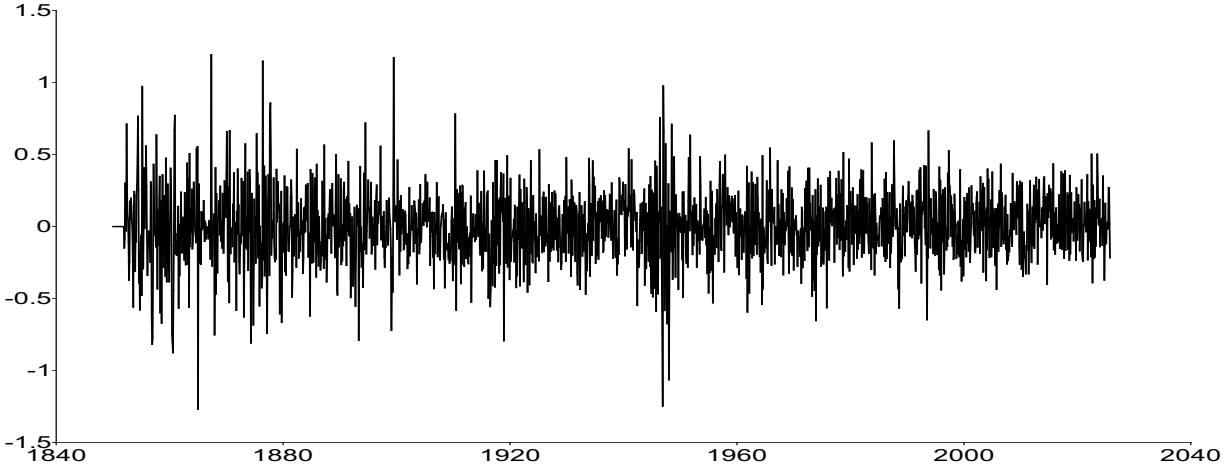

(b) Northern Hemisphere temperature anomalies, scaled error term v_t for t-FI-QAR

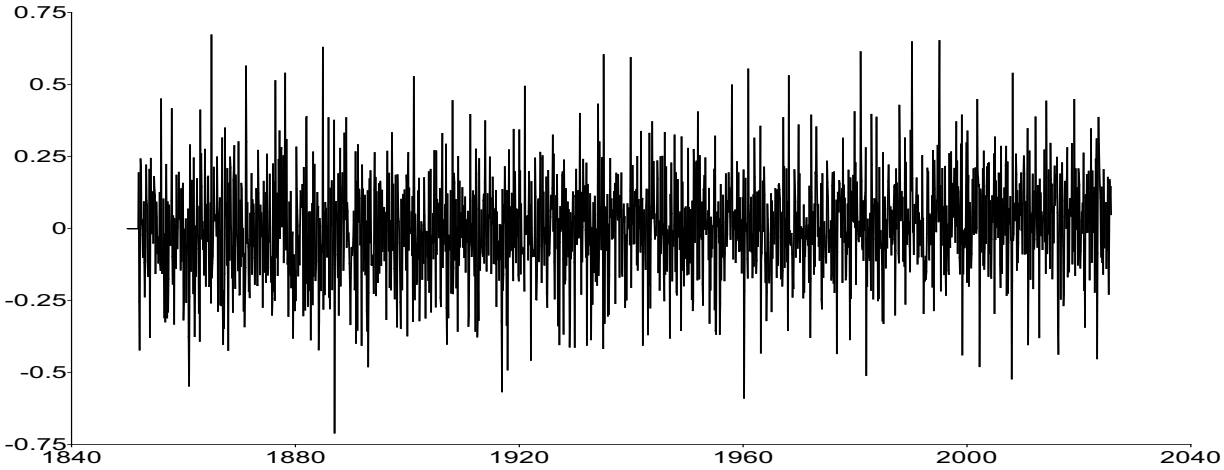

(c) Southern Hemisphere temperature anomalies, scaled error term v_t for t-FI-QAR

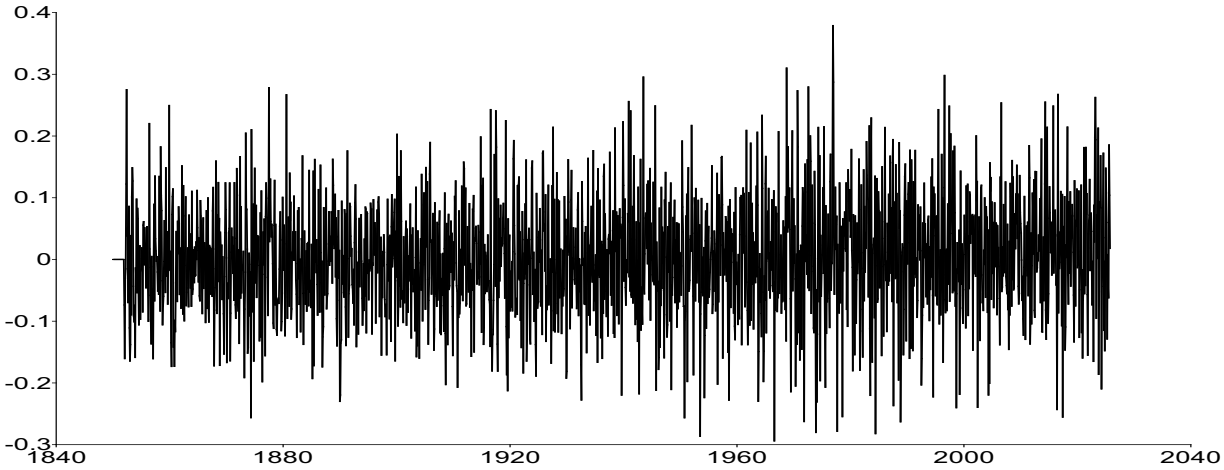

Figure A12. Scaled error term v_t from January 1850 to October 2025 for the t-FI(d_t)-QAR(p) model.

(a) Arctic temperature anomalies, location score function $u_{\mu,t}$ for t-FI-QAR

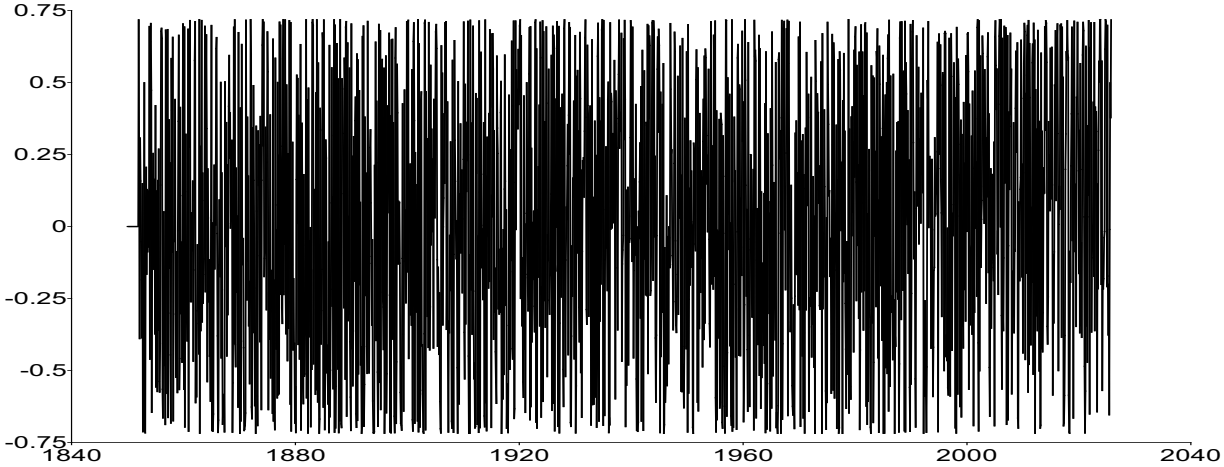

(b) Antarctic temperature anomalies, location score function $u_{\mu,t}$ for t-FI-QAR

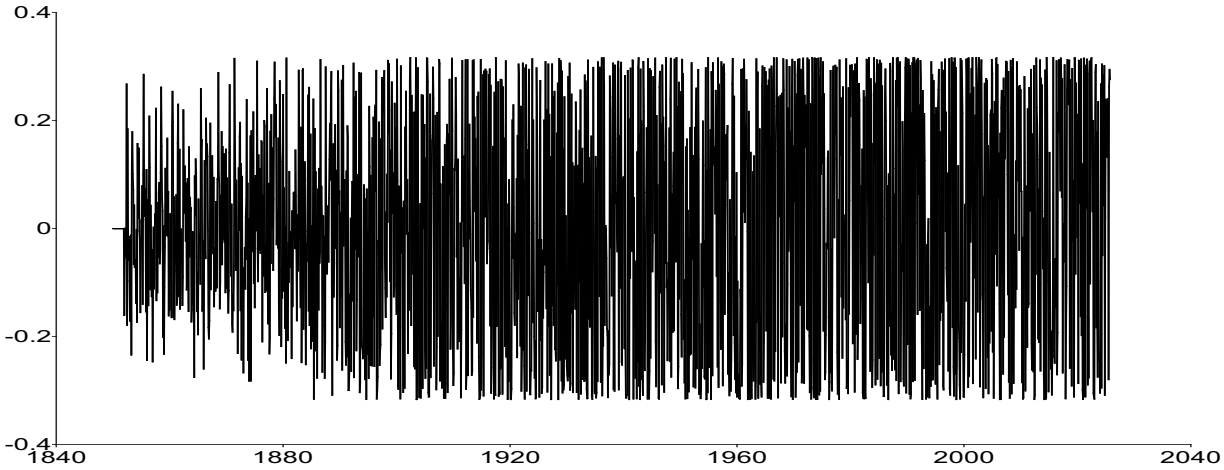

(c) Atlantic Ocean temperature anomalies, location score function $u_{\mu,t}$ for t-FI-QAR

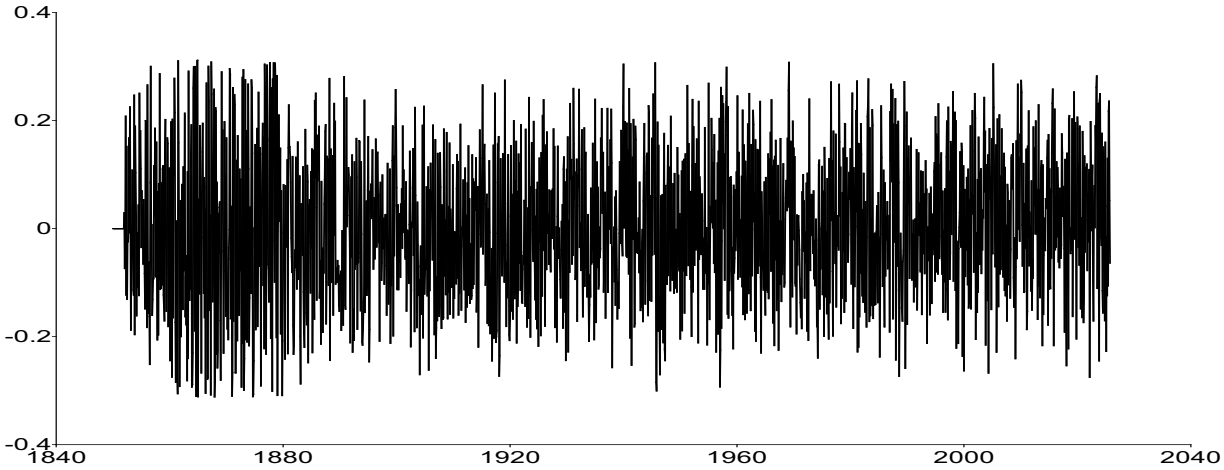

Figure A13. Location score function $u_{\mu,t}$ from January 1850 to October 2025 for the t-FI(d_t)-QAR(p) model.

(a) Northeast Pacific Ocean temperature anomalies, location score function $u_{\mu,t}$ for t-FI-QAR

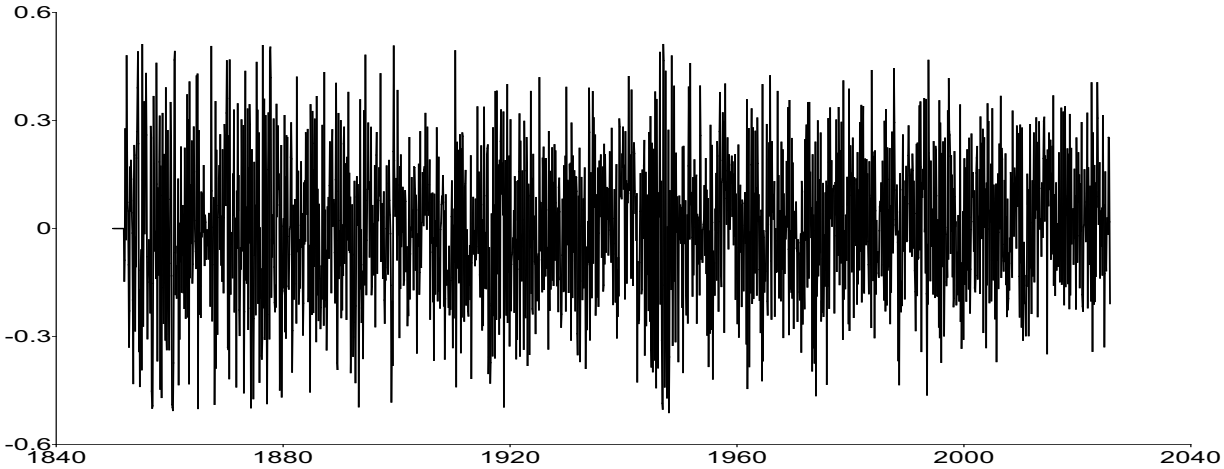

(b) Northern Hemisphere temperature anomalies, location score function $u_{\mu,t}$ for t-FI-QAR

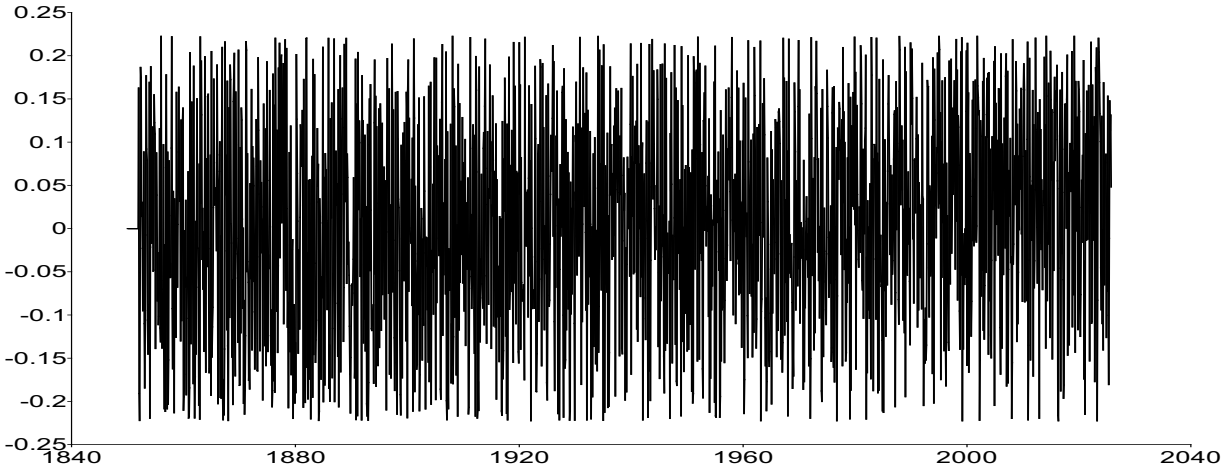

(c) Southern Hemisphere temperature anomalies, location score function $u_{\mu,t}$ for t-FI-QAR

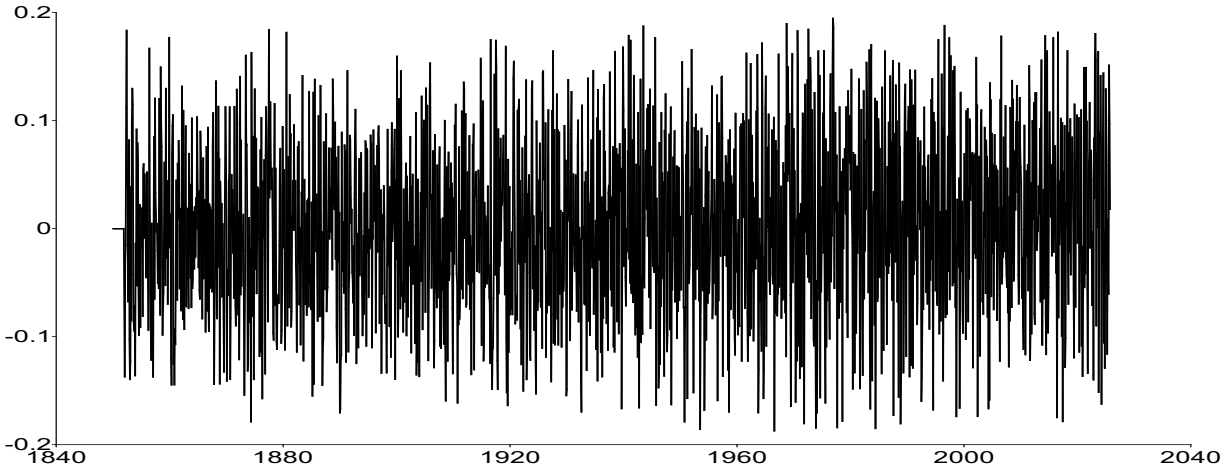

Figure A14. Location score function $u_{\mu,t}$ from January 1850 to October 2025 for the t-FI(d_t)-QAR(p) model.

(a) Arctic temperature anomalies, degree of fractional integration score function $u_{d,t}$ for t-FI-QAR

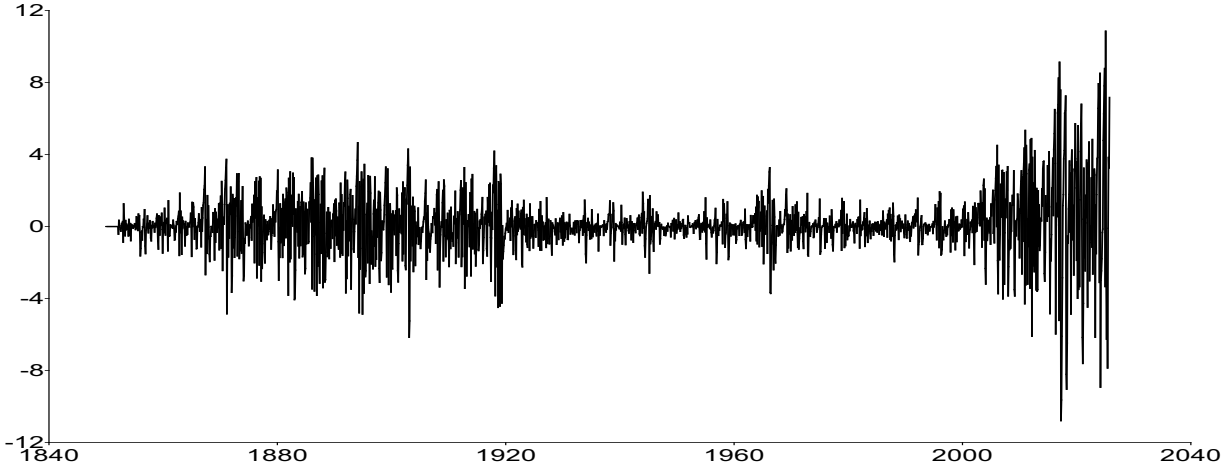

(b) Antarctic temperature anomalies, degree of fractional integration score function $u_{d,t}$ for t-FI-QAR

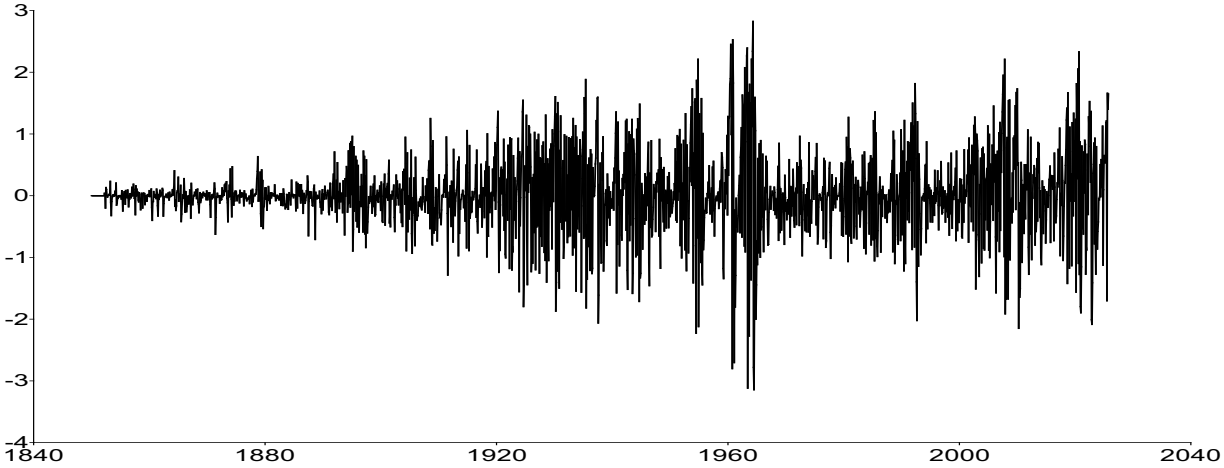

(c) Atlantic Ocean temperature anomalies, degree of fractional integration score function $u_{d,t}$ for t-FI-QAR

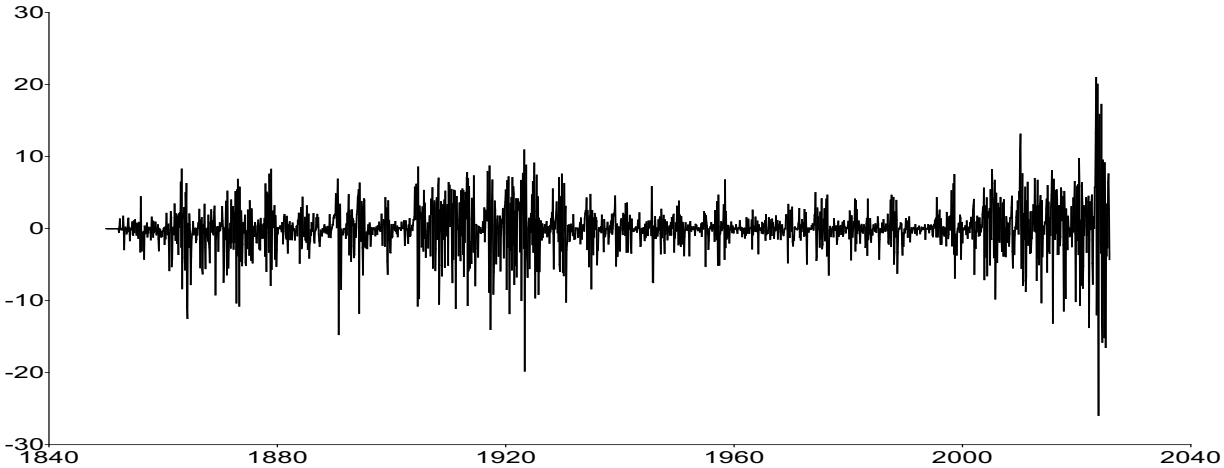

Figure A15. Degree of fractional integration score function $u_{d,t}$ from January 1850 to October 2025 for the t-FI(d_t)-QAR(p) model.

(a) Northeast Pacific Ocean temperature anomalies, degree of fractional integration score function $u_{d,t}$ for t-FI-QAR

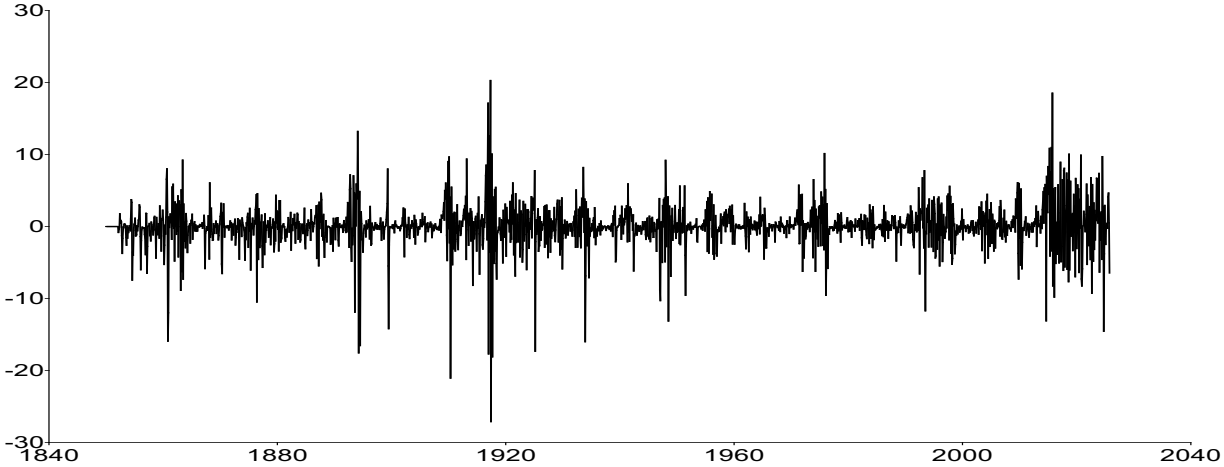

(b) Northern Hemisphere temperature anomalies, degree of fractional integration score function $u_{d,t}$ for t-FI-QAR

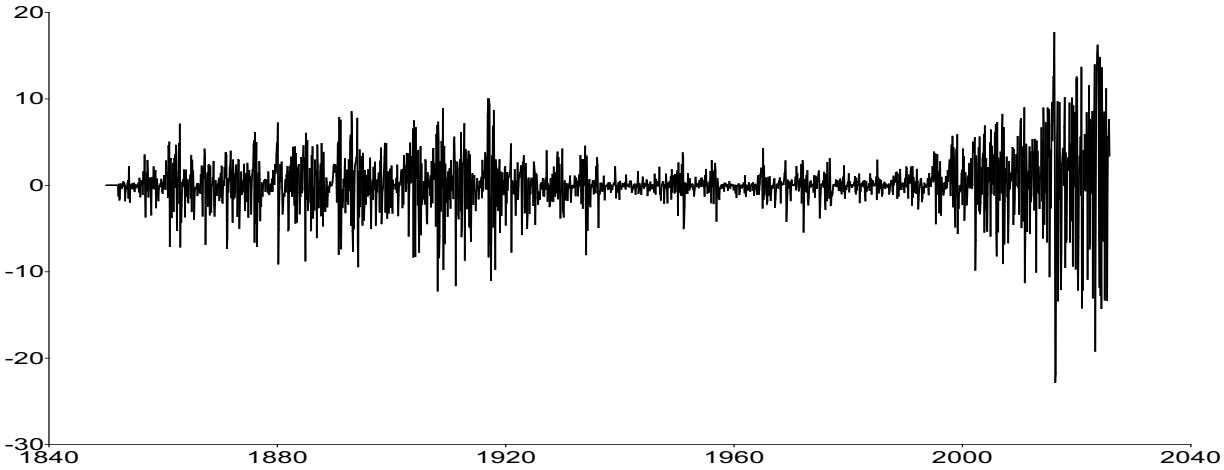

(c) Southern Hemisphere temperature anomalies, degree of fractional integration score function $u_{d,t}$ for t-FI-QAR

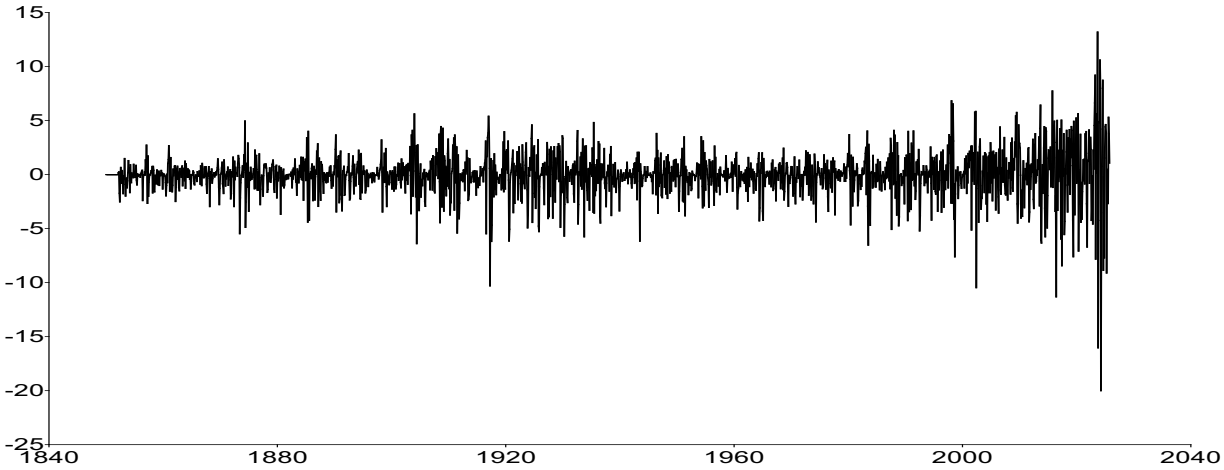

Figure A16. Degree of fractional integration score function $u_{d,t}$ from January 1850 to October 2025 for the t-FI(d_t)-QAR(p) model.

Supplementary Material B

Figure B1. Impact of shocks on updating terms: $u_{\mu,t}$ as a function of ϵ_t from January 1850 to October 2025 for the t-FI(d_t)-QAR(p)-Beta-t-EGARCH and t-FI(d_t)-QAR(p)-Beta-t-EIGARCH models.

Figure B2. Impact of shocks on updating terms: $u_{\mu,t}$ as a function of ϵ_t from January 1850 to October 2025 for the t-FI(d_t)-QAR(p)-Beta-t-EGARCH and t-FI(d_t)-QAR(p)-Beta-t-EIGARCH models.

Figure B3. Impact of shocks on updating terms: $u_{d,t}$ as a function of ϵ_t from January 1850 to October 2025 for the t-FI(d_t)-QAR(p)-Beta-t-EGARCH and t-FI(d_t)-QAR(p)-Beta-t-EIGARCH models.

Figure B4. Impact of shocks on updating terms: $u_{d,t}$ as a function of ϵ_t from January 1850 to October 2025 for the t-FI(d_t)-QAR(p)-Beta-t-EGARCH and t-FI(d_t)-QAR(p)-Beta-t-EIGARCH models.

Figure B5. Impact of shocks on updating terms: $u_{\lambda,t}$ as a function of ϵ_t from January 1850 to October 2025 for the t-FI(d_t)-QAR(p)-Beta-t-EGARCH and t-FI(d_t)-QAR(p)-Beta-t-EIGARCH models.

Figure B6. Impact of shocks on updating terms: $u_{\lambda,t}$ as a function of ϵ_t from January 1850 to October 2025 for the t-FI(d_t)-QAR(p)-Beta-t-EGARCH and t-FI(d_t)-QAR(p)-Beta-t-EIGARCH models.

Figure B7. Evolution of y_t (black) and μ_t (red) from January 1850 to October 2025 for the t-FI(d_t)-QAR(p)-Beta-t-EGARCH and t-FI(d_t)-QAR(p)-Beta-t-EIGARCH models.

Figure B8. Evolution of y_t (black) and μ_t (red) from January 1850 to October 2025 for the t-FI(d_t)-QAR(p)-Beta-t-EGARCH and t-FI(d_t)-QAR(p)-Beta-t-EIGARCH models.

Figure B9. Degree of fractional integration of temperature anomalies d_t from January 1850 to October 2025 for the t-FI(d_t)-QAR(p)-Beta-t-EGARCH and t-FI(d_t)-QAR(p)-Beta-t-EIGARCH models.

Figure B10. Degree of fractional integration of temperature anomalies d_t from January 1850 to October 2025 for the t-FI(d_t)-QAR(p)-Beta-t-EGARCH and t-FI(d_t)-QAR(p)-Beta-t-EIGARCH models.

Figure B11. Log scale λ_t from January 1850 to October 2025 for the t-FI(d_t)-QAR(p)-Beta-t-EGARCH and t-FI(d_t)-QAR(p)-Beta-t-EIGARCH models.

Figure B12. Log scale λ_t from January 1850 to October 2025 for the t-FI(d_t)-QAR(p)-Beta-t-EGARCH and t-FI(d_t)-QAR(p)-Beta-t-EIGARCH models.

Figure B13. Conditional standard deviation σ_t from January 1850 to October 2025 for the t-FI(d_t)-QAR(p)-Beta-t-EGARCH and t-FI(d_t)-QAR(p)-Beta-t-EIGARCH models.

Figure B14. Conditional standard deviation σ_t from January 1850 to October 2025 for the t-FI(d_t)-QAR(p)-Beta-t-EGARCH and t-FI(d_t)-QAR(p)-Beta-t-EIGARCH models.

Figure B15. Standardized error term ϵ_t from January 1850 to October 2025 for the t-FI(d_t)-QAR(p)-Beta-t-EGARCH and t-FI(d_t)-QAR(p)-Beta-t-EIGARCH models.

Figure B16. Standardized error term ϵ_t from January 1850 to October 2025 for the t-FI(d_t)-QAR(p)-Beta-t-EGARCH and t-FI(d_t)-QAR(p)-Beta-t-EIGARCH models.

Figure B17. Scaled error term v_t from January 1850 to October 2025 for the t-FI(d_t)-QAR(p)-Beta-t-EGARCH and t-FI(d_t)-QAR(p)-Beta-t-EIGARCH models.

Figure B18. Scaled error term v_t from January 1850 to October 2025 for the t-FI(d_t)-QAR(p)-Beta-t-EGARCH and t-FI(d_t)-QAR(p)-Beta-t-EIGARCH models.

Figure B19. Location score function $u_{\mu,t}$ from January 1850 to October 2025 for the t-FI(d_t)-QAR(p)-Beta-t-EGARCH and t-FI(d_t)-QAR(p)-Beta-t-EIGARCH models.

Figure B20. Location score function $u_{\mu,t}$ from January 1850 to October 2025 for the t-FI(d_t)-QAR(p)-Beta-t-EGARCH and t-FI(d_t)-QAR(p)-Beta-t-EIGARCH models.

Figure B21. Degree of fractional integration score function $u_{d,t}$ from January 1850 to October 2025 for the t-FI(d_t)-QAR(p)-Beta-t-EGARCH and t-FI(d_t)-QAR(p)-Beta-t-EIGARCH models.

Figure B22. Degree of fractional integration score function $u_{d,t}$ from January 1850 to October 2025 for the t-FI(d_t)-QAR(p)-Beta-t-EGARCH and t-FI(d_t)-QAR(p)-Beta-t-EIGARCH models.

Figure B23. Log scale score function $u_{\lambda,t}$ from January 1850 to October 2025 for the t-FI(d_t)-QAR(p)-Beta-t-EGARCH and t-FI(d_t)-QAR(p)-Beta-t-EIGARCH models.

Figure B24. Log scale score function $u_{\lambda,t}$ from January 1850 to October 2025 for the t-FI(d_t)-QAR(p)-Beta-t-EGARCH and t-FI(d_t)-QAR(p)-Beta-t-EIGARCH models.

(a) Arctic temperature anomalies, $u_{\mu,t}$ as a function of ϵ_t for t-FI-QAR-Beta-t-EGARCH

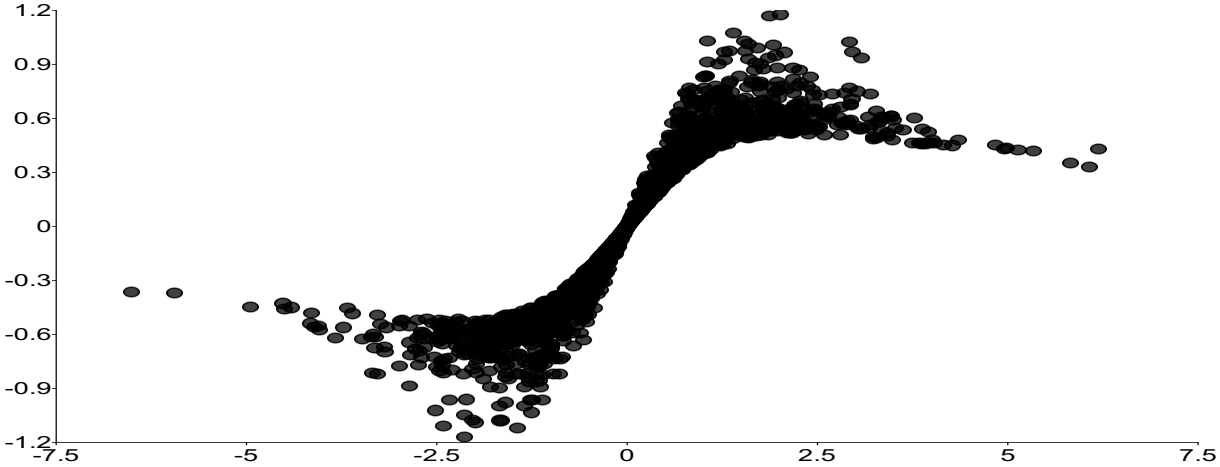

(b) Antarctic temperature anomalies, $u_{\mu,t}$ as a function of ϵ_t for t-FI-QAR-Beta-t-EIGARCH

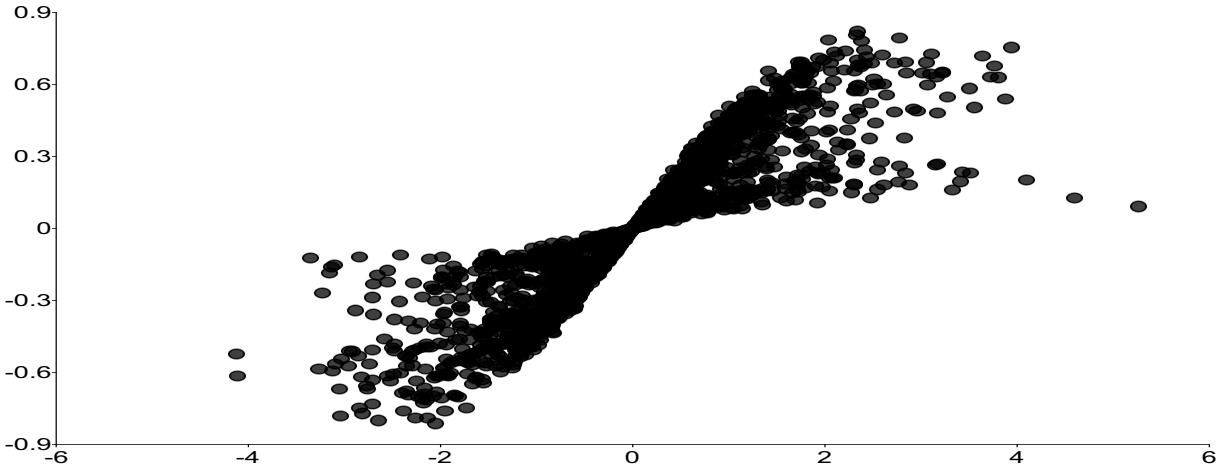

(c) Atlantic Ocean temperature anomalies, $u_{\mu,t}$ as a function of ϵ_t for t-FI-QAR-Beta-t-EGARCH

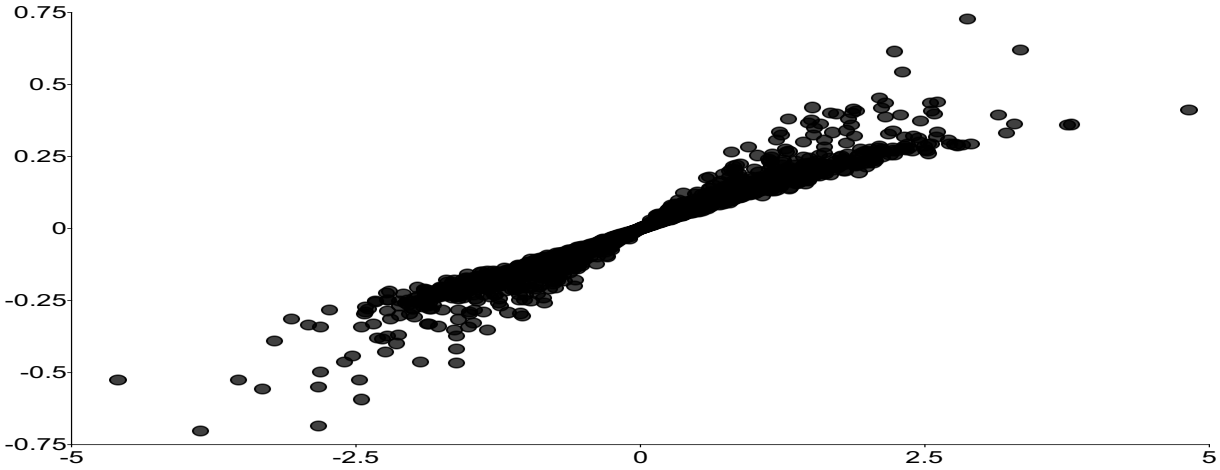

Figure B1. Impact of shocks on updating terms: $u_{\mu,t}$ as a function of ϵ_t from January 1850 to October 2025 for the t-FI(d_t)-QAR(p)-Beta-t-EGARCH and t-FI(d_t)-QAR(p)-Beta-t-EIGARCH models.

(a) Northeast Pacific Ocean temperature anomalies, $u_{\mu,t}$ as a function of ϵ_t for t-FI-QAR-Beta-t-EGARCH

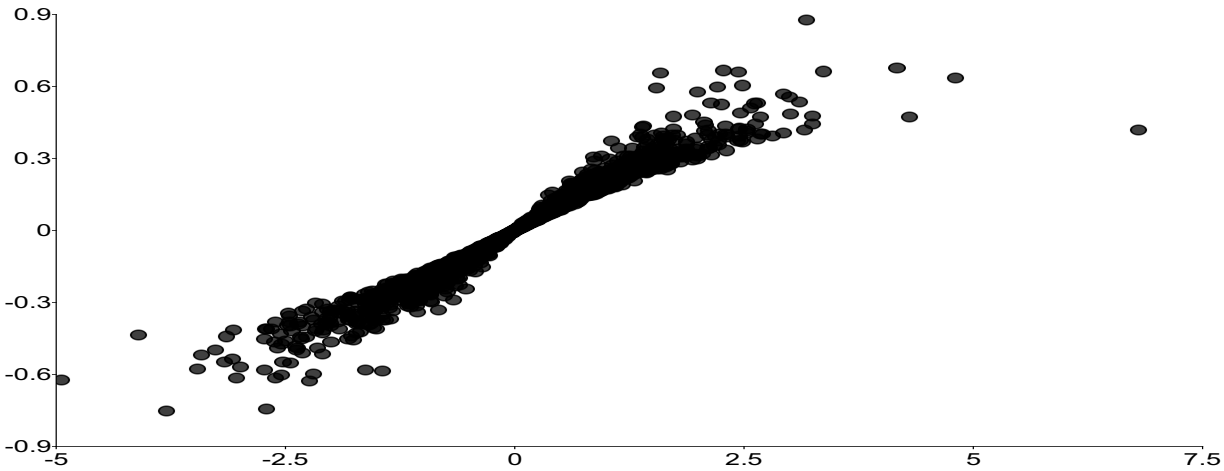

(b) Northern Hemisphere temperature anomalies, $u_{\mu,t}$ as a function of ϵ_t for t-FI-QAR-Beta-t-EGARCH

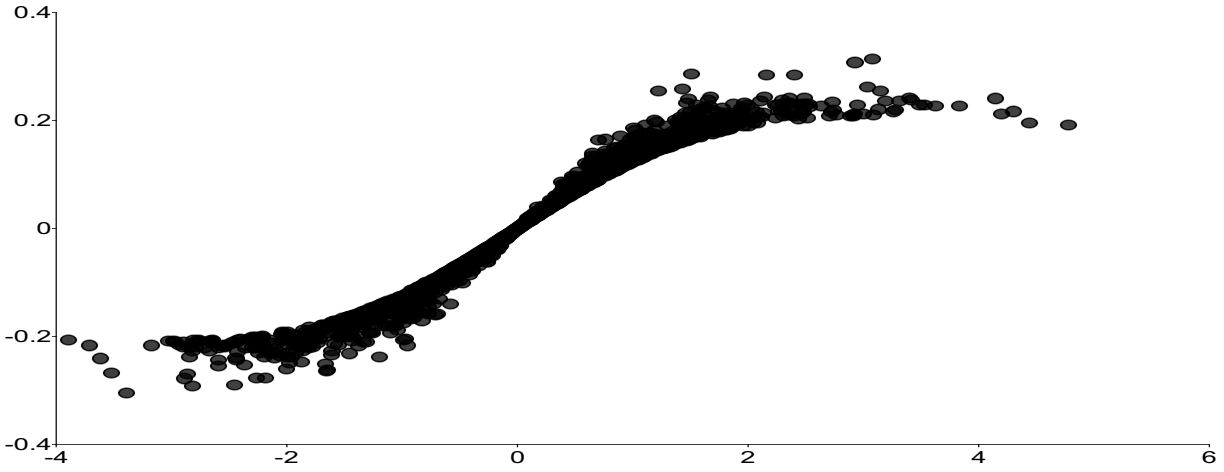

(c) Southern Hemisphere temperature anomalies, $u_{\mu,t}$ as a function of ϵ_t for t-FI-QAR-Beta-t-EIGARCH

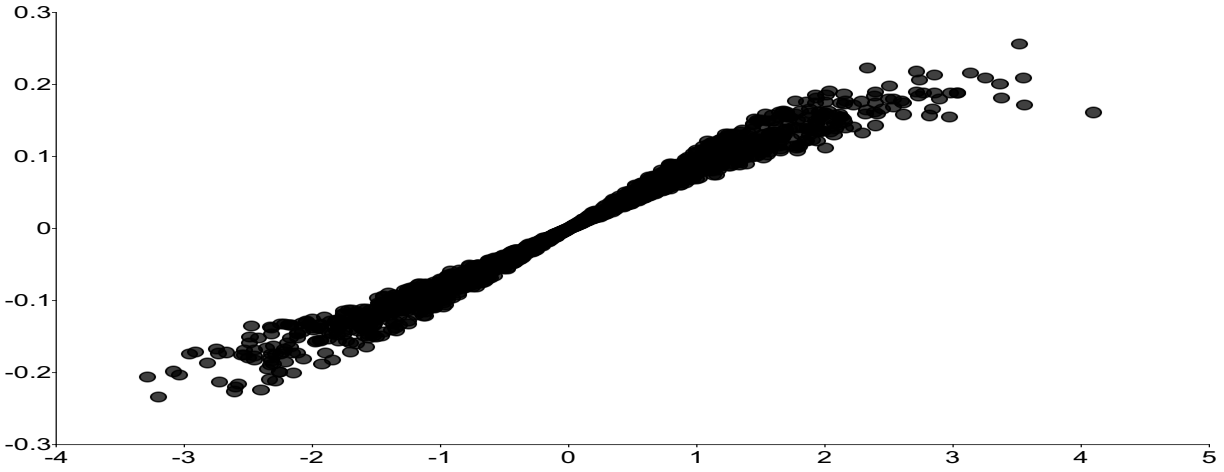

Figure B2. Impact of shocks on updating terms: $u_{\mu,t}$ as a function of ϵ_t from January 1850 to October 2025 for the t-FI(d_t)-QAR(p)-Beta-t-EGARCH and t-FI(d_t)-QAR(p)-Beta-t-EIGARCH models.

(a) Arctic temperature anomalies, $u_{d,t}$ as a function of ϵ_t for t-FI-QAR-Beta-t-EGARCH

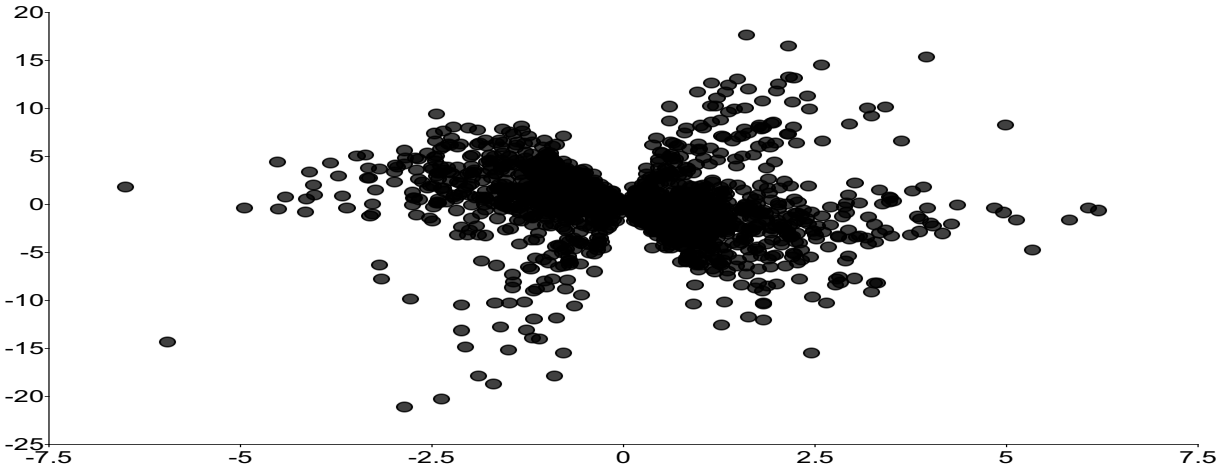

(b) Antarctic temperature anomalies, $u_{d,t}$ as a function of ϵ_t for t-FI-QAR-Beta-t-EIGARCH

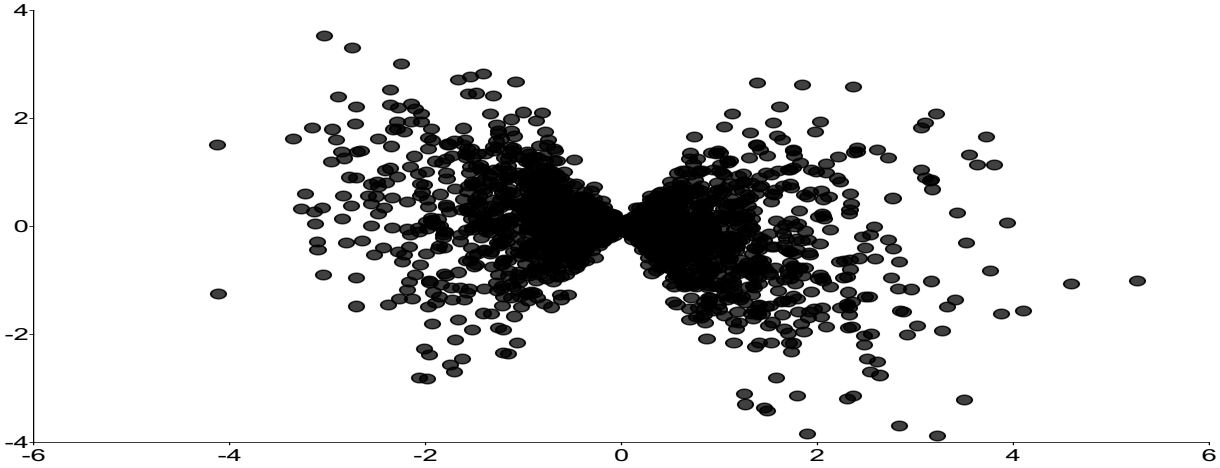

(c) Atlantic Ocean temperature anomalies, $u_{d,t}$ as a function of ϵ_t for t-FI-QAR-Beta-t-EGARCH

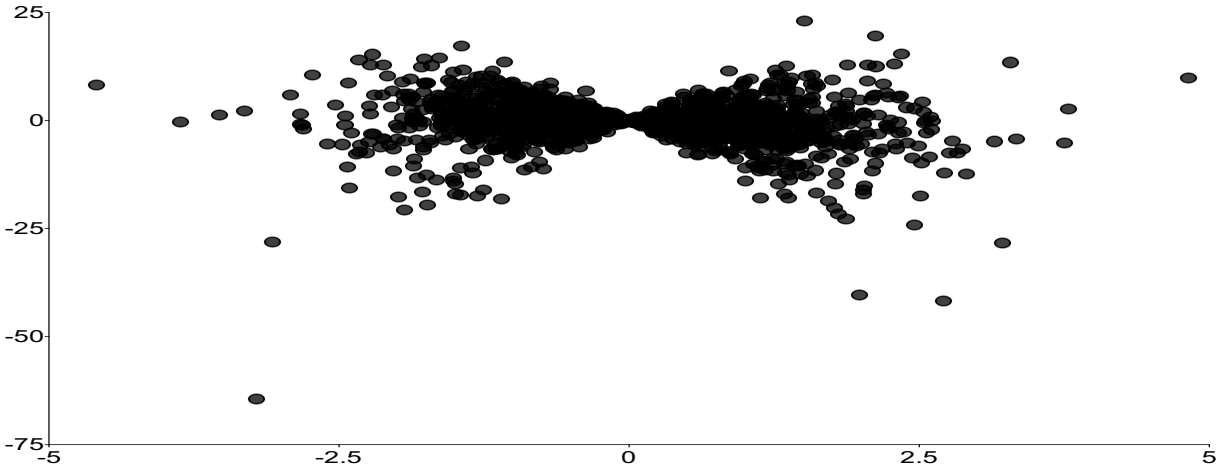

Figure B3. Impact of shocks on updating terms: $u_{d,t}$ as a function of ϵ_t from January 1850 to October 2025 for the t-FI(d_t)-QAR(p)-Beta-t-EGARCH and t-FI(d_t)-QAR(p)-Beta-t-EIGARCH models.

(a) Northeast Pacific Ocean temperature anomalies, $u_{d,t}$ as a function of ϵ_t for t-FI-QAR-Beta-t-EGARCH

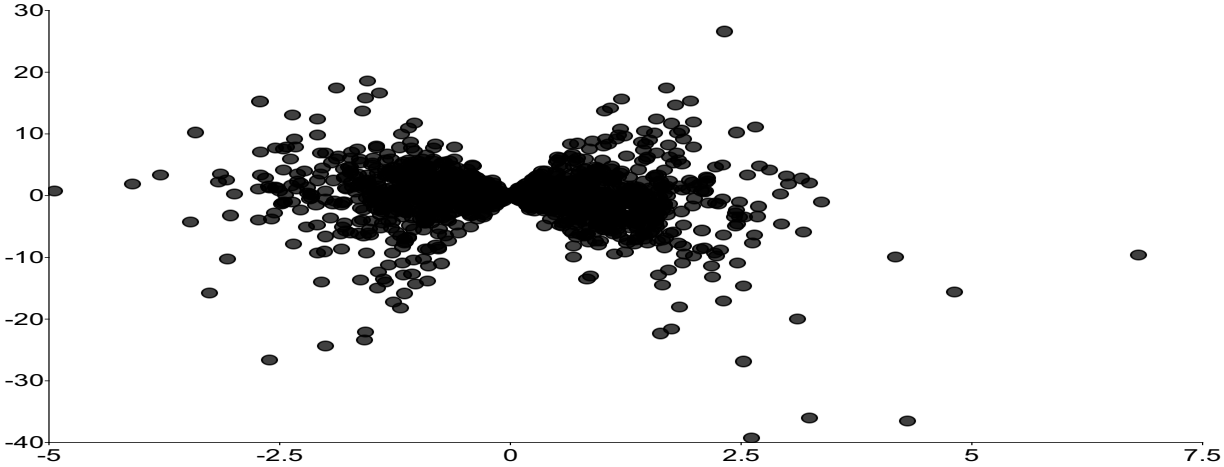

(b) Northern Hemisphere temperature anomalies, $u_{d,t}$ as a function of ϵ_t for t-FI-QAR-Beta-t-EGARCH

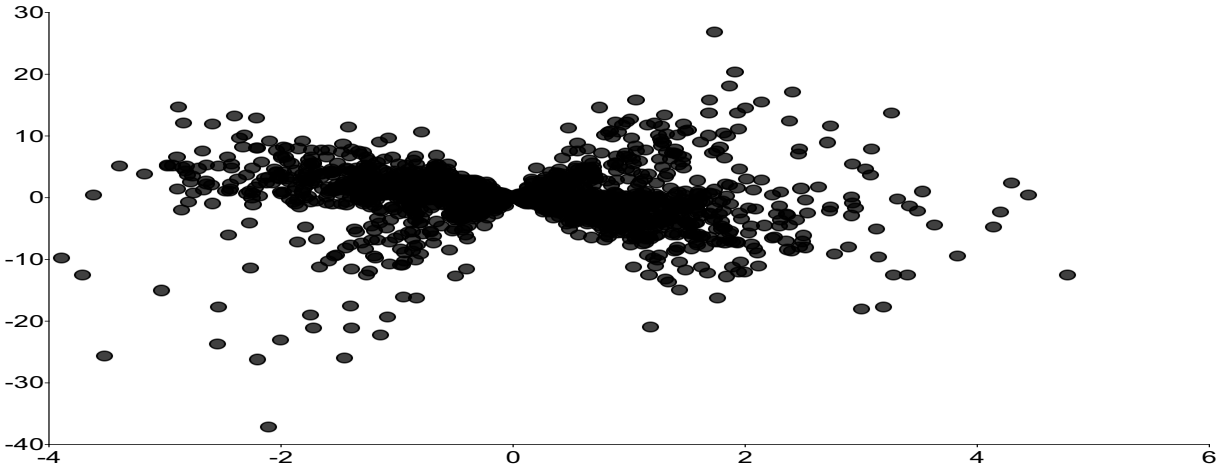

(c) Southern Hemisphere temperature anomalies, $u_{d,t}$ as a function of ϵ_t for t-FI-QAR-Beta-t-EIGARCH

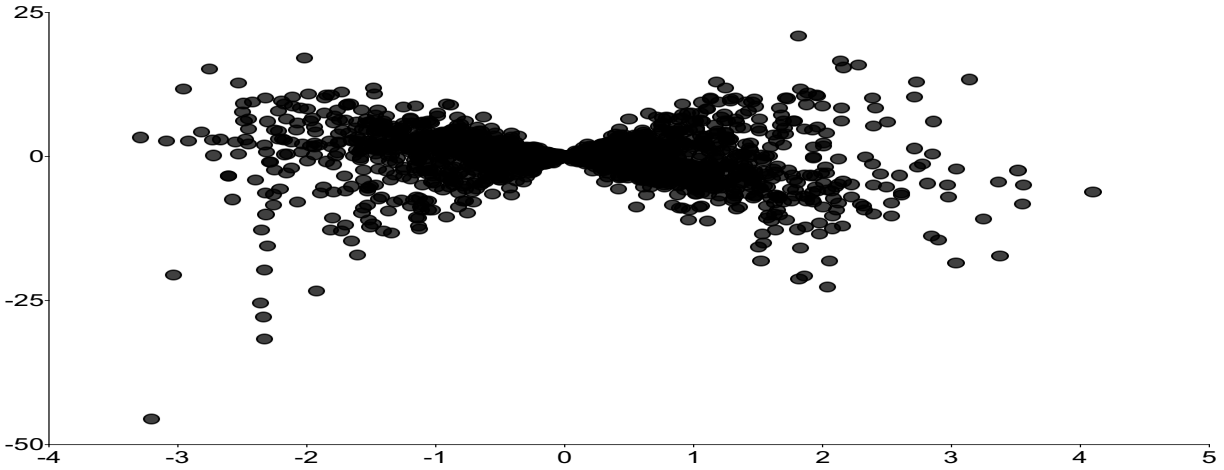

Figure B4. Impact of shocks on updating terms: $u_{d,t}$ as a function of ϵ_t from January 1850 to October 2025 for the t-FI(d_t)-QAR(p)-Beta-t-EGARCH and t-FI(d_t)-QAR(p)-Beta-t-EIGARCH models.

(a) Arctic temperature anomalies, $u_{\lambda,t}$ as a function of ϵ_t for t-FI-QAR-Beta-t-EGARCH

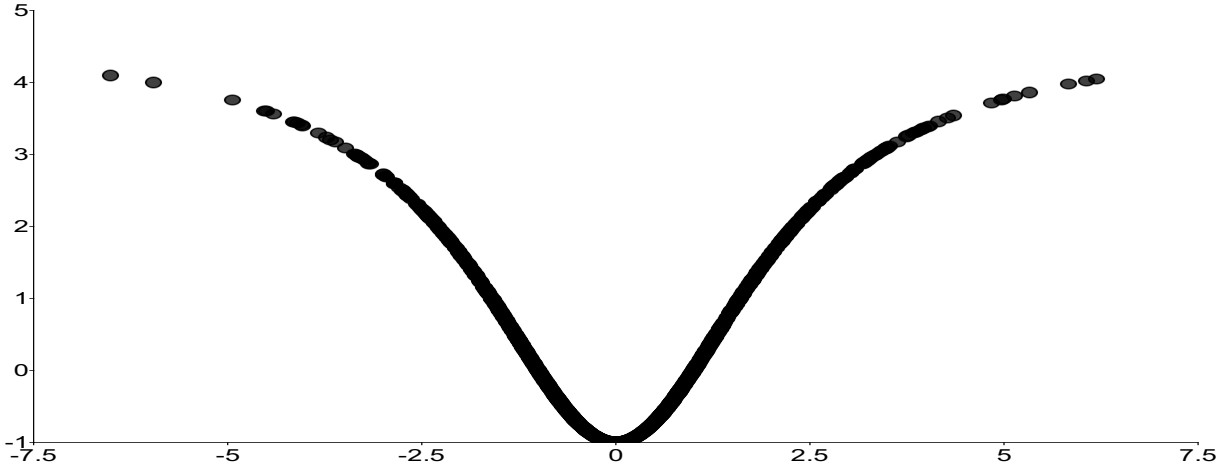

(b) Antarctic temperature anomalies, $u_{\lambda,t}$ as a function of ϵ_t for t-FI-QAR-Beta-t-EIGARCH

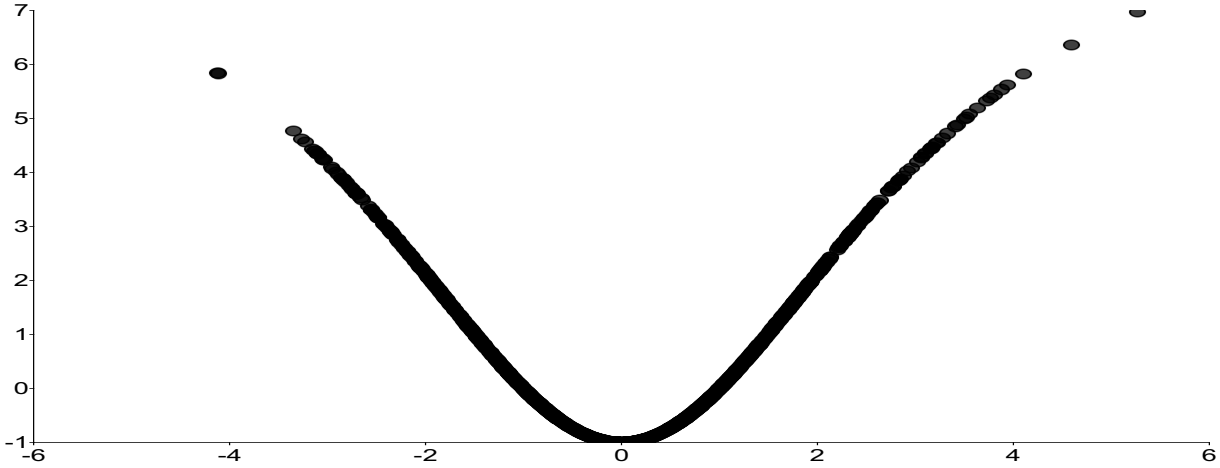

(c) Atlantic Ocean temperature anomalies, $u_{\lambda,t}$ as a function of ϵ_t for t-FI-QAR-Beta-t-EGARCH

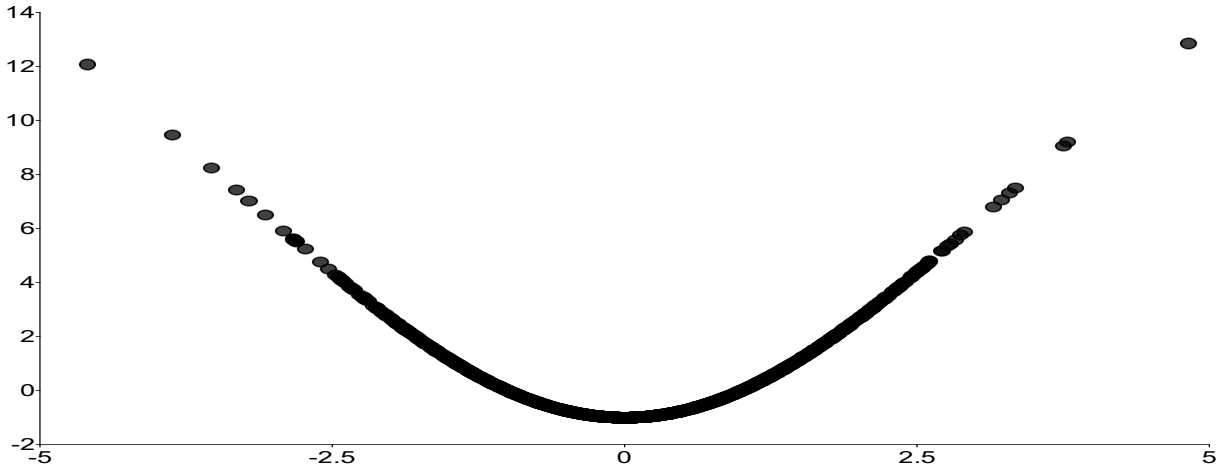

Figure B5. Impact of shocks on updating terms: $u_{\lambda,t}$ as a function of ϵ_t from January 1850 to October 2025 for the t-FI(d_t)-QAR(p)-Beta-t-EGARCH and t-FI(d_t)-QAR(p)-Beta-t-EIGARCH models.

(a) Northeast Pacific Ocean temperature anomalies, $u_{\lambda,t}$ as a function of ϵ_t for t-FI-QAR-Beta-t-EGARCH

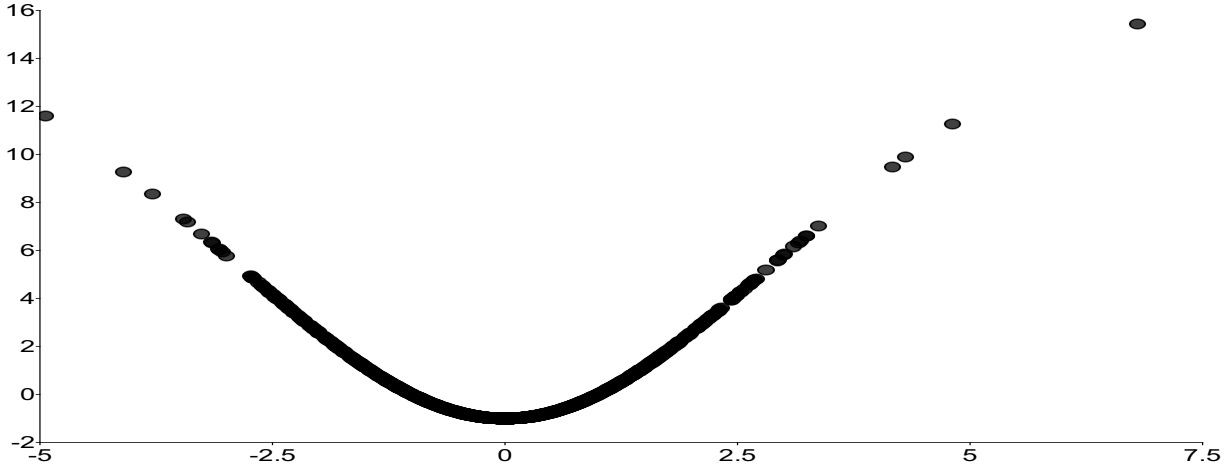

(b) Northern Hemisphere temperature anomalies, $u_{\lambda,t}$ as a function of ϵ_t for t-FI-QAR-Beta-t-EGARCH

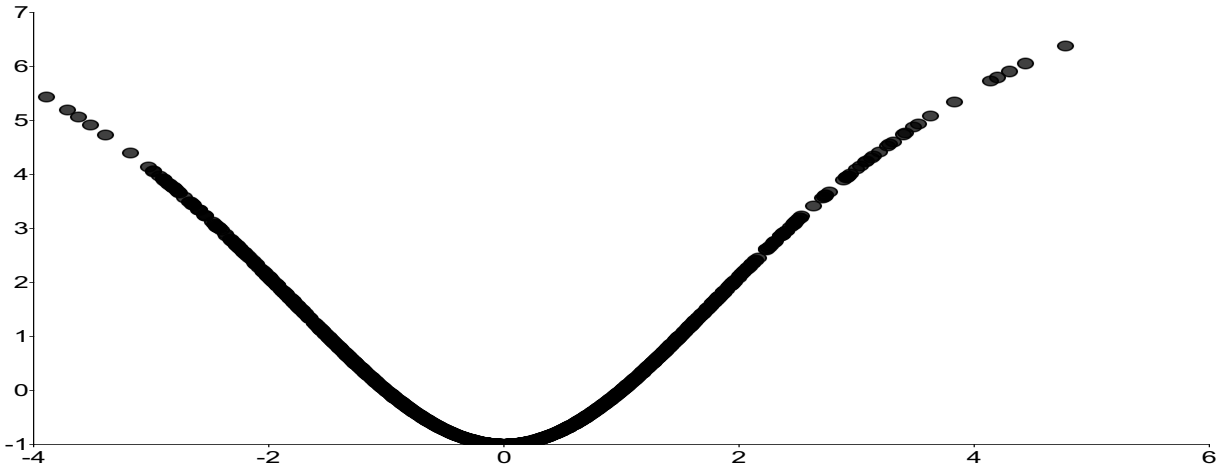

(c) Southern Hemisphere temperature anomalies, $u_{\lambda,t}$ as a function of ϵ_t for t-FI-QAR-Beta-t-EIGARCH

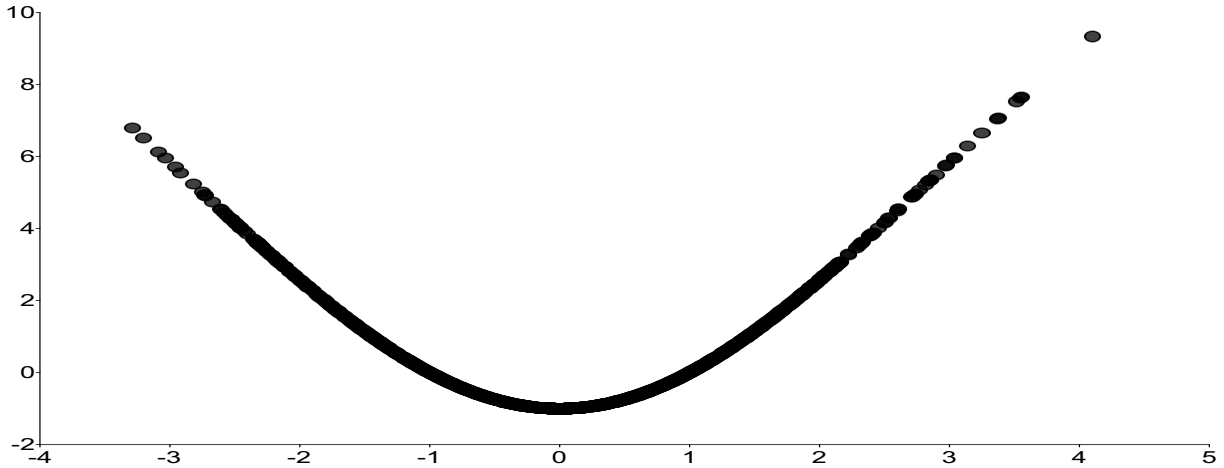

Figure B6. Impact of shocks on updating terms: $u_{\lambda,t}$ as a function of ϵ_t from January 1850 to October 2025 for the t-FI(d_t)-QAR(p)-Beta-t-EGARCH and t-FI(d_t)-QAR(p)-Beta-t-EIGARCH models.

(a) Arctic temperature anomalies, y_t and μ_t for t-FI-QAR-Beta-t-EGARCH

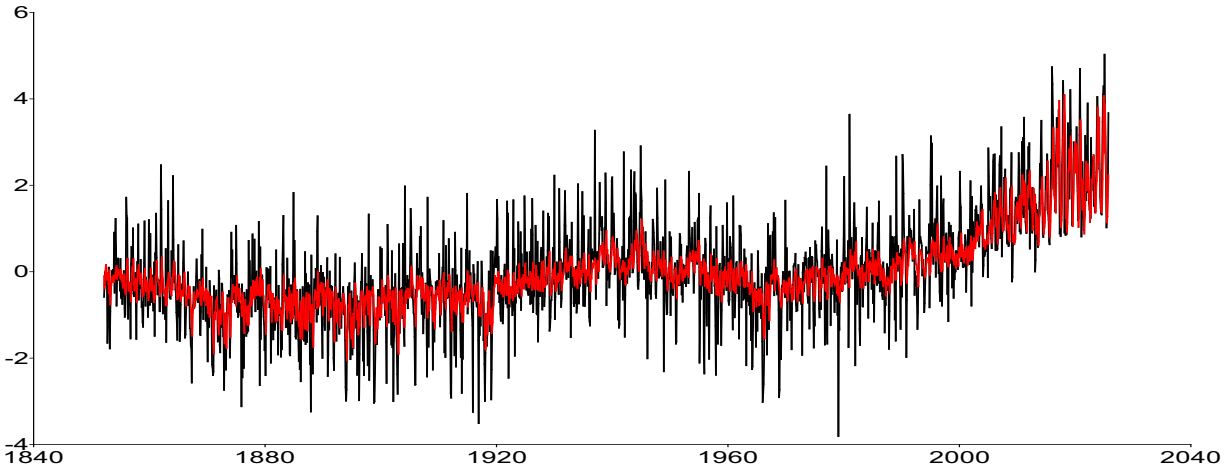

(b) Antarctic temperature anomalies, y_t and μ_t for t-FI-QAR-Beta-t-EIGARCH

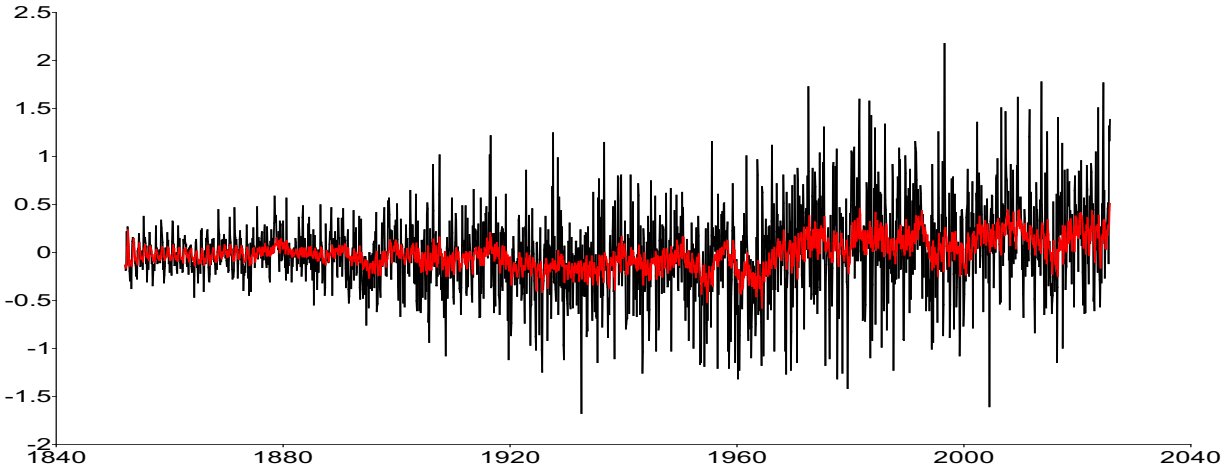

(c) Atlantic Ocean temperature anomalies, y_t and μ_t for t-FI-QAR-Beta-t-EGARCH

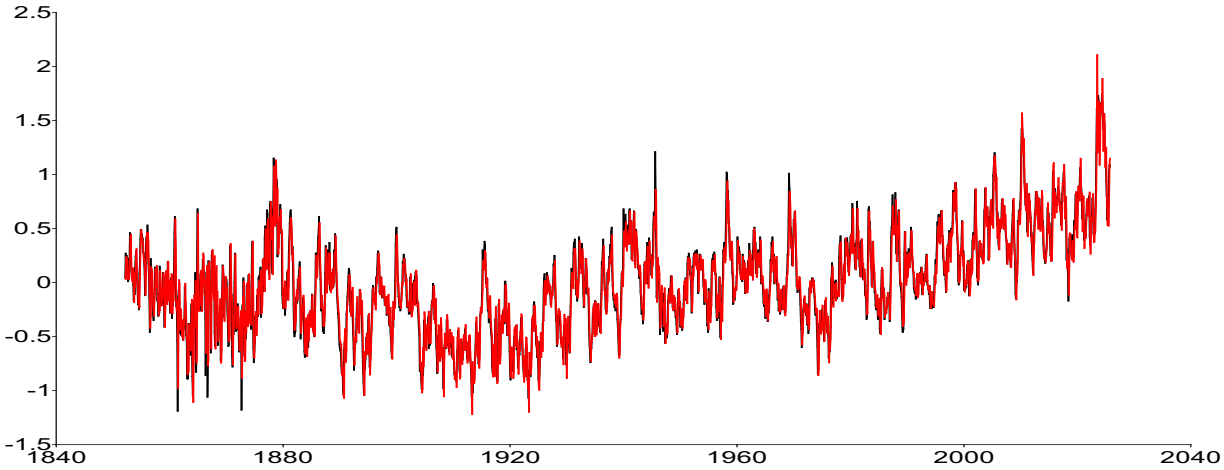

Figure B7. Evolution of y_t (black) and μ_t (red) from January 1850 to October 2025 for the t-FI(d_t)-QAR(p)-Beta-t-EGARCH and t-FI(d_t)-QAR(p)-Beta-t-EIGARCH models.

(a) Northeast Pacific Ocean temperature anomalies, y_t and μ_t for t-FI-QAR-Beta-t-EGARCH

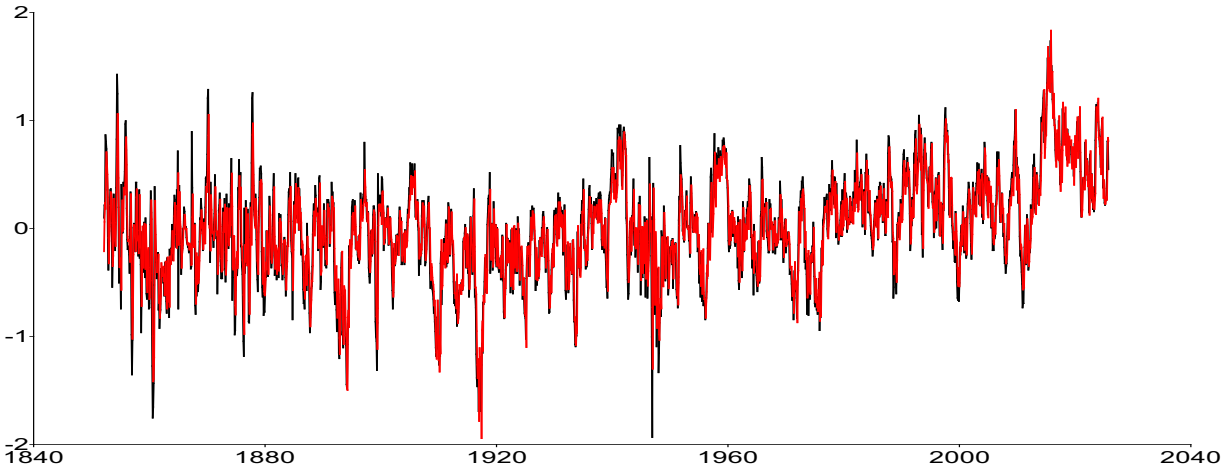

(b) Northern Hemisphere temperature anomalies, y_t and μ_t for t-FI-QAR-Beta-t-EGARCH

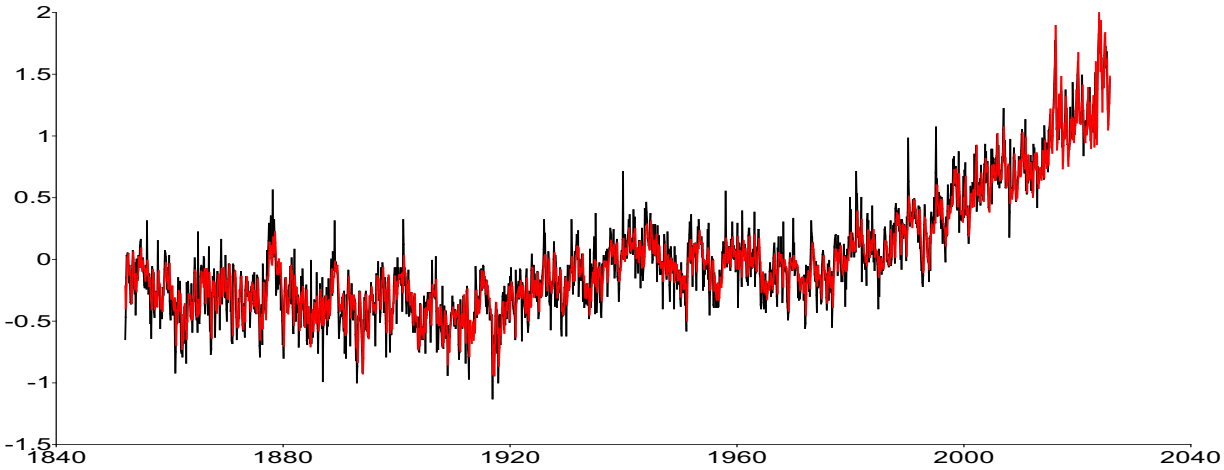

(c) Southern Hemisphere temperature anomalies, y_t and μ_t for t-FI-QAR-Beta-t-EIGARCH

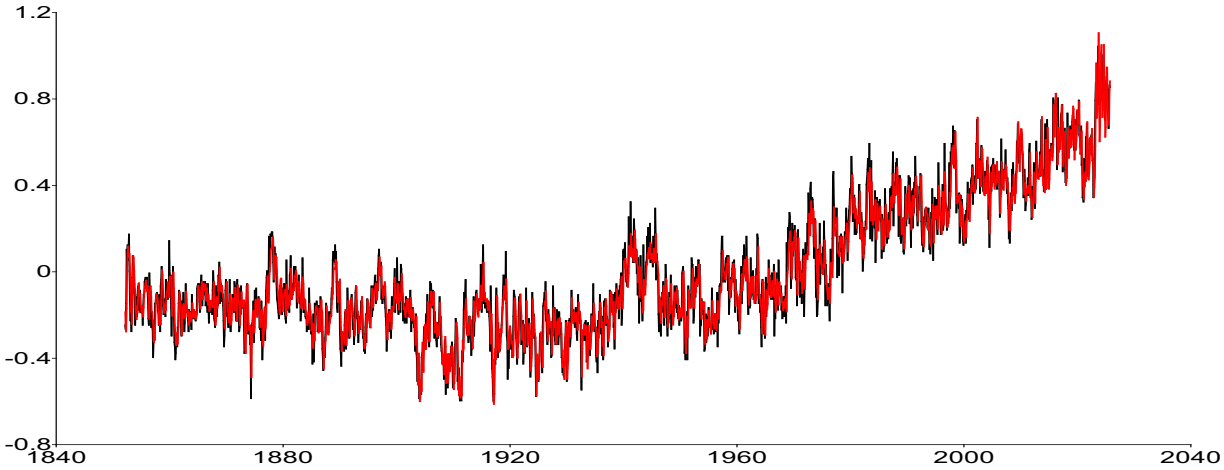

Figure B8. Evolution of y_t (black) and μ_t (red) from January 1850 to October 2025 for the t-FI(d_t)-QAR(p)-Beta-t-EGARCH and t-FI(d_t)-QAR(p)-Beta-t-EIGARCH models.

(a) Arctic temperature anomalies, degree of fractional integration d_t for t-FI-QAR-Beta-t-EGARCH

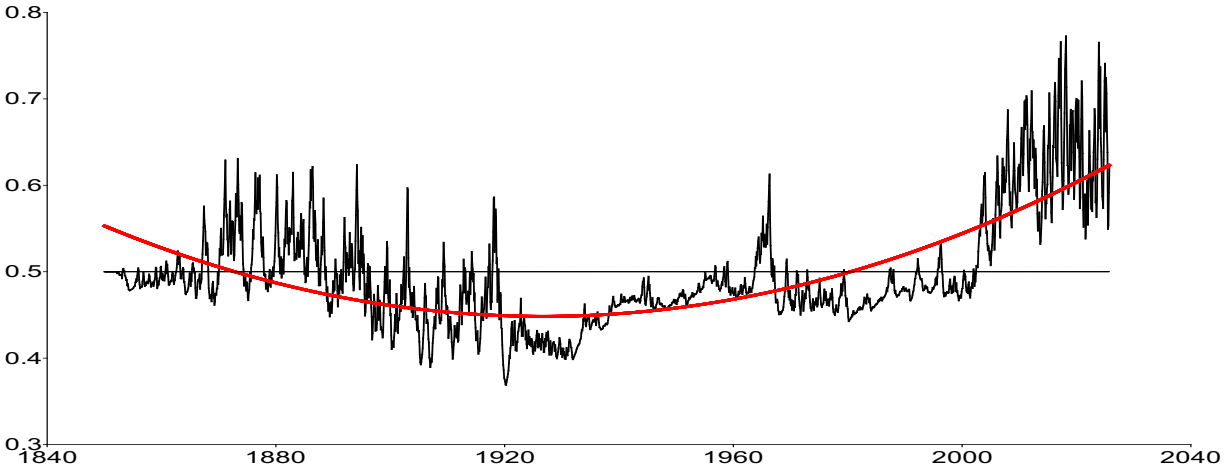

(b) Antarctic temperature anomalies, degree of fractional integration d_t for t-FI-QAR-Beta-t-EIGARCH

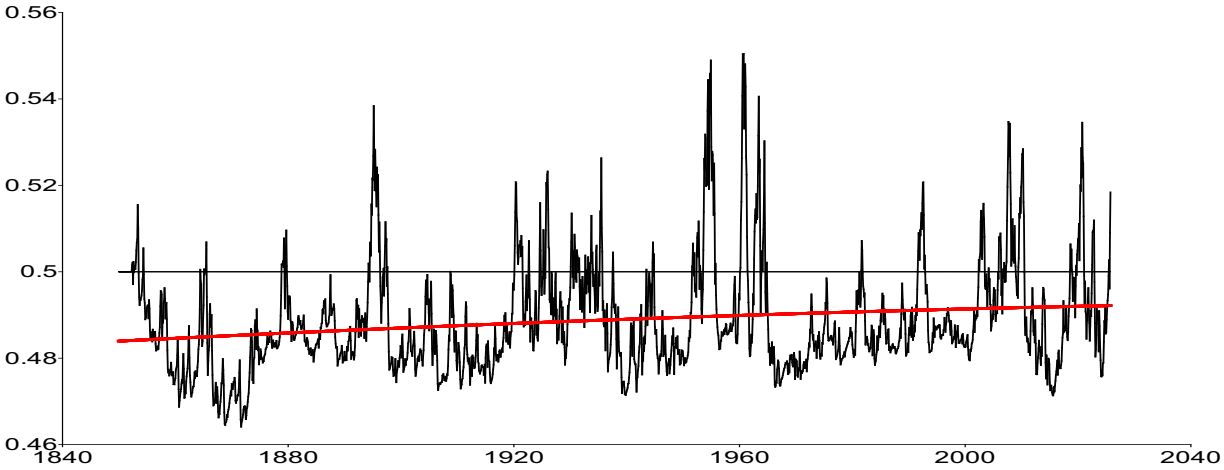

(c) Atlantic Ocean temperature anomalies, degree of fractional integration d_t for t-FI-QAR-Beta-t-EGARCH

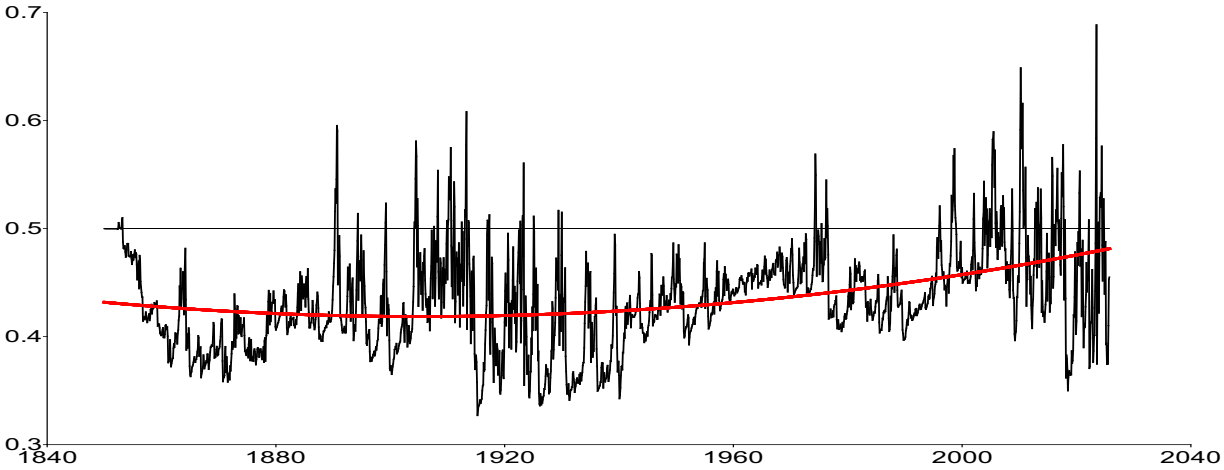

Figure B9. Degree of fractional integration of temperature anomalies d_t from January 1850 to October 2025 for the t-FI(d_t)-QAR(p)-Beta-t-EGARCH and t-FI(d_t)-QAR(p)-Beta-t-EIGARCH models. *Notes:* We present the degree of fractional integration of temperature anomalies d_t (black) and the fitted quadratic polynomial (red).

(a) Northeast Pacific Ocean temperature anomalies, degree of fractional integration d_t for t-FI-QAR-Beta-t-EGARCH

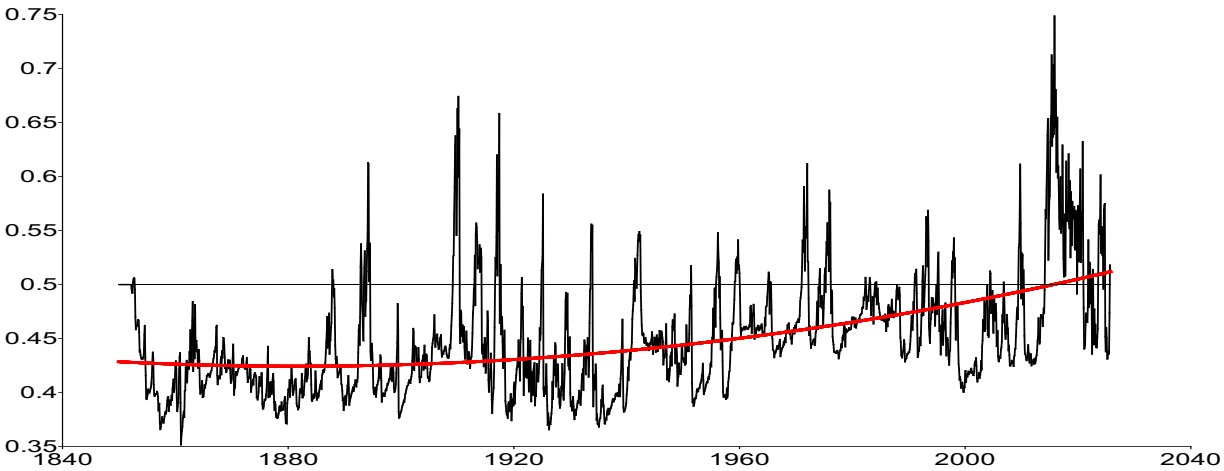

(b) Northern Hemisphere temperature anomalies, degree of fractional integration d_t for t-FI-QAR-Beta-t-EGARCH

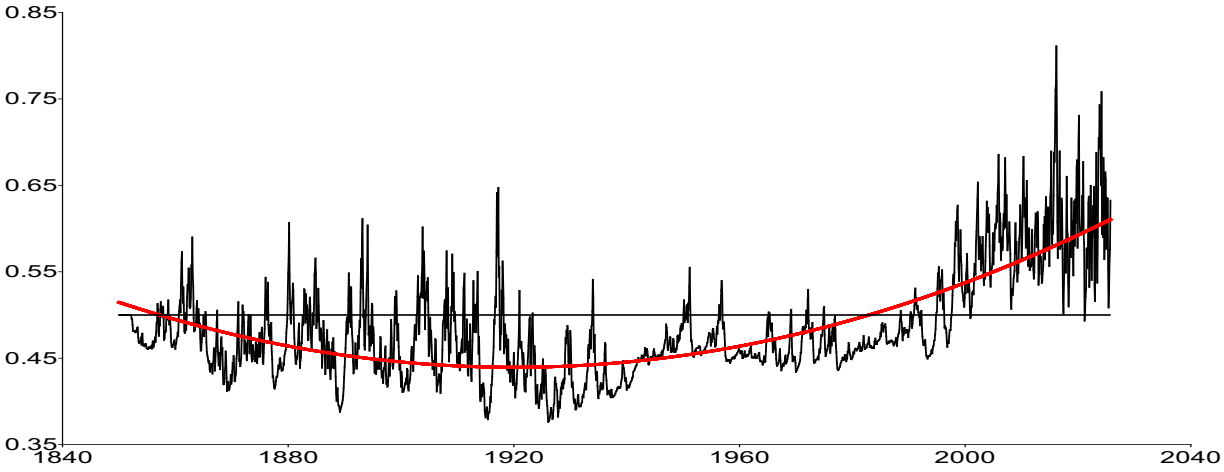

(c) Southern Hemisphere temperature anomalies, degree of fractional integration d_t for t-FI-QAR-Beta-t-EIGARCH

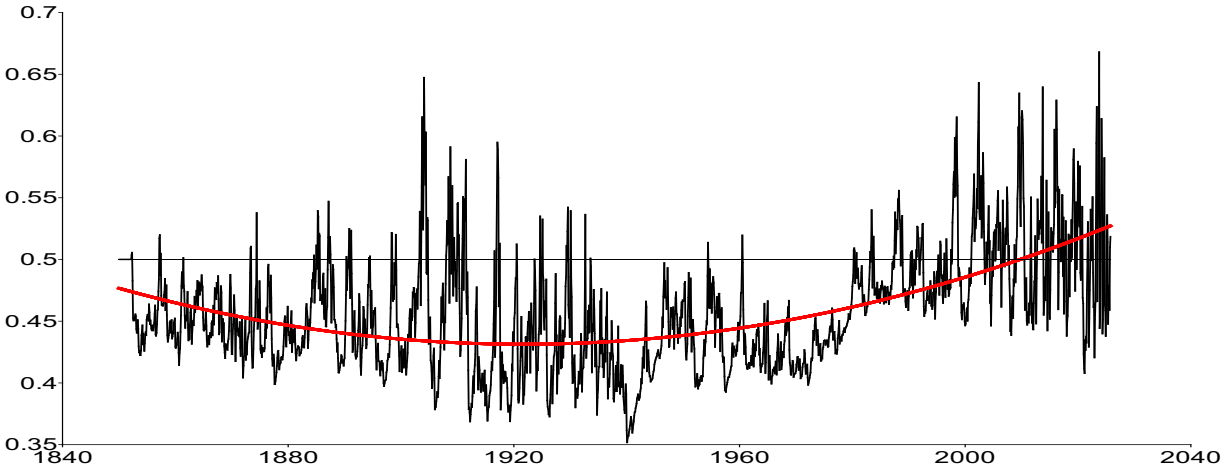

Figure B10. Degree of fractional integration of temperature anomalies d_t from January 1850 to October 2025 for the t-FI(d_t)-QAR(p)-Beta-t-EGARCH and t-FI(d_t)-QAR(p)-Beta-t-EIGARCH models. *Notes:* We present the degree of fractional integration of temperature anomalies d_t (black) and the fitted quadratic polynomial (red).

(a) Arctic temperature anomalies, log scale λ_t for t-FI-QAR-Beta-t-EGARCH

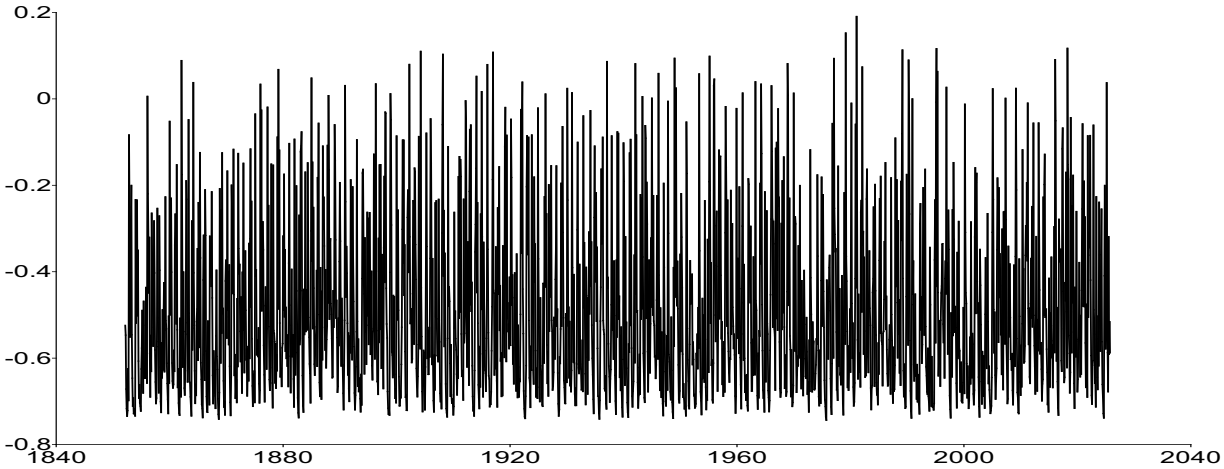

(b) Antarctic temperature anomalies, log scale λ_t for t-FI-QAR-Beta-t-EIGARCH

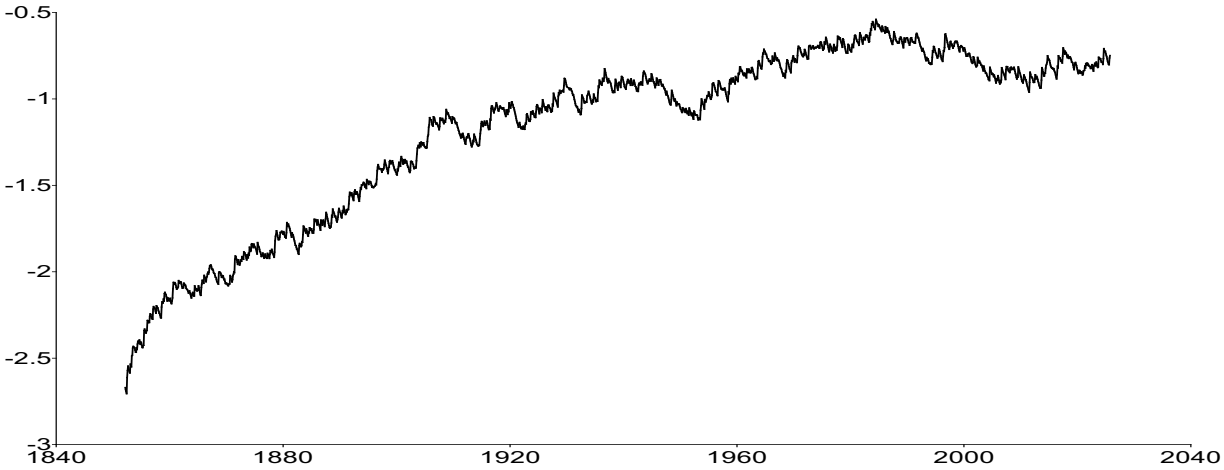

(c) Atlantic Ocean temperature anomalies, log scale λ_t for t-FI-QAR-Beta-t-EGARCH

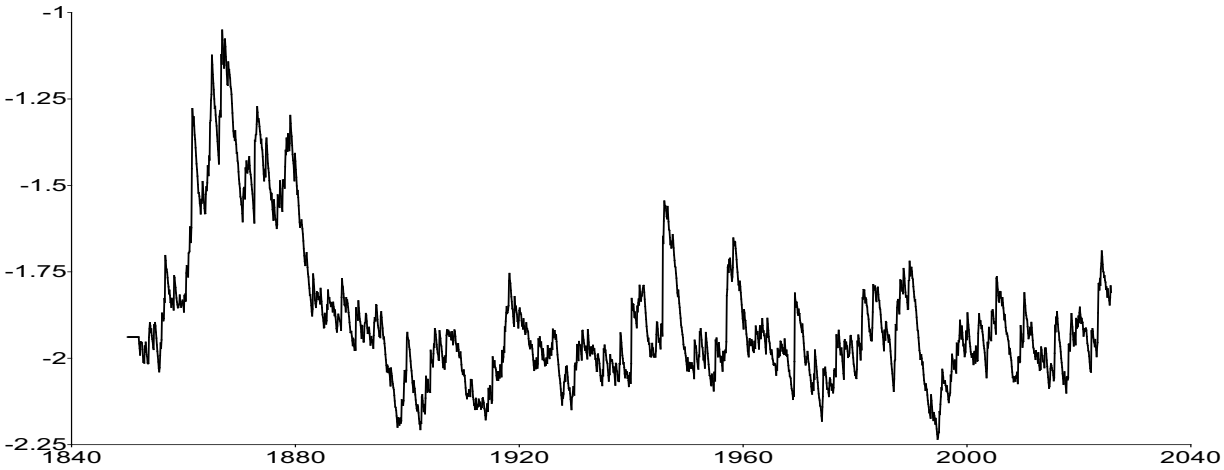

Figure B11. Log scale λ_t from January 1850 to October 2025 for the t-FI(d_t)-QAR(p)-Beta-t-EGARCH and t-FI(d_t)-QAR(p)-Beta-t-EIGARCH models.

(a) Northeast Pacific Ocean temperature anomalies, log scale λ_t for t-FI-QAR-Beta-t-EGARCH

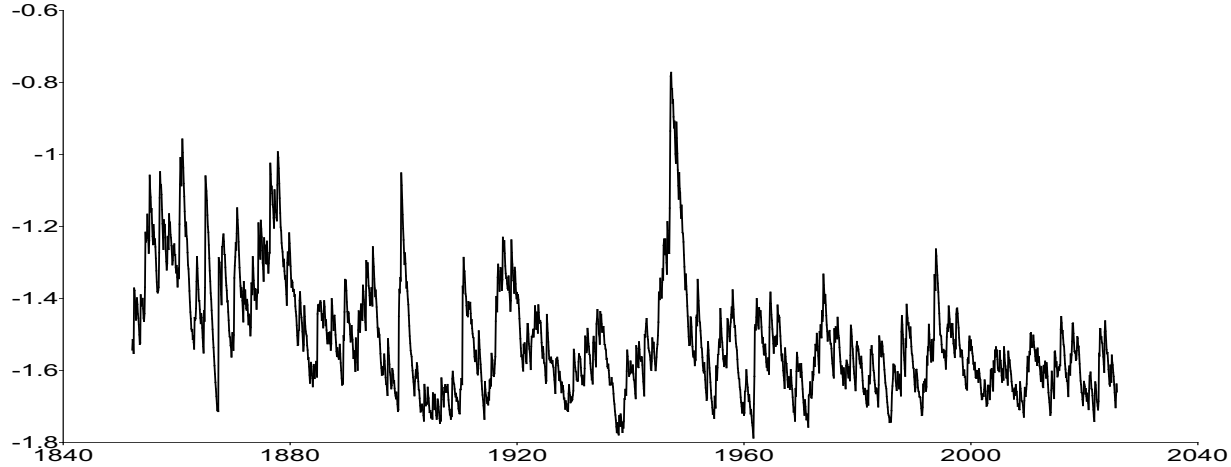

(b) Northern Hemisphere temperature anomalies, log scale λ_t for t-FI-QAR-Beta-t-EGARCH

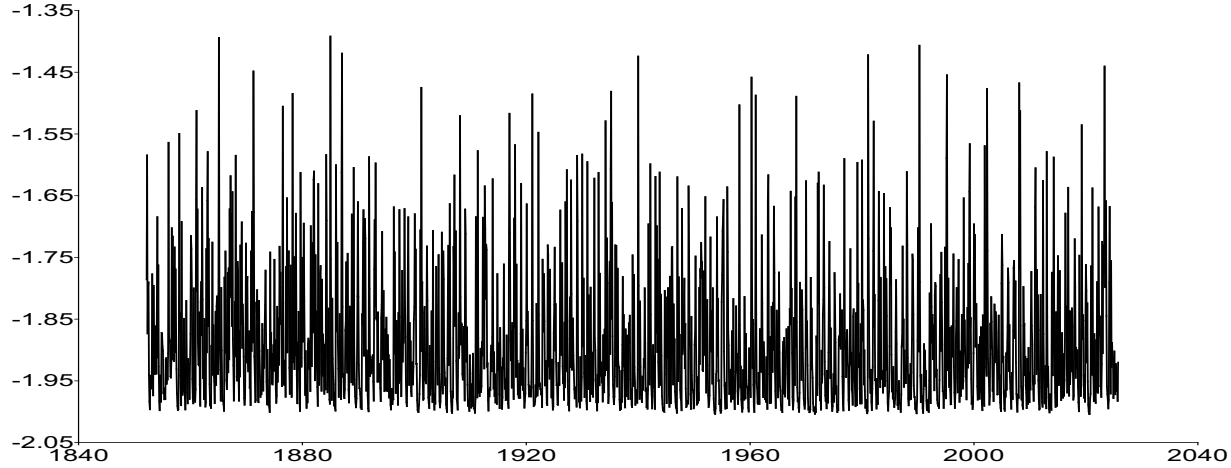

(c) Southern Hemisphere temperature anomalies, log scale λ_t for t-FI-QAR-Beta-t-EIGARCH

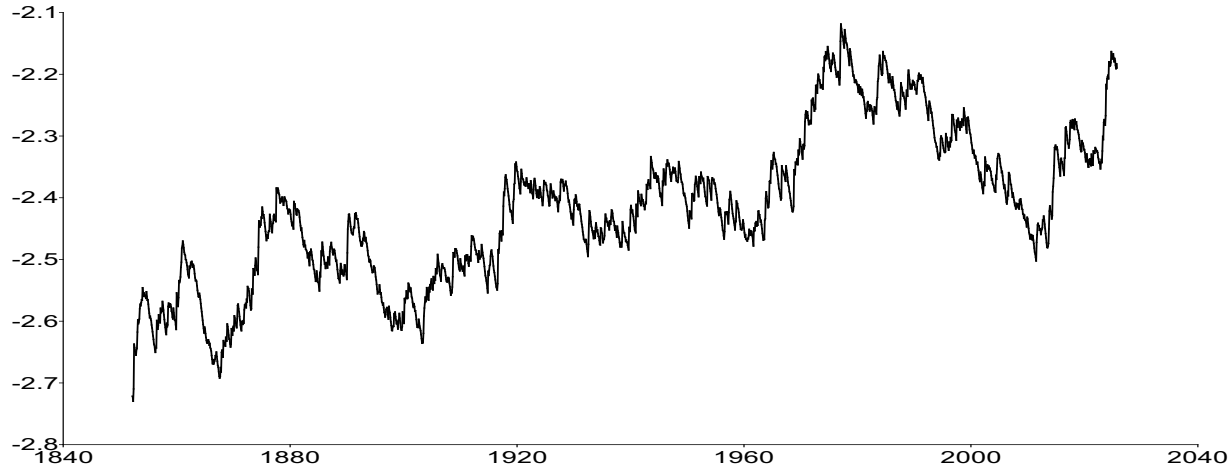

Figure B12. Log scale λ_t from January 1850 to October 2025 for the t-FI(d_t)-QAR(p)-Beta-t-EGARCH and t-FI(d_t)-QAR(p)-Beta-t-EIGARCH models.

(a) Arctic temperature anomalies, conditional standard deviation σ_t for t-FI-QAR-Beta-t-EGARCH

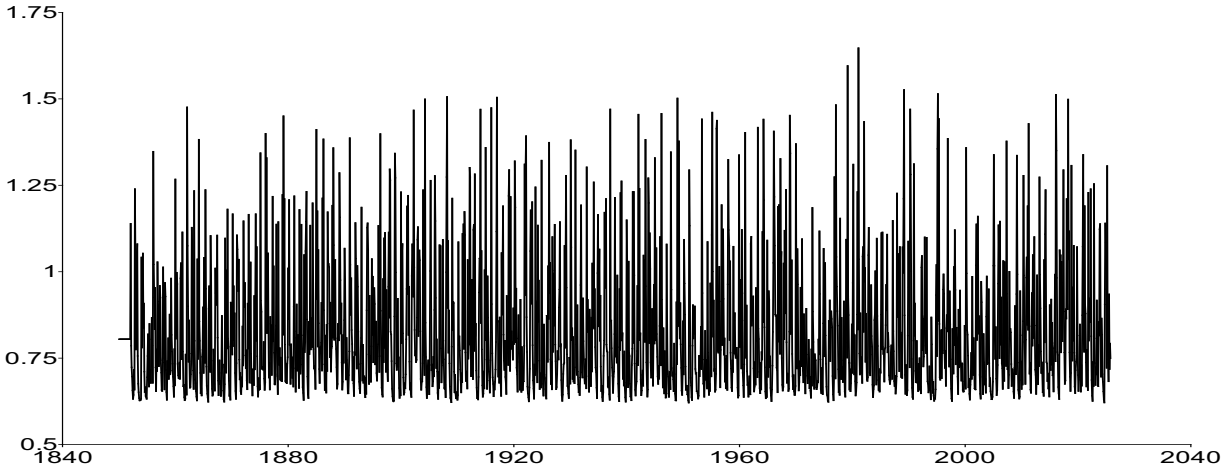

(b) Antarctic temperature anomalies, conditional standard deviation σ_t for t-FI-QAR-Beta-t-EIGARCH

(c) Atlantic Ocean temperature anomalies, conditional standard deviation σ_t for t-FI-QAR-Beta-t-EGARCH

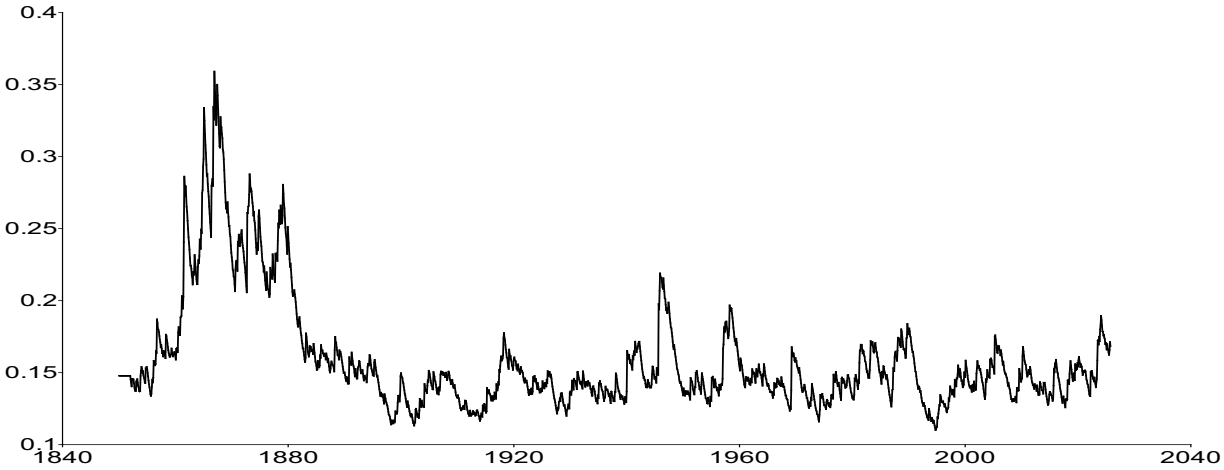

Figure B13. Conditional standard deviation σ_t from January 1850 to October 2025 for the t-FI(d_t)-QAR(p)-Beta-t-EGARCH and t-FI(d_t)-QAR(p)-Beta-t-EIGARCH models.

(a) Northeast Pacific Ocean temperature anomalies, conditional standard deviation σ_t for t-FI-QAR-Beta-t-EGARCH

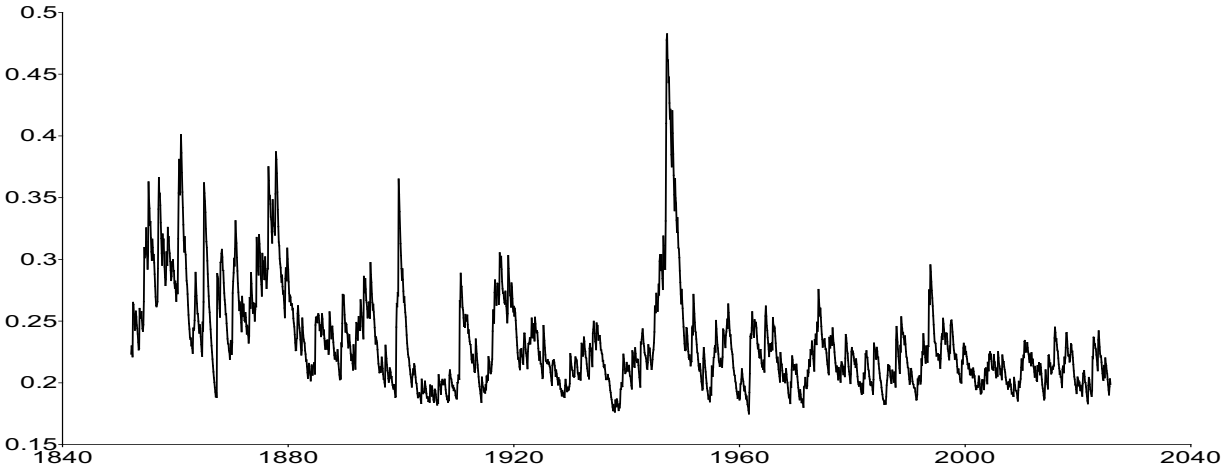

(b) Northern Hemisphere temperature anomalies, conditional standard deviation σ_t for t-FI-QAR-Beta-t-EGARCH

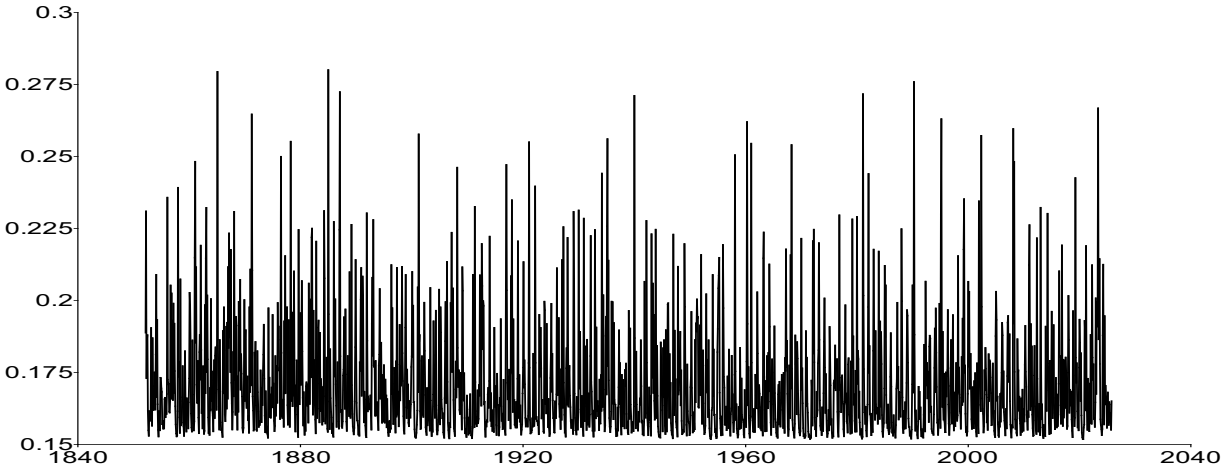

(c) Southern Hemisphere temperature anomalies, conditional standard deviation σ_t for t-FI-QAR-Beta-t-EIGARCH

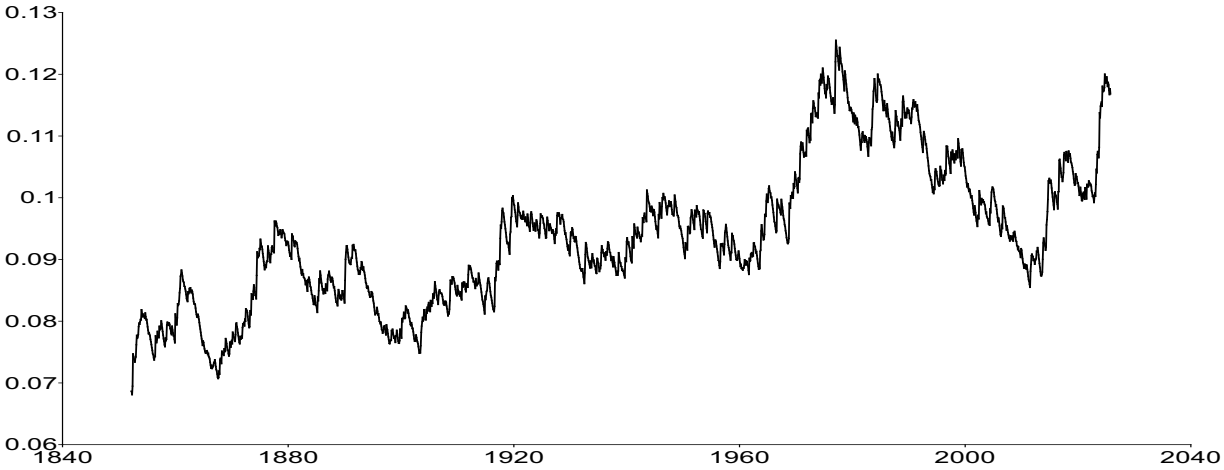

Figure B14. Conditional standard deviation σ_t from January 1850 to October 2025 for the t-FI(d_t)-QAR(p)-Beta-t-EGARCH and t-FI(d_t)-QAR(p)-Beta-t-EIGARCH models.

(a) Arctic temperature anomalies, standardized error term ϵ_t for t-FI-QAR-Beta-t-EGARCH

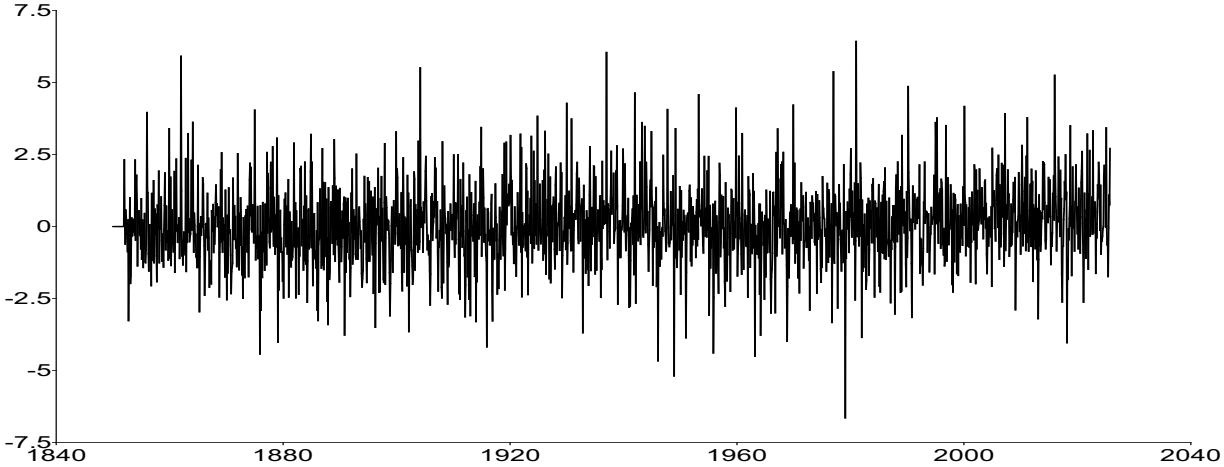

(b) Antarctic temperature anomalies, standardized error term ϵ_t for t-FI-QAR-Beta-t-EIGARCH

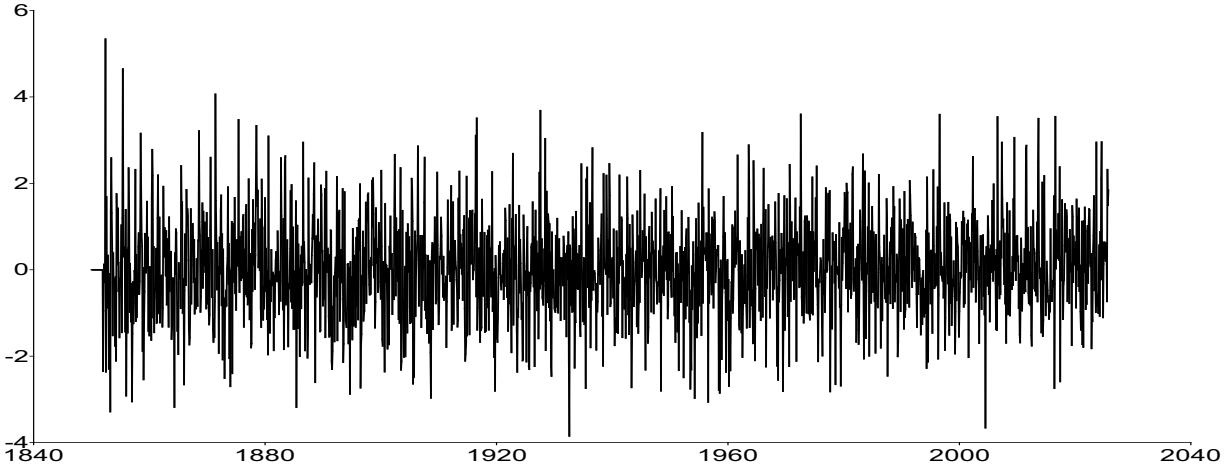

(c) Atlantic Ocean temperature anomalies, standardized error term ϵ_t for t-FI-QAR-Beta-t-EGARCH

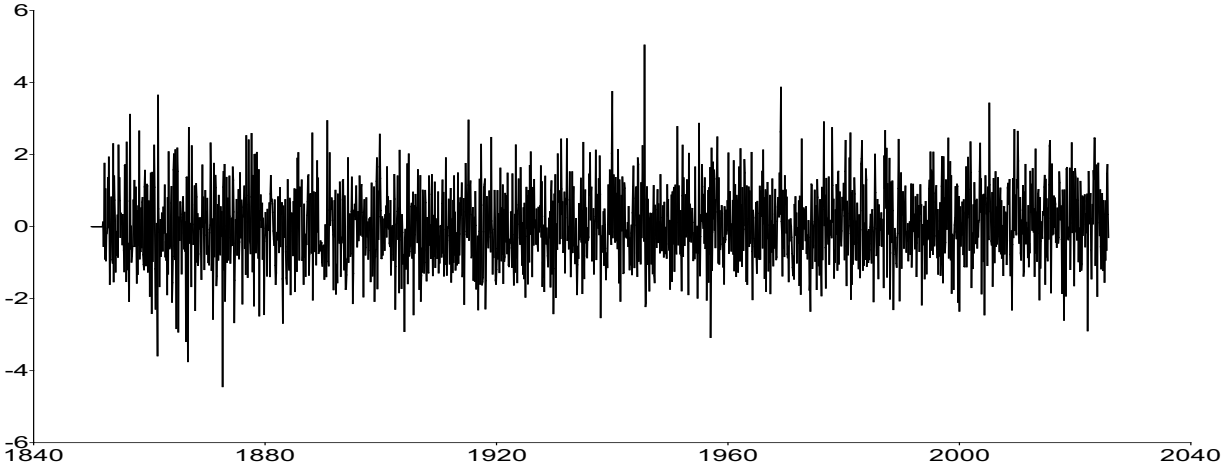

Figure B15. Standardized error term ϵ_t from January 1850 to October 2025 for the t-FI(d_t)-QAR(p)-Beta-t-EGARCH and t-FI(d_t)-QAR(p)-Beta-t-EIGARCH models.

(a) Northeast Pacific Ocean temperature anomalies, standardized error term ϵ_t for t-FI-QAR-Beta-t-EGARCH

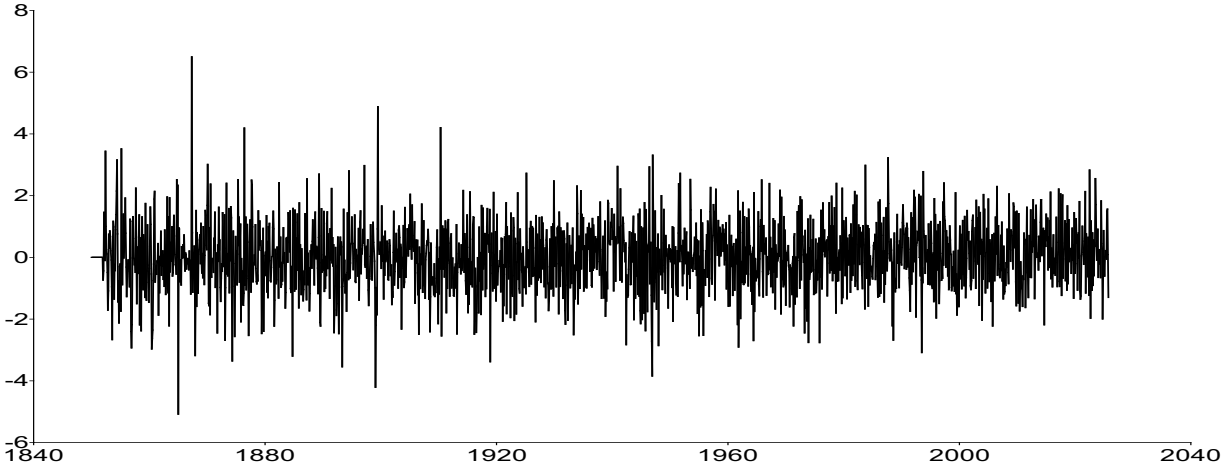

(b) Northern Hemisphere temperature anomalies, standardized error term ϵ_t for t-FI-QAR-Beta-t-EGARCH

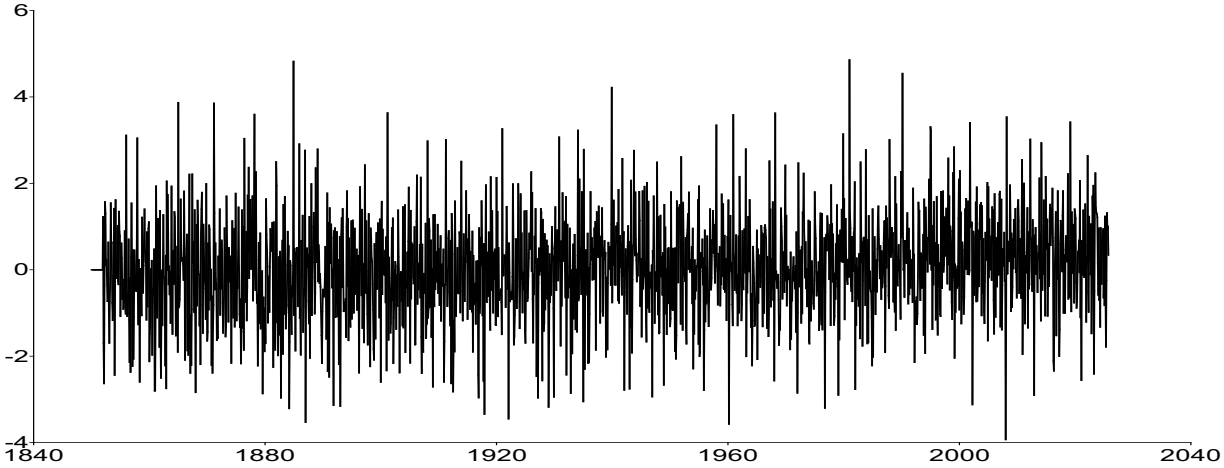

(c) Southern Hemisphere temperature anomalies, standardized error term ϵ_t for t-FI-QAR-Beta-t-EIGARCH

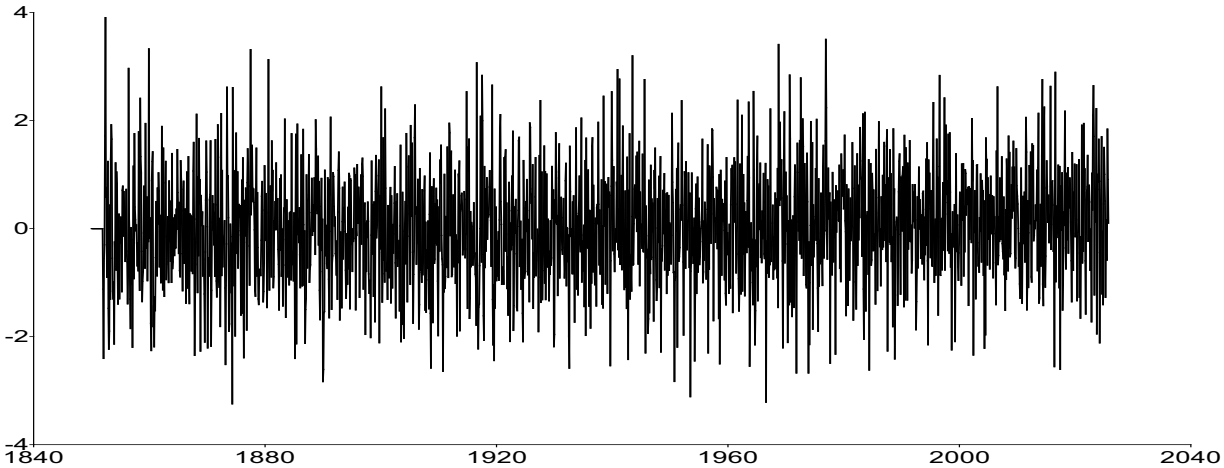

Figure B16. Standardized error term ϵ_t from January 1850 to October 2025 for the t-FI(d_t)-QAR(p)-Beta-t-EGARCH and t-FI(d_t)-QAR(p)-Beta-t-EIGARCH models.

(a) Arctic temperature anomalies, scaled error term v_t for t-FI-QAR-Beta-t-EGARCH

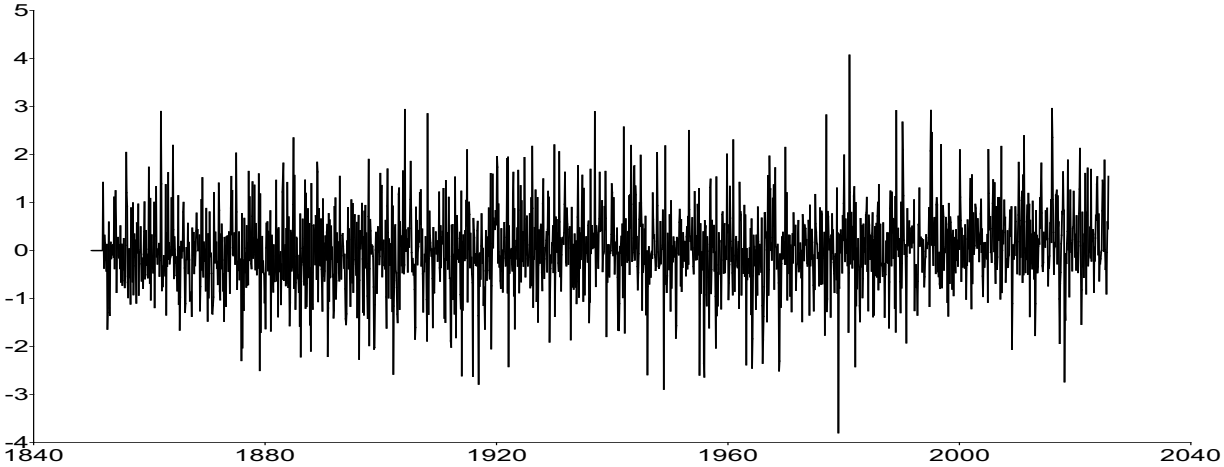

(b) Antarctic temperature anomalies, scaled error term v_t for t-FI-QAR-Beta-t-EIGARCH

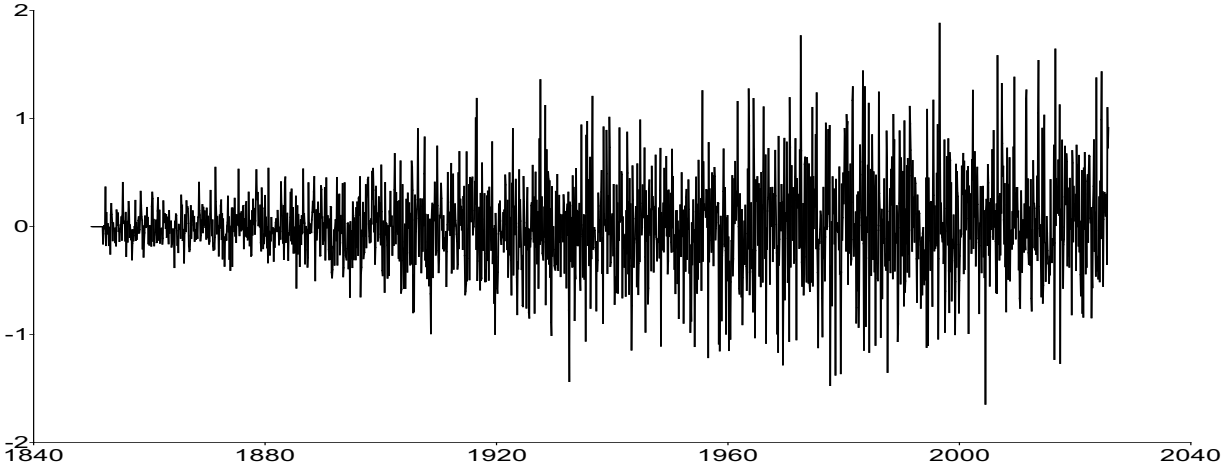

(c) Atlantic Ocean temperature anomalies, scaled error term v_t for t-FI-QAR-Beta-t-EGARCH

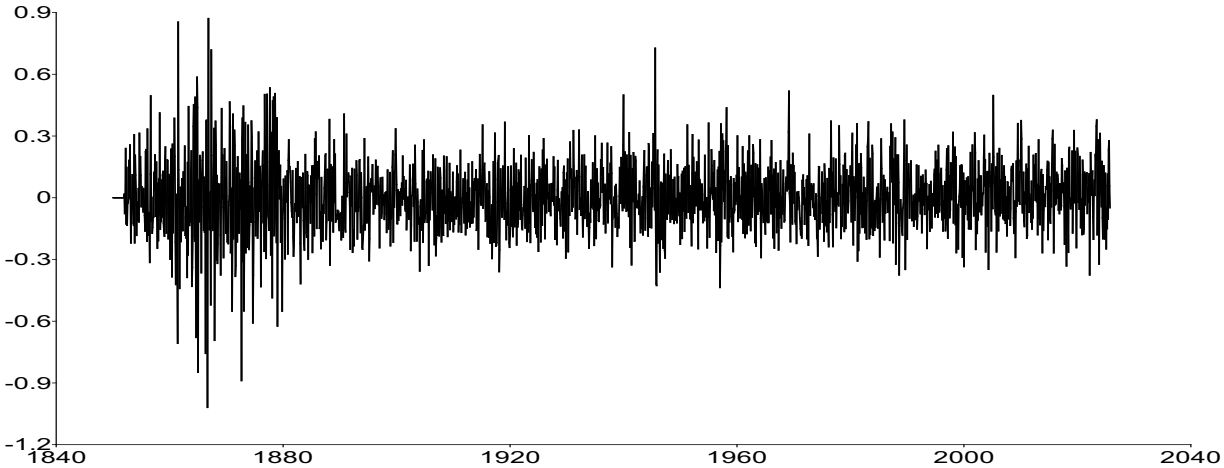

Figure B17. Scaled error term v_t from January 1850 to October 2025 for the t-FI(d_t)-QAR(p)-Beta-t-EGARCH and t-FI(d_t)-QAR(p)-Beta-t-EIGARCH models.

(a) Northeast Pacific Ocean temperature anomalies, scaled error term v_t for t-FI-QAR-Beta-t-EGARCH

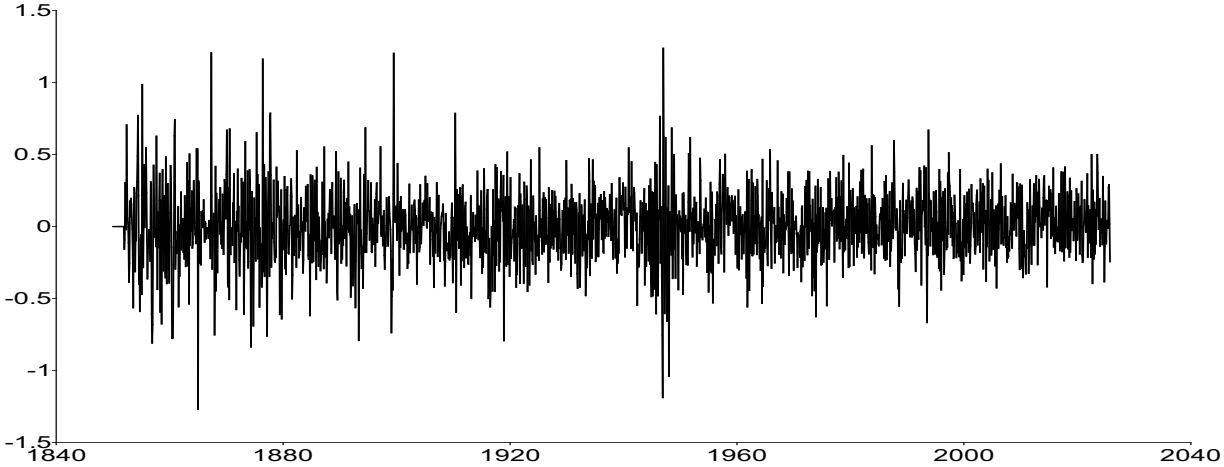

(b) Northern Hemisphere temperature anomalies, scaled error term v_t for t-FI-QAR-Beta-t-EGARCH

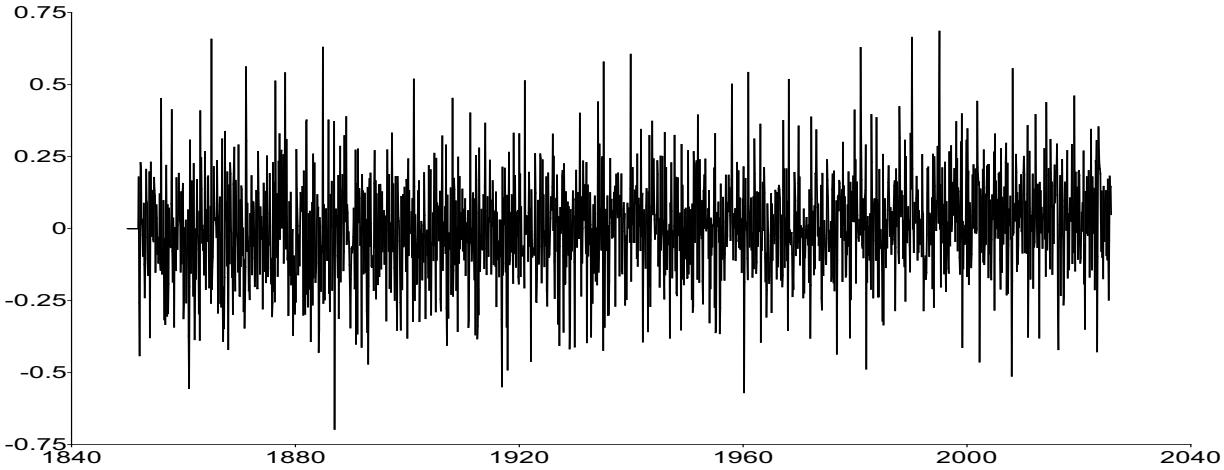

(c) Southern Hemisphere temperature anomalies, scaled error term v_t for t-FI-QAR-Beta-t-EIGARCH

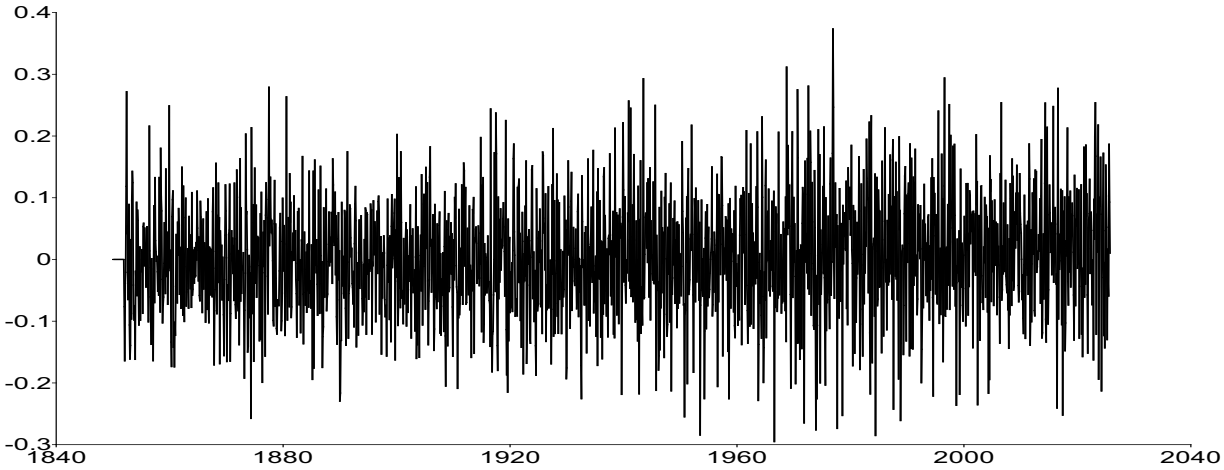

Figure B18. Scaled error term v_t from January 1850 to October 2025 for the t-FI(d_t)-QAR(p)-Beta-t-EGARCH and t-FI(d_t)-QAR(p)-Beta-t-EIGARCH models.

(a) Arctic temperature anomalies, location score function $u_{\mu,t}$ for t-FI-QAR-Beta-t-EGARCH

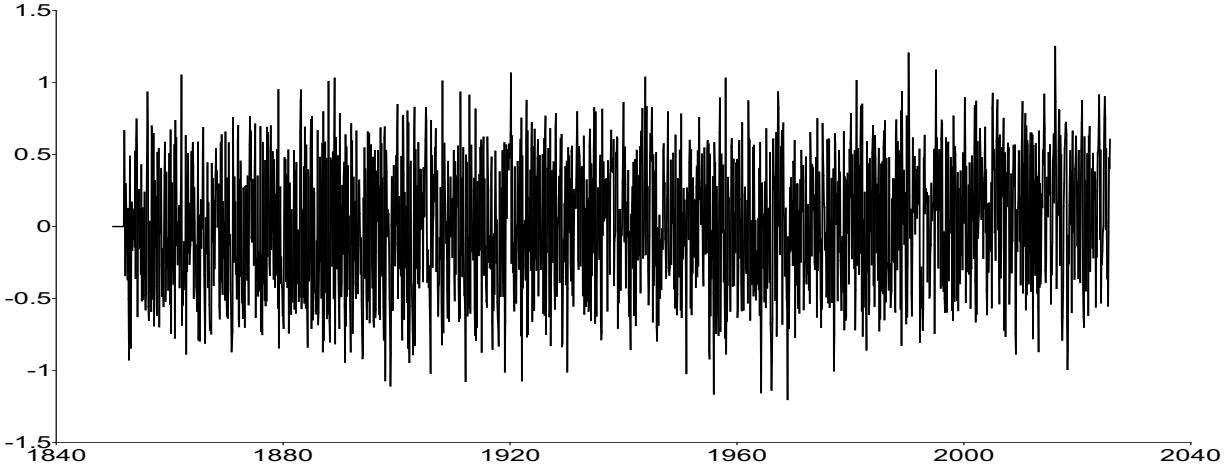

(b) Antarctic temperature anomalies, location score function $u_{\mu,t}$ for t-FI-QAR-Beta-t-EIGARCH

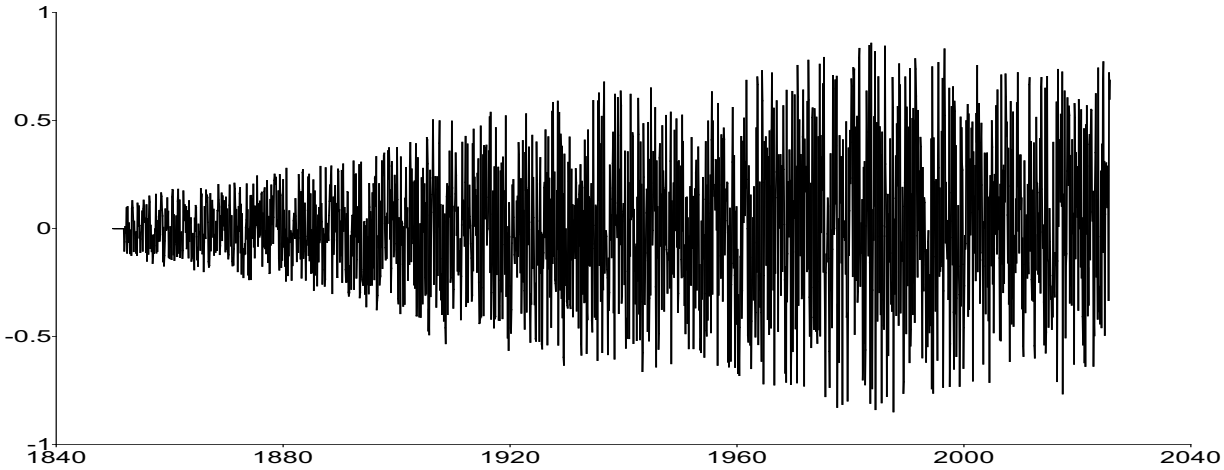

(c) Atlantic Ocean temperature anomalies, location score function $u_{\mu,t}$ for t-FI-QAR-Beta-t-EGARCH

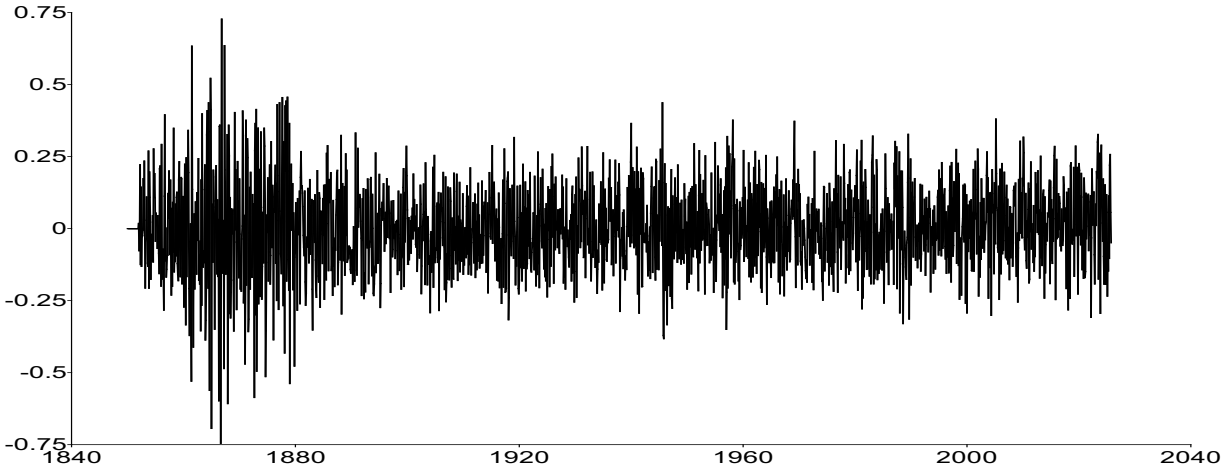

Figure B19. Location score function $u_{\mu,t}$ from January 1850 to October 2025 for the t-FI(d_t)-QAR(p)-Beta-t-EGARCH and t-FI(d_t)-QAR(p)-Beta-t-EIGARCH models.

(a) Northeast Pacific Ocean temperature anomalies, location score function $u_{\mu,t}$ for t-FI-QAR-Beta-t-EGARCH

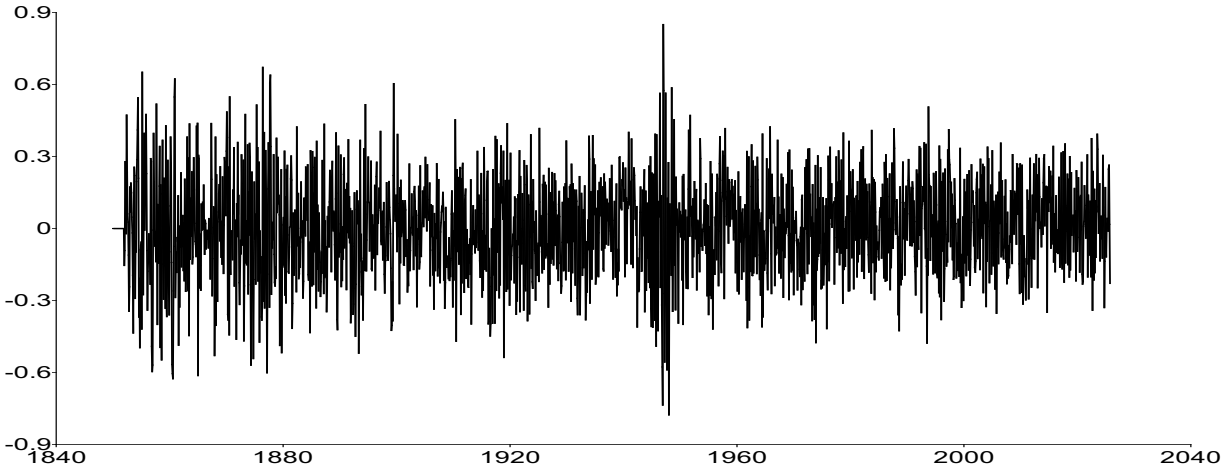

(b) Northern Hemisphere temperature anomalies, location score function $u_{\mu,t}$ for t-FI-QAR-Beta-t-EGARCH

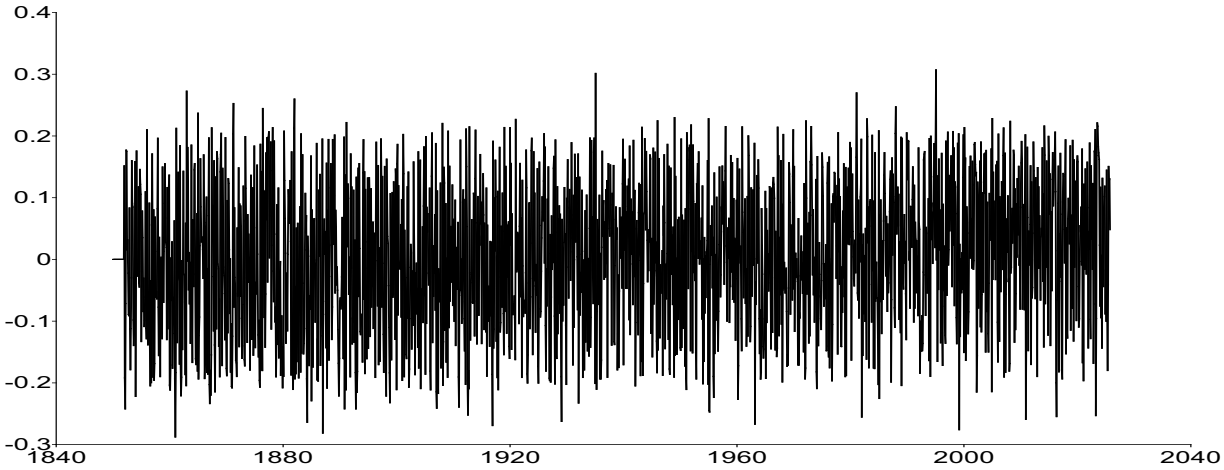

(c) Southern Hemisphere temperature anomalies, location score function $u_{\mu,t}$ for t-FI-QAR-Beta-t-EIGARCH

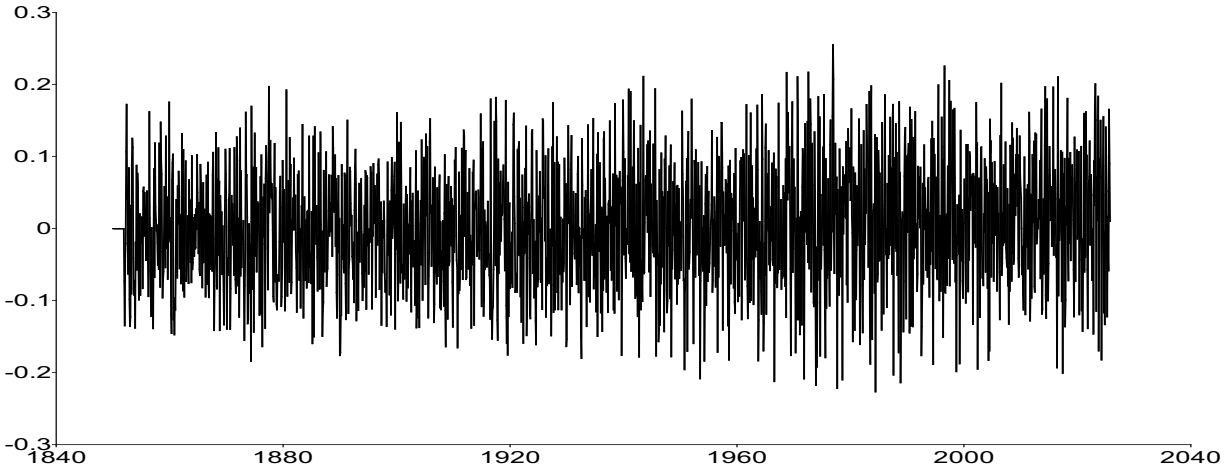

Figure B20. Location score function $u_{\mu,t}$ from January 1850 to October 2025 for the t-FI(d_t)-QAR(p)-Beta-t-EGARCH and t-FI(d_t)-QAR(p)-Beta-t-EIGARCH models.

(a) Arctic temperature anomalies, degree of fractional integration score function $u_{d,t}$ for t-FI-QAR-Beta-t-EGARCH

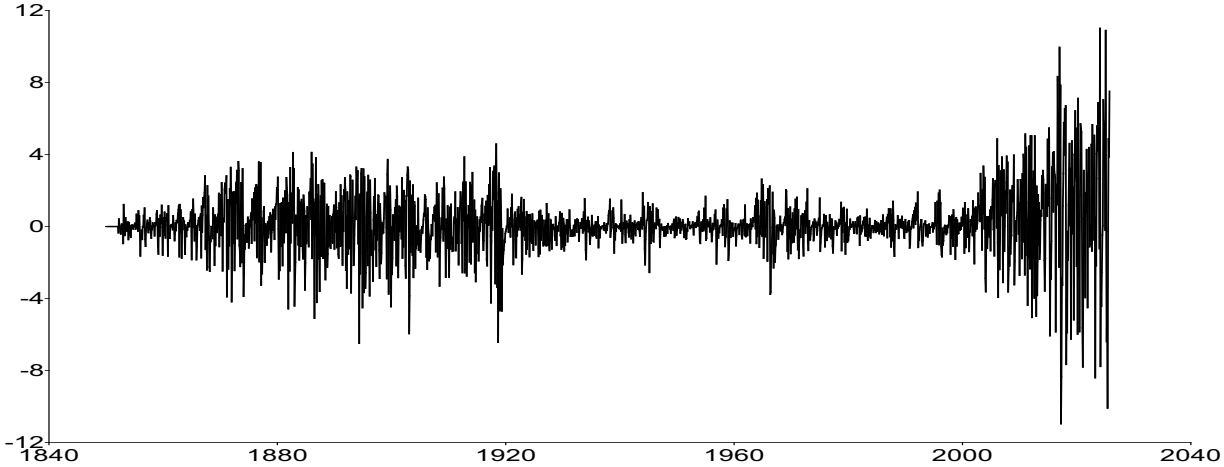

(b) Antarctic temperature anomalies, degree of fractional integration score function $u_{d,t}$ for t-FI-QAR-Beta-t-EIGARCH

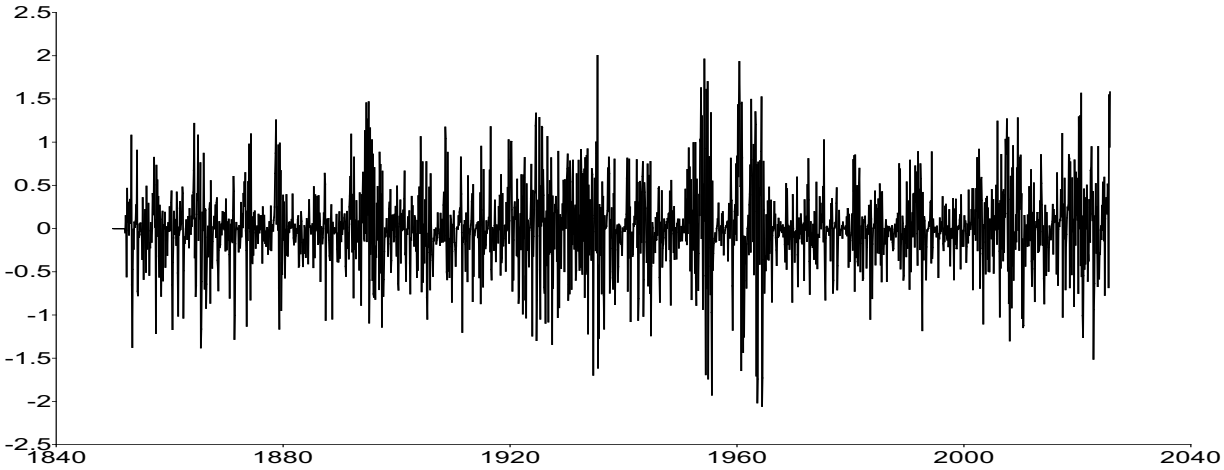

(c) Atlantic Ocean temperature anomalies, degree of fractional integration score function $u_{d,t}$ for t-FI-QAR-Beta-t-EGARCH

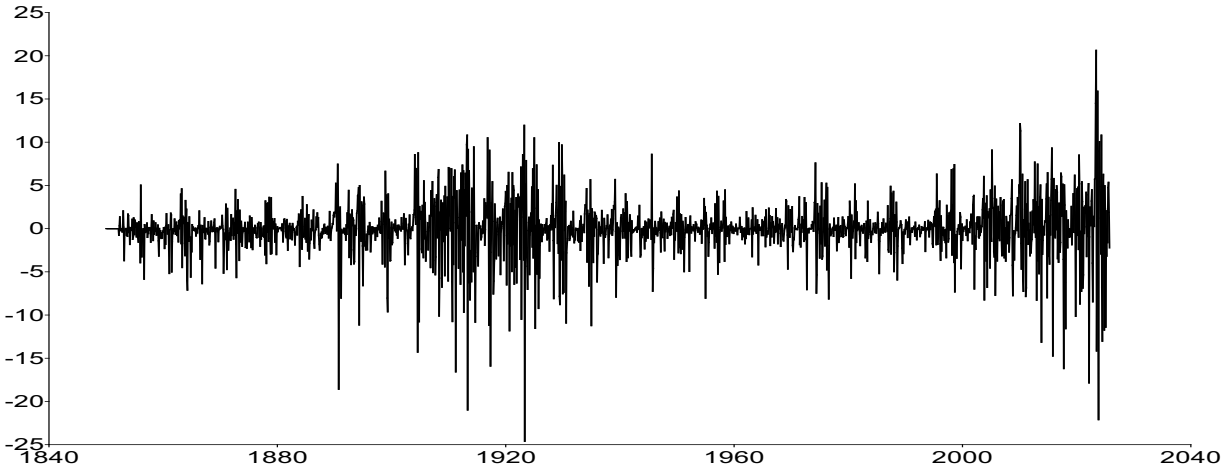

Figure B21. Degree of fractional integration score function $u_{d,t}$ from January 1850 to October 2025 for the t-FI(d_t)-QAR(p)-Beta-t-EGARCH and t-FI(d_t)-QAR(p)-Beta-t-EIGARCH models.

(a) Northeast Pacific Ocean temperature anomalies, degree of fractional integration score function $u_{d,t}$ for t-FI-QAR-Beta-t-EGARCH

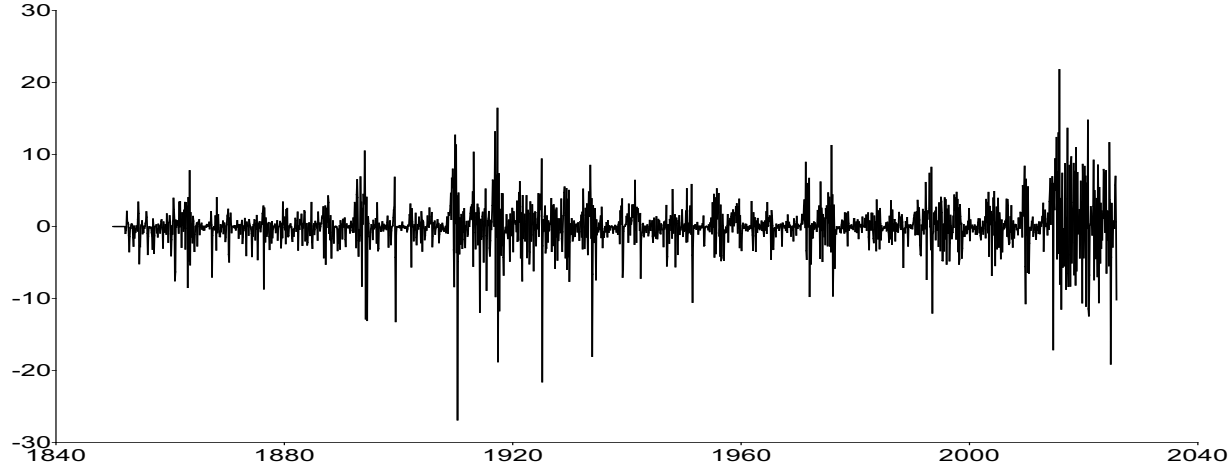

(b) Northern Hemisphere temperature anomalies, degree of fractional integration score function $u_{d,t}$ for t-FI-QAR-Beta-t-EGARCH

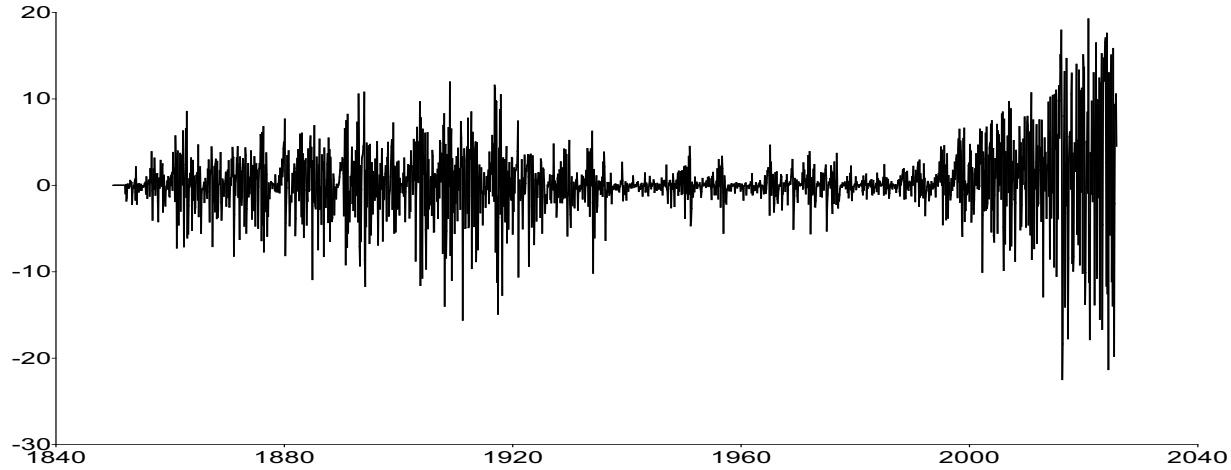

(c) Southern Hemisphere temperature anomalies, degree of fractional integration score function $u_{d,t}$ for t-FI-QAR-Beta-t-EIGARCH

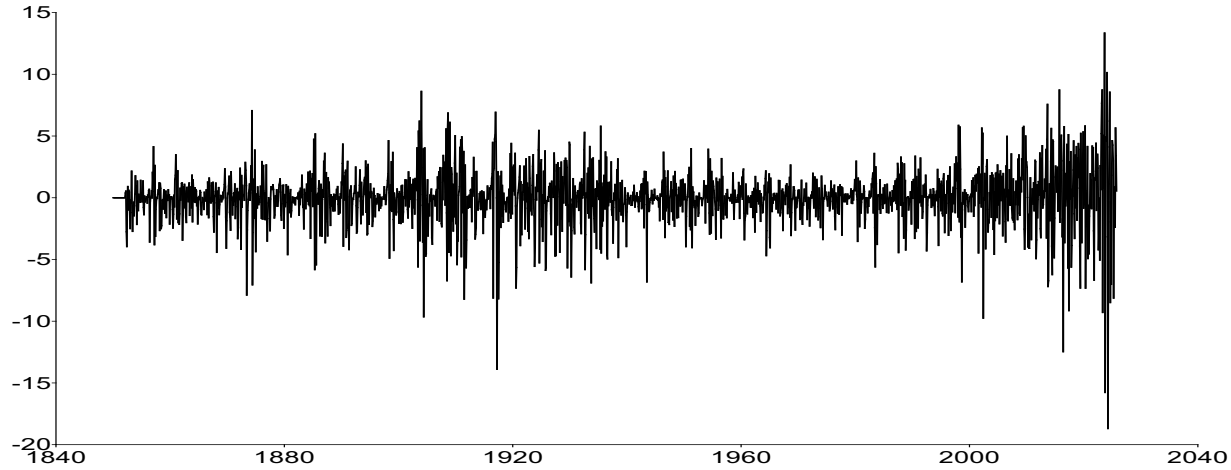

Figure B22. Degree of fractional integration score function $u_{d,t}$ from January 1850 to October 2025 for the t-FI(d_t)-QAR(p)-Beta-t-EGARCH and t-FI(d_t)-QAR(p)-Beta-t-EIGARCH models.

(a) Arctic temperature anomalies, log scale score function $u_{\lambda,t}$ for t-FI-QAR-Beta-t-EGARCH

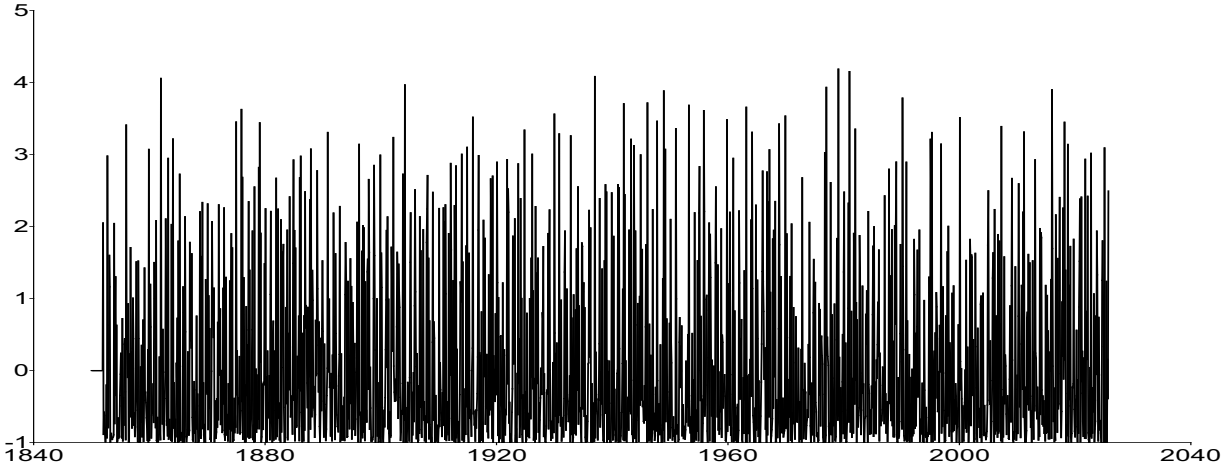

(b) Antarctic temperature anomalies, log scale score function $u_{\lambda,t}$ for t-FI-QAR-Beta-t-EIGARCH

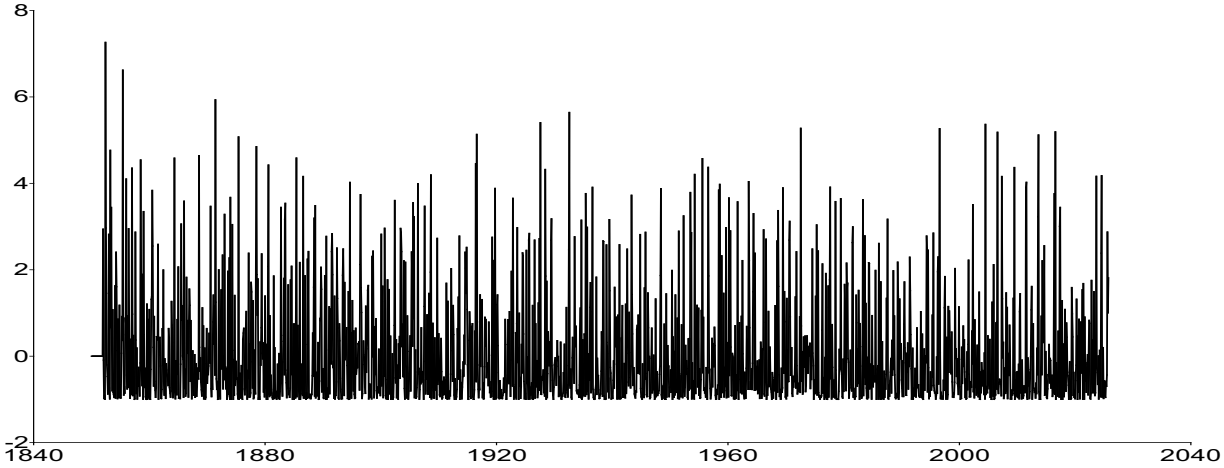

(c) Atlantic Ocean temperature anomalies, log scale score function $u_{\lambda,t}$ for t-FI-QAR-Beta-t-EGARCH

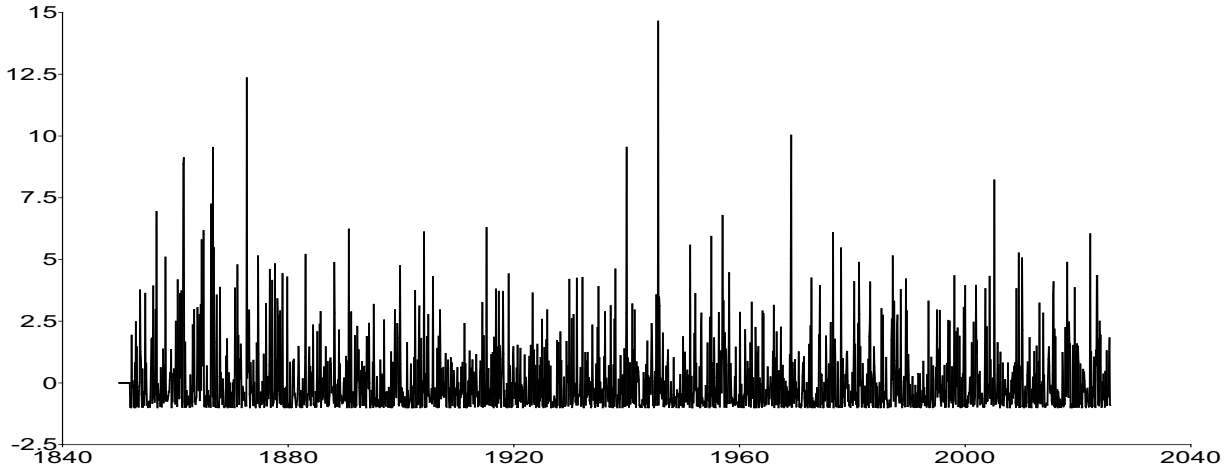

Figure B23. Log scale score function $u_{\lambda,t}$ from January 1850 to October 2025 for the t-FI(d_t)-QAR(p)-Beta-t-EGARCH and t-FI(d_t)-QAR(p)-Beta-t-EIGARCH models.

(a) Northeast Pacific Ocean temperature anomalies, log scale score function $u_{\lambda,t}$ for t-FI-QAR-Beta-t-EGARCH

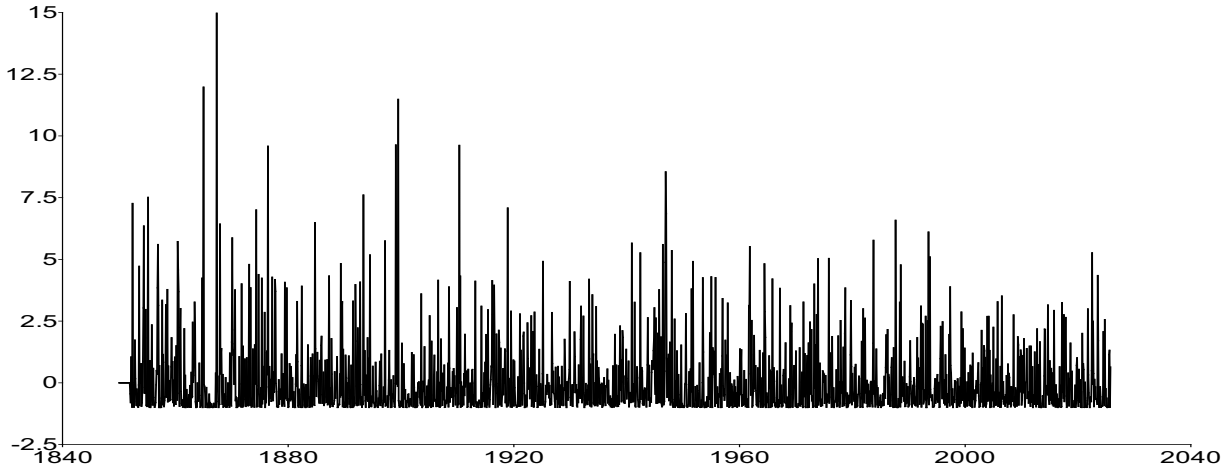

(b) Northern Hemisphere temperature anomalies, log scale score function $u_{\lambda,t}$ for t-FI-QAR-Beta-t-EGARCH

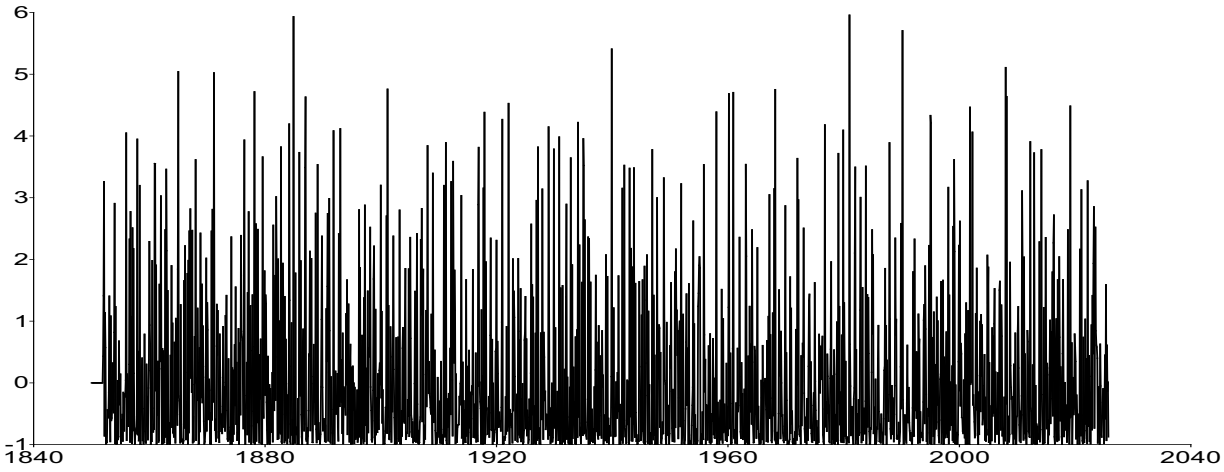

(c) Southern Hemisphere temperature anomalies, log scale score function $u_{\lambda,t}$ for t-FI-QAR-Beta-t-EIGARCH

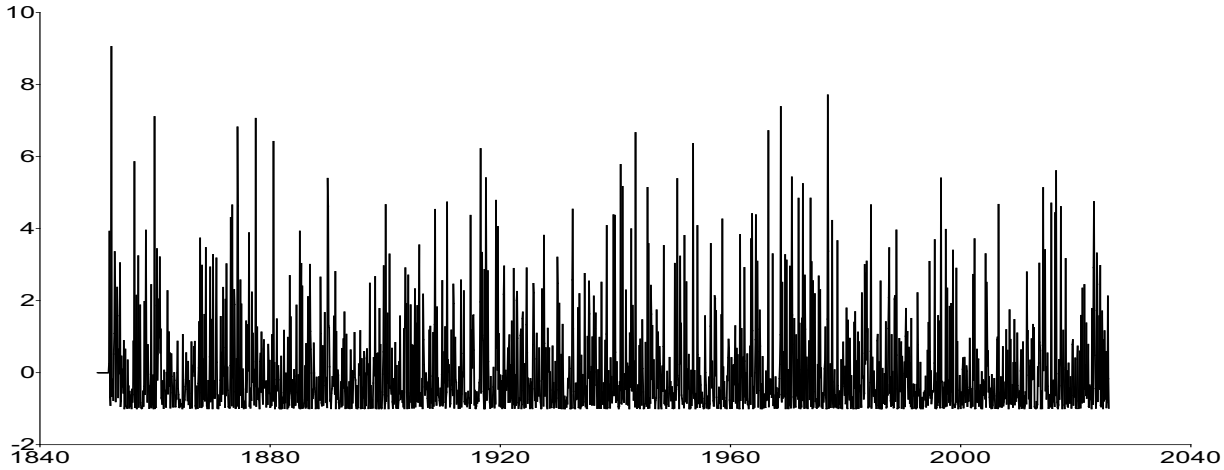

Figure B24. Log scale score function $u_{\lambda,t}$ from January 1850 to October 2025 for the t-FI(d_t)-QAR(p)-Beta-t-EGARCH and t-FI(d_t)-QAR(p)-Beta-t-EIGARCH models.